OPTICAL EXPRESSIONS OF ION-PAIR INTERACTIONS IN MINERALS

Thesis by

Stephanie Margaret Mattson

In Partial Fulfillment of the Requirements

for the Degree of

Doctor of Philosophy

California Institute of Technology

Pasadena, California

1985

(Submitted January 11, 1985)

Acknowledgments

My special thanks are due to George Rossman, my thesis advisor, for the many enjoyable discussions we have had regarding this thesis and related topics and the freedom to follow my own direction. I have also appreciated the interest expressed by Edward Stolper in my progress and activities.

I would like to gratefully acknowledge the influence of my interactions and collaborations with my fellow graduate students. In particular, the support, help and ideas of Roger Aines, Anne Hofmeister, Gerry Fine, Cleve Solomon and Greg Miller have been of great value.

Samples for this research were kindly provided by Pete Dunn (Smithsonian Institution), Pete Flusser (Los Angeles), Robert Gaal and Peter Keller (Gemmological Institute of America), Julius Petsch (Idar-Oberstein), and Roger Burns (MIT). Mössbauer spectra and helpful discussions were provided by Wayne Dollase (UCLA), Glen Waychunas (Stanford), Georg Amthauer (Marburg) and Roger Burns (MIT). My appreciation is also extended to members of Peter Rice's group (USC) for assistance in obtaining the magnetic susceptibility data and Edward Stolper (Caltech) for the use of controlled atomosphere ovens. This study was funded in part by NSF grants EAR 8212540 and EAR 7904801 and a grant from the Gemmological Institute of America.

Abstract

Clusters of transition element cations in neighboring sites frequently govern the optical properties of minerals. This is particularly true of Fe-bearing minerals which may exhibit several types of ion-pair transitions. In this thesis four different types of interactions were distinguished: intensified spin-forbidden transitions of Fe^{3+} clusters, intensified Fe^{2+} spin-allowed transitions of Fe^{2+}-Fe^{3+} clusters, heteronuclear charge transfer transitions of Fe^{2+}-Ti^{4+} and Mn^{2+}-Ti^{4+} clusters, and homonuclear charge transfer transitions of Fe^{2+}-Fe^{3+} clusters.

The optical characteristics of Fe^{3+} in red Fe^{3+}-rich and black Fe^{3+},Fe^{2+}-rich tourmalines were examined by absorption spectroscopy in the visible and near-infrared, Mössbauer spectroscopy and magnetic susceptibility measurements. Intense optical absorption features at 485 and 540 nm were assigned to transitions of exchange-coupled Fe^{3+} pairs in two different site combinations. Absorption spectra at variable temperatures and of samples which were oxidized and reduced were used to establish these assignments. Site assignments were based on intensity ratios in different polarizations according to the polarization of these transitions along the vector between the interacting cations. The 485 nm band occurs at an unusually low energy for Fe^{3+} in silicate minerals. Similar behavior was observed in the spectrum of coalingite, a Mg,Fe-hydroxy

carbonate, and has been proposed to result from magnetic exchange in large, edge-shared octahedra. The antiferromagnetic exchange which is generally associated with intensity increases in Fe^{3+} clusters was confirmed by variable temperature magnetic susceptibility measurements. The Mössbauer spectrum of a red tourmaline with 3.4% Fe exhibits an unusual decrease in width of peaks by ~30% from 298 K to 5 K which may be related to an unusual interaction between Fe^{3+} and trace amounts of Fe^{2+}.

Optical absorption and Mössbauer studies of Fe^{2+}-bearing tourmalines with variable Fe^{3+} contents were used to examine Fe^{2+} transitions which are intensified through an interaction with Fe^{3+} neighbors. The variation of molar absorptivity of Fe^{2+} bands with the fraction of Fe^{2+} in Fe^{2+}-Fe^{3+} pairs indicates that Fe^{3+} ions increase the absorptivity of Fe^{2+} bands to ~1200 $M^{-1}cm^{-1}$ as compared to ~5 $M^{-1}cm^{-1}$ for non-interacting Fe^{2+}. Approximately equal degrees of intensification were observed for both components of the $^5T_2 \rightarrow {}^5E$ Fe^{2+} transition as well as for Fe^{2+} in two different sites. Although the detailed behavior of non-interacting Fe^{2+} ions differ in Mg-tourmalines and Li,Al-tourmalines, the characteristics of Fe^{2+}-Fe^{3+} absorption are constant. Intensity increases were restricted to the polarization which coincided with the vector between the Fe^{2+} and Fe^{3+} ions. The intensified Fe^{2+} transitions are characterized by an unusual temperature response. The integrated intensity of these transitions

increases by 10-50% at 83 K as compared to 296 K. The positions and widths of the intensified transitions maintain the values of the non-interacting Fe^{2+}. Tourmalines with the lowest Fe^{3+} contents were the gemmy Li,Al-tourmalines which generally form in pockets within pegmatites. Fe,Mg-tourmalines exhibited consistently higher Fe^{3+} contents than any of the Li-bearing tourmalines examined. Oxidation of Fe^{2+} which resulted from gamma irradiation of blue Li-tourmalines which contained several percent each of MnO and FeO could be monitored by increases in Fe^{2+} intensity in one polarization.

Fe^{2+}-Ti^{4+} charge transfer transitions were examined in minerals which contain stoichiometric quantities of Fe and Ti--taramellite, neptunite, and traskite--and tourmaline. The wavelength of these transitions ranged between 400 and 500 nm, and the halfwidths ranged between 7000 and 9000 cm^{-1}. These characteristics can generally be used to assign Fe^{2+}-Ti^{4+} charge transfer transitions. The molar absorptivities of these transitions, however, exhibit very large variations. The molar absorptivity of Fe^{2+}-Ti^{4+} charge transfer in neptunite is ~225 $M^{-1}cm^{-1}$ in beta polarization, in taramellite it is ~1300 $M^{-1}cm^{-1}$ and in tourmaline it is ~4000 $M^{-1}cm^{-1}$. Tentative assignments of Fe^{2+}-Ti^{4+} in more dilute minerals generally compare favorably with the energy and width stated above. However, sapphire and other Al-minerals such as kyanite have very different characteristics for bands assigned to Fe^{2+}-Ti^{4+}

charge transfer. The Fe^{2+}–Ti^{4+} charge transfer transition in taramellite exhibits no change in integrated intensity with decreasing temperature but increases by 15% from 296 K to 83 K in tourmaline. Mn^{2+}–Ti^{4+} charge transfer was also assigned to a transition at 320 nm in two unusual yellow tourmalines.

The characteristics of Fe^{2+}–Fe^{3+} charge transfer transitions were reviewed in light of recent data and with regard to their utility as diagnostic criteria. A correlation between charge transfer energy and the separation of the interacting cations proposed by Smith and Strens (1976) could not be supported by the expanded data base. Temperature variations of charge transfer transition areas were also examined. The magnetic behavior of two minerals which exhibited different temperature responses were investigated. General agreement with the theories of Cox (1980) and Girerd (1983) that suggest that ferromagnetic exchange should produce intensity increases at low temperature and that antiferromagnetic exchange produces intensity decreases was confirmed by these examples of Fe^{2+}–Fe^{3+} charge transfer but could not explain the temperature response of Fe^{2+}–Ti^{4+} charge transfer transitions. In any case, an increase in intensity with decreasing temperature, which is generally expected on the basis of experimental observations, cannot be used in a negative sense to eliminate a charge transfer assignment. The large width of charge transfer transitions is

generally the most useful diagnostic criterion.

Cox, PA (1980) Electron transfer between exchange-coupled ions in a mixed-valency compound. Chem Phys Lett 69:340-343

Girerd, J-J (1983) Electron transfer between magnetic ions in mixed valence binuclear systems. J Chem Phys 79:1766-1775

Smith, G and Strens RGJ (1976) Intervalence transfer absorption in some silicate, oxide and phosphate minerals. In: The Physics and Chemistry of Minerals and Rocks, Strens, RGJ (ed.). New York: Wiley and Sons, pp. 583-612

Table of Contents

Acknowledgments		ii
Abstract		iii
Extended Table of Contents		ix
Chapter 1	Introduction	1
Chapter 2	Fe^{3+}–Fe^{3+} Interactions in Tourmaline	9
Chapter 3	Fe^{2+}–Fe^{3+} Interactions in Tourmaline	48
Chapter 4	Heteronuclear Charge Transfer in Minerals	89
Chapter 5	Characteristics of Intervalence Charge Transfer in Minerals	120
Chapter 6	Summary	146
Appendix		151

Extended Table of Contents

Chapter 1 Introduction 1
References 7

Chapter 2 Fe^{3+}–Fe^{3+} Interactions in Tourmaline 9
Introduction 10
Experimental 13
Results and Discussion 17
Magnetic Moment 17
Mössbauer Spectroscopy 20
Optical Spectroscopy 24
Fe^{3+}–Fe^{3+} pairs in the trimer 26
Fe^{3+}–Fe^{3+} pairs in the helix 33
Structural Effects 38
Summary 41
References 43

Chapter 3 Fe^{2+}–Fe^{3+} Interactions in Tourmaline 48
Introduction 49
Experimental 52
Results and Discussion 57
Intensity of Fe2+ absorption in Fe^{2+}–Fe^{3+}groups 63
Diagnostic Attributes of Intensified Fe^{2+} Transitions 69
$Fe^{2+}Fe^{3+}$ Charge Transfer in Tourmaline 74
Site Assignments of Fe^{2+} Absorption 76
Application to Radiation Effects 79
Summary 83
References 85

Chapter 4 Heteronuclear Charge Transfer in Minerals 89
Introduction 90
Experimental 92
Results
Taramellite 95
Neptunite 99
Traskite 101
Tourmaline 103
Mn^{2+}–Ti^{4+} Charge Transfer 108
Discussion 111
References 116

Chapter 5 Characteristics of Intervalence Charge Transfer in Minerals 120
Introduction 121
Experimental
Results and Discussion
Charge Transfer Energies 124
Effect of Temperature on Intensity 126

Widths of Charge Transfer Transitions 137
Summary 140
References 142

Chapter 6 Summary 146

Appendix OH Vibrations as a Chemical Probe in Tourmaline 151

Chapter 1

Introduction

Optical absorption bands of transition element ions are often used to determine the concentration of these ions in solution. The extension of such analytical capabilities to solids, in particular to minerals, has met with limited success. Difficulties have arisen in part because transition elements are often partitioned into multiple sites in minerals which have different optical properties which complicate the analysis of optical data from which more information (i.e. site occupancy) is required. When the sites are very different, as in orthopyroxenes (Goldman and Rossman 1979), quantitative site occupancies may be determinable. More significant problems result from the complicated chemistries of natural materials and the possibility of interactions among cations.

Dramatic color changes which attended the mixing of transition element cations of differing valence were the first indications of the properties associated with multiple cations. These color changes were later attributed to optical transitions which involved the transfer of electrons between neighboring cations. These intervalence charge transfer transitions were investigated extensively in chemical systems (Robin and Day 1967; Allen and Hush 1967). Their importance to the fields of physics, biology and geology has been more gradually recognized (Brown 1980). The initial emphasis on systems with highly controlled chemistries produced a large amount of data on charge transfer between cations of the same element which differed

in their oxidation states. The most important mineralogical example of this group is Fe^{2+}–Fe^{3+} charge transfer. Charge transfer between cations of different elements and different valences received very little attention. Transitions which occurred in Ti-bearing minerals were often assigned to Ti^{3+}–Ti^{4+} charge transfer without consideration of more abundant Fe^{2+}–Ti^{4+} ion-pairs (e.g. in tourmaline, Faye et al. 1968). Although these errors have generally been rectified, there are very few unequivocal examples of Fe^{2+}–Ti^{4+} charge transfer. Burns (1981) has reviewed current assignments of intervalence charge transfer transitions in Fe,Ti-minerals. In a few cases, simple assignments of transitions to Fe^{2+}–Fe^{3+} vs Fe^{2+}–Ti^{4+} charge transfer is not yet possible.

The amount of information available through the analysis of intervalence charge transfer transitions is potentially greater than that available from crystal field transitions. Site occupancies of cations can possibly be determined by intensity ratios in various polarizations according to the polarization of charge transfer transitions along the vector between the interacting cations. The involvement of multiple cations suggests that the evaluation of preferential ordering of cations should also be possible. The large relative intensities of charge transfer transitions indicate their potential as sensitive probes of cations which are weakly absorbing, such as Fe^{3+}, or which do not exhibit electronic transitions in the visible or

near-infrared, such as Ti^{4+}. These applications, however, require quantitative measures of absorbance vs concentration which are generally known to orders of magnitude accuracy if at all in minerals. Quantitative studies have been hampered by the difficulty of producing synthetic crystals suitable for optical studies, the complex chemistries of many minerals, and experimental difficulties associated with preparing sections which transmit enough light for the most concentrated systems. The last of these was recently surmounted, permitting the evaluation of quantitative Fe^{2+}-Fe^{3+} charge transfer intensities in several minerals (Amthauer and Rossman 1984).

In addition to producing intervalence charge transfer transitions which cannot be generated by the superposition of the characteristic absorptions of the individual cations, ion-pair interactions can also produce changes in the characteristic absorption of individual cations. This effect was first noted for groups of Mn^{2+} ions (Lohr and McClure 1968) and has since been found in Fe^{3+} clusters (Murray 1974). The normally weak spin-forbidden bands of these ions can be intensified by two orders of magnitude through antiferromagnetic exchange. It is generally believed that this intensification occurs through a circumvention of the spin-selection rules via simultaneous transitions in coupled ion-pairs. The most common mineralogical examples of this effect are found in iron sulfates (Rossman 1975). Smith (1978) proposed that the

spin-allowed bands of Fe^{2+} ions were intensified through an interaction with Fe^{3+} ions. Although this intensification cannot be justified on theoretical grounds, the behavior of these transitions, particularly with regard to temperature response, is also inconsistent with the current theory of crystal field transitions. The magnitude of the intensity increase was not evaluated. The utility of intensified Fe^{2+} transitions as probes of Fe^{3+} ions is greatly dependent on the magnitude of the intensity increase. However, the possible corruption of expected concentration vs intensity correlations of transitions in which this effect is not recognized are significant even at fairly low increases.

The basic requirement of all of these transitions is that transition element ion-pairs involve next-nearest neighbor cations which share one to three nearest neighbor anions. Transition elements in minerals often occupy edge-sharing octahedra in clusters from dimers up to chains and sheets of octahedra. Several common minerals combine these structures with complex chemistries to produce spectra that consist of multiple ion-pair transitions as well as transitions of single ions. Reliable characteristics which can be used to differentiate among these transitions are essential for the interpretation of such spectra but are not yet available for all three types of ion-pair transitions.

The purposes of this study were twofold, to provide reliable characteristics of ion-pair transitions in minerals

such that assignments of transitions can be more certain, and to evaluate quantitative absorption intensities such that concentrations and site occupancies can be evaluated from intensities of ion-pair transitions. The study of intensified Fe^{2+} transitions was focused upon tourmalines (Chapter 3) because of their relative abundance and wide range of compositions among the minerals discussed by Smith (1978). However, the chemical complexity of tourmalines required a fairly complete understanding of the spectroscopy of Fe-bearing tourmalines. Chapter 2 presents the spectroscopy of Fe^{3+} in tourmaline and Fe^{2+}-Ti^{4+} and Mn^{2+}-Ti^{4+} charge transitions in tourmaline are included in Chapter 4. Stoichiometric Fe,Ti-minerals are emphasized in the study of Fe^{2+}-Ti^{4+} charge transfer (Chapter 4) because of the possibility of quantitative as well as qualitative evaluations. The characteristics of Fe^{2+}-Fe^{3+} charge transfer are reexamined in Chapter 5 to evaluate theoretical and experimental discrepancies and to incorporate more recent experimental data. Chapter 6 concludes the main body of the thesis with a summary discussion. A short section on the interpretation of OH vibrational overtones in tourmalines is presented in the appendix.

REFERENCES

Allen, GC and Hush, NS (1967) Intervalence transfer absorption. Part 1. Qualitative evidence for intervalence-transfer absorption in inorganic systems in solution and in the solid state. Prog Inorg Chem 8:357-389

Amthauer, G and Rossman, GR (1984) Mixed valence of iron in minerals with cation clusters. Phys Chem Minerals 11:37-51

Brown, DB, ed. (1980) Mixed Valence Compounds. Theory and Applications in Chemistry, Physics, Geology, and Biology. Holland: Reidel, 519 pp.

Burns, RG (1981) Intervalence transitions in mixed-valence minerals of iron and titanium. Ann Rev Earth Planet Sci 9:345-383

Faye, GH, Manning, PG and Nickel, EH (1968) An interpretation of the polarized optical absorption spectra of tourmaline, cordierite, chloritoid and vivianite. Am Mineral 53:1174-1201

Goldman, DG and Rossman, GR (1979) Determination of quantitative cation distribution in orthopyroxenes from electronic absorption spectra. Phys Chem Minerals 4:43-53

Lohr, LL Jr and McClure, DS (1968) Optical spectra of divalent manganese salts. II. The effect of interionic coupling on absorption strength. J Chem Phys 49:3516-3521

Murray, KS (1974) Binuclear oxo-bridged iron (III) complexes. Coord Chem Rev 12:1-35

Robin, MB and Day, P (1967) Mixed valence chemistry--a survey and classification. Adv Inorg Chem Radiochem 10:248-422

Rossman, GR (1975) Spectroscopic and magnetic studies of ferric iron hydroxy sulfates: intensification of color in ferric iron clusters bridged by a single hydroxide ion. Am Mineral 60:698-704

Smith, G (1978) Evidence for absorption by exchange-coupled Fe^{2+}-Fe^{3+} pairs in the near infra-red spectra of minerals. Phys Chem Minerals 3:375-383

Chapter 2

Fe^{3+} - Fe^{3+} Interactions in Tourmaline

(Accepted for publication in Physics and Chemistry of Minerals

George Rossman coauthor)

Introduction

The presence of Fe^{3+} in minerals is usually easily determined by its characteristic optical absorption bands. The consistency of these features in many silicates has made quite puzzling their apparent absence in tourmaline and micas. Fe^{3+} has a large role in the optical spectroscopy of tourmaline through its interaction with Fe^{2+} (Smith 1978; Faye et al. 1974; Wilkins et al. 1969). Some natural samples have been shown to contain substantial amounts of Fe^{3+} by other methods (Hermon et al. 1973; Saegusa et al. 1979; Walenta and Dunn 1979). However, in spite of the prevalence of Fe^{2+}-Fe^{3+} interactions in tourmaline, consistent independent optical evidence of Fe^{3+} has not been recognized. Even in buergerite, nearly the Fe^{3+}-tourmaline end-member, only Fe^{2+} features were recognized (Manning 1969). The discrimination of Fe^{3+} bands in tourmaline has been hampered both by a complex composition in which other chromophoric ions are generally present and by low levels of Fe^{3+} in the gemmy samples which have been preferentially studied. Spectral features have been previously assigned to Fe^{3+} in tourmaline by Manning (1969) and Smith (1978). However, these assignments refer to different features. Furthermore, bands at these positions are rarely encountered in tourmaline. Unusual red tourmalines from Kenya were reported to contain only trace amounts of transition elements other than iron (Bank 1974; Dunn et al. 1975). Our preliminary study of these samples indicated a very low Fe^{2+}/Fe^{3+} ratio and the potential to isolate Fe^{3+} optical features.

In addition to features of individual cations, in minerals such as tourmaline, neighboring transition elements interact to produce optical features which are more intense than those of isolated ions. These

transitions frequently dominate the spectra of minerals in which the sites occupied by transition elements are linked directly to similar sites. In tourmaline, interactions among cation pairs can occur in 3 possible site combinations (Buerger et al. 1962). They are highly favored by edge-shared connections and short next-nearest neighbor distances (295-305 pm). Transition elements are known to substitute into two 6-coordinate sites which form helices (Z-site) and trimers (Y-site) (Fig. 1). The linkage of these groups provides pairs within the trimer, within the helix and in combination. The site occupancy of Fe^{3+} is potentially quite variable as evidenced by the existence of two Fe^{3+} end-members: buergerite, $NaFe^{3+}_3Al_6Si_6O_{18}(BO_3)_3(O_3OH)$ (Donnay et al. 1966) and ferridravite, $NaMg_3Fe^{3+}_6Si_6O_{18}(BO_3)_3(OH)_4$ (Walenta and Dunn 1974). Fe^{3+} site occupancy in tourmaline has been firmly established only in buergerite by X-ray structure refinement (Barton 1969). Structure refinements of more typical tourmalines have suffered from the inability to differentiate Fe^{2+} from Fe^{3+} (Fortier and Donnay 1975). Mössbauer studies of Fe^{3+} in tourmaline have suffered from the general dominance of Fe^{2+} peaks as well as the relative insensitivity of Fe^{3+} peaks to site geometry. Optical transitions of multiple cations provide another measure of site occupancy which will be explored here.

The spectroscopy and color of most tourmalines are dominated by an interaction between Fe^{2+} and Fe^{3+} which intensifies Fe^{2+} absorption bands (Smith 1978). Although this interaction occurs in other minerals, in tourmaline it is particularly pronounced. The expected signature of such interactions, Fe^{2+}-Fe^{3+} intervalence charge transfer, has been assigned to a comparatively weak feature. These characteristics of ion-pair interactions can provide a sensitive probe of oxidation states and

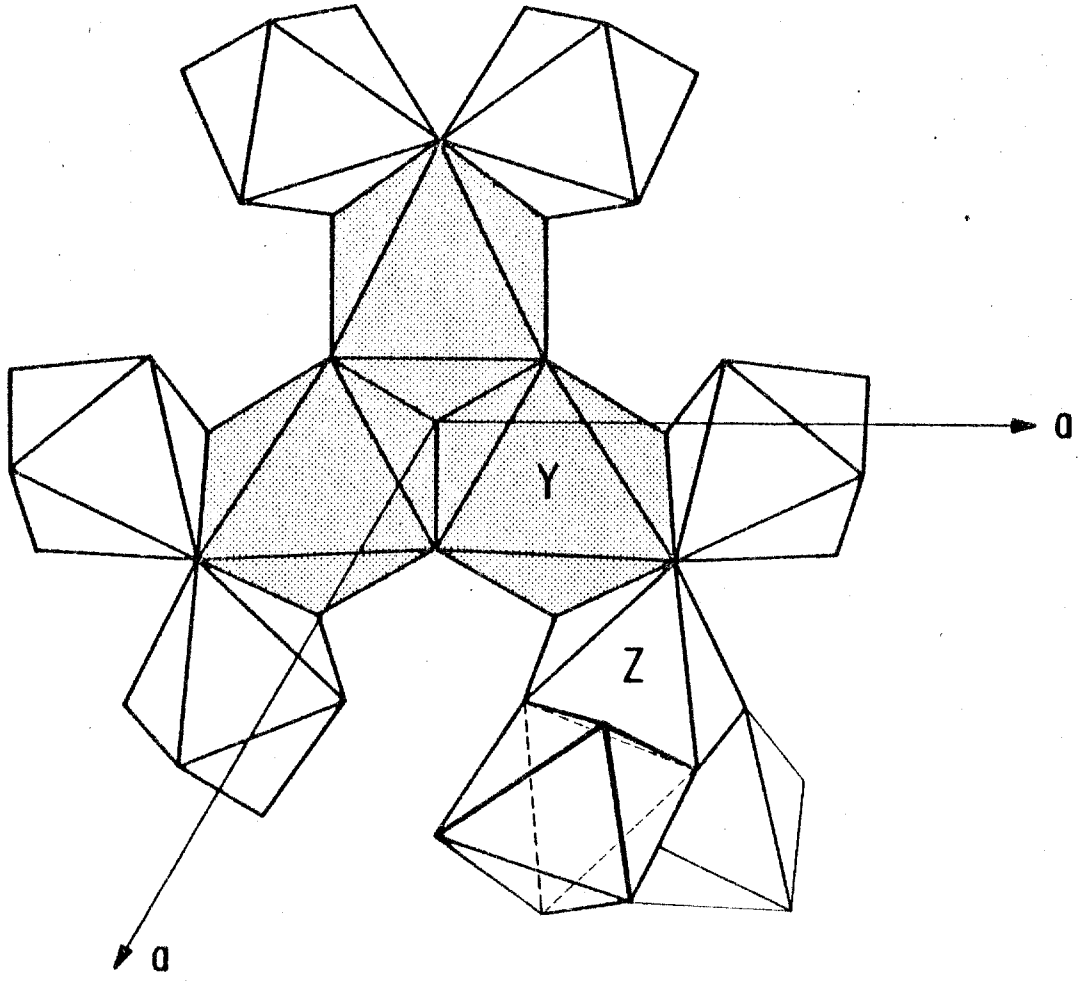

Fig. 1. (001) projection of a portion of the tourmaline structure showing the trimer and helix formed by the sites in which transition elements occur and the connections among these sites.

site occupancies of Fe cations in minerals, but they must be understood in regard to the factors which govern their intensity. Tourmaline provides an extreme version of Fe^{2+}-Fe^{3+} interactions and furnishes the opportunity to study the factors involved in these effects. The recognition and understanding of the optical properties of Fe^{3+} is essential to this study.

Experimental

Sample localities are presented in Table 1. Chemical analyses were obtained using a MAC5-SA5 electron microprobe. Data reduction was accomplished using the methods of Bence and Albee (1968). Partial sample compositions are shown in Table 2. Formula proportions were calculated using Mg + Fe + Ti + Mn + Al + Si = 15.

Magnetic susceptibility measurements were taken on a S.H.E. model VTS magnetometer/susceptometer. The raw data were corrected for the Al sample container and fit to combined paramagnetic and antiferromagnetically-coupled components. The exchange-coupled components were modelled as 'dimers' and 'trimers' of equivalent ions interacting isotropically through Heisenberg intracluster exchange (O'Connor 1982); g=2.0 was assumed for all groups. The magnetic moment of Fe^{3+} was assumed to be the spin-only value of 5.92 B.M. which is consistent among similar high-spin compounds (König 1966). Because the magnetic moment of Fe^{2+} is somewhat more variable in oxide coordination, this parameter was varied between 4.9 and 5.4 B.M..

The Mössbauer spectra of sample 1 were taken by Georg Amthauer using conventional techniques described in Amthauer et al. (1976). The mirror symmetric, simultaneously recorded spectra (512 channels each)

Table 1. Sample Descriptions

Sample #	Mineral Name	Color[a]	Locality	Archival Code
1	Dravite	red	Osarara, Narok District Kenya	NMNH # 126030
2	Dravite	red	Kenya	CIT # 13764
3	Uvite	orange-red	Brumado, Bahia, Brazil	CIT # 13765
4	Dravite	red	Diamantina area Minas Gerais, Brazil	NMNH # 137101
5	Dravite	red	Chipata, Zambia	CIT # 15053
6	Schorl	yellow[b]	Schindler Claim, Cahuilla Mt. Southern California	CIT # 13763
7	Uvite	green[c]	Pierrepont, New York	NMNH # 81511
8	Schorl	green[c]	Santa Cruz, Sonora, Mexico	NMNH # R15504
9	Dravite	brown[c]	Madagascar	Harvard # 108796
10	Dravite	brown[c]	Syndenham, Ontario	CIT # 2884
11	Buergerite	brown	Mexquitic, Mexico	CIT # 8207
12	Coalingite	yellow	Near Dallas Gem Mine San Benito Co., California	CIT # 7298

NMNH: U.S. National Museum of Natural History
CIT: Calfornia Institute of Technology
[a] Macroscopic color unless otherwise indicated [b] color of oxidized sample
[c] macroscopically black, color quoted is E⊥c color in thin section

Table 2. Electron Microprobe Partial Analyses (wt.%)

Sample	1[b]	2	3[b]	4	5	6	7	8	9	10
Na_2O	2.72	1.98	0.80	1.77	2.33	1.34	1.44	1.86	1.67	1.58
CaO	0.06	0.84	3.69	1.64	0.14	0.05	2.92	1.98	2.42	2.61
K_2O	0.07	0.07	0.03	0.11	0.02	0.05	0.05	0.05	0.08	0.04
MgO	9.45	9.46	12.8	10.1	10.0	0.48	10.8	6.48	8.58	10.9
FeO[a]	4.32	2.10	1.93	4.46	2.06	13.3	8.23	18.1	13.4	7.84
MnO	tr	0.12	tr	0.22	-	0.36	-	tr	tr	tr
TiO_2	0.27	0.20	0.58	0.22	0.18	0.05	0.55	1.18	1.69	0.72
Al_2O_3	32.0	33.9	29.3	31.0	33.9	35.3	26.3	22.2	23.6	26.5
SiO_2	36.7	37.1	36.7	36.1	36.7	35.5	35.2	34.0	34.4	35.3
F	tr	tr	0.1	0.1	-	-	1.6	0.5	1.1	1.6
Formula Proportions										
Na	0.88	0.62	0.24	0.56	0.72	0.44	0.47	0.63	0.56	0.51
Ca	0.01	0.14	0.64	0.28	0.03	0.01	0.52	0.37	0.44	0.46
K	0.02	0.01	0.01	0.02	0	0.01	0.01	0.01	0.02	0.01
Mg	2.27	2.27	3.09	2.46	2.40	0.12	2.70	1.69	2.20	2.72
Fe	0.58	0.28	0.26	0.60	0.28	1.87	1.15	2.64	1.92	1.09
(Fe^{3+})[c]	(0.53)	(0.25)	(0.23)	(0.53)	(0.26)	(1.87)	(0.55)	(0.93)[d]	(1.19)	(0.59)
Mn	0	0.02	0	0.03	0	0.05	0	0.01	0	0
Ti	0.03	0.02	0.07	0.03	0.02	0.01	0.07	0.15	0.22	0.09
Al	6.12	6.44	5.60	5.97	6.40	7.00	5.18	4.56	4.76	5.22
Si	5.99	5.97	5.96	5.90	5.89	5.96	5.91	5.94	5.90	5.89
F	0	0	0.1	0	0	0	0.8	0.3	0.6	0.8

[a] total Fe [b] contains trace amounts of V or Cr
[c] calculated using calibrated optical absorption except where noted
[d] minimum value based on charge balance in the absence of H-defects

were folded and fit using a modified version of 'MOSFIT' (Kulscar, Nagy, and Verbiest--Leuven, Belgium). The fitting was constrained to symmetric doublets having the same isomer shift. These constraints were employed because the outer doublet is poorly constrained by the spectra. No significant improvement or difference in the fits was obtained by independent isomer shifts. One-doublet fits required unusually large quadratic backgrounds and were 1.5-2 times poorer fits as measured by chi-squared. The final parameters are shown in Table 4. The isomer shift is quoted relative to sodium nitroprusside. A Mössbauer spectrum of sample 3 was obtained by W. Dollase at UCLA and was similar to that of sample 1 at 298 K but with a lower signal to noise ratio. Independent Mössbauer data on sample 7 indicates ~60% Fe^{3+} (RG Burns personal communication).

Optical spectra were obtained in a manner described in Amthauer and Rossman (1984). In addition to Mössbauer data for samples 1, 3, and 7, calibrated Fe^{2+} absorption (Chapter 3) was used to determine the relative amounts of ferrous and ferric iron. The assignment of various transitions to ferric vs. ferrous iron was based upon spectra of oxidized and reduced samples. Sample 1 was oxidized by heating in air at 1073 K for 15 and 40 hours and sample 6 for 7 hours. Oxidation via this treatment has been confirmed by Mössbauer studies (Gorelikova et al. 1976). Reduction of sample 1 was accomplished by heating at 1073 K for 8 hours in a H_2/CO_2 mixture set at the iron/wüstite buffer. Molar absorptivities are given in units of liters/mole/cm ($M^{-1}cm^{-1}$).

Results and Discussion

Magnetic Moment

The magnetic moment of solids and its variation with temperature provide information regarding oxidation state and the extent of interaction among paramagnetic ions. In materials such as the tourmalines of this study the degree of ordering can also be indicated. The temperature dependence of the magnetic moment of sample 1 is shown in Fig. 2 together with the calculated values. The decreasing moment with decreasing temperature indicates a small antiferromagnetic interaction. The solid line represents a calculation for a combination of the most probable components based on stoichiometry and the simplest model: non-interacting ferrous and ferric iron, two populations of ferric iron 'dimers' and a population of ferric iron 'trimers'. The parameters of this calculation are presented in Table 3. This distribution is in rough agreement with a random distribution of Fe^{3+} within the trimer -- 67% Fe in $Fe^{3+}X_2$, 30% in $Fe_2^{3+}X$, and 3% in Fe_3^{3+} (X: other cations in the trimer). A small proportion of iron in the helix would decrease the percentage of 'dimer' and 'trimer' leading to somewhat better agreement with the data. Preferential association of Fe^{3+} is inconsistent with the observations. The strength of the interaction between adjacent Fe^{3+} ions is indicated by the coupling constant, J. Values of -14 and -14.5 cm^{-1} are slightly larger than edge-shared dimers (J = -8 to -11 cm^{-1}, Schugar et al. 1969; Wu et al. 1972) and roughly one half of that for the trimeric iron(III) carboxylates (Long et al. 1973; Earnshaw et al. 1966). The coupling constants are thus consistent with any of the 3 edge-shared pairs, and the agreement of the calculated distribution within the trimer with the

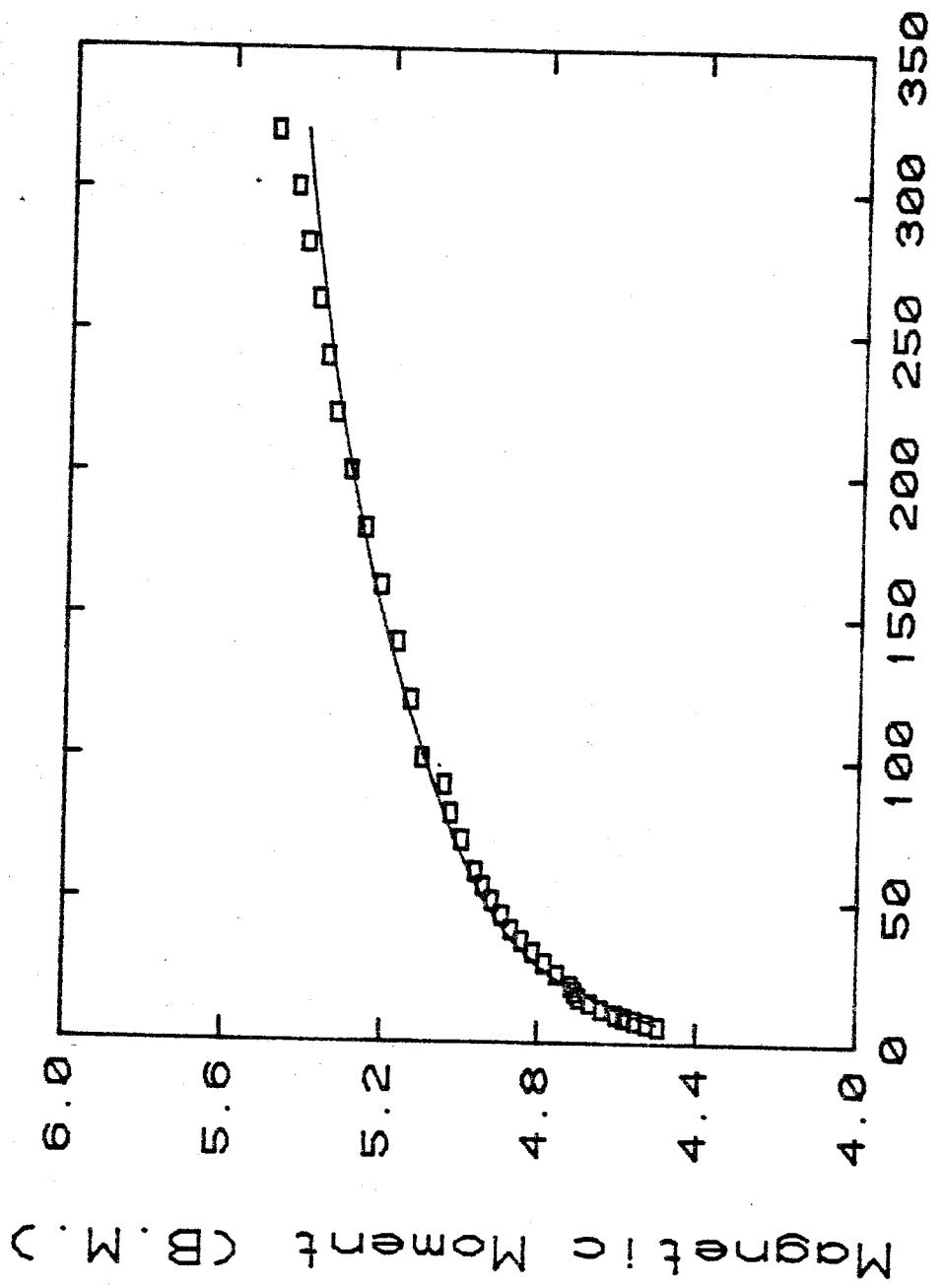

Fig. 2. Temperature dependence of the effective magnetic moment of sample 1. Rectangles represent the observed data. The solid line is a calculation for the parameters presented in Table 3.

Table 3. Calculated Magnetic Parameters for Sample 1

	Percentage	μ_B[a] (B.M.)	J[b] (cm^{-1})
Non-interacting Fe^{3+}	55	5.92	
Non-interacting Fe^{2+}	7.5	5.2	
Binuclear Fe^{3+} cluster #1	20		-14.5
Binuclear Fe^{3+} cluster #2	15		-1.25
Trinuclear Fe^{3+} cluster	2.5		-14

[a] magnetic moment in Bohr magnetons (assumed standard values 298 K)
[b] coupling constant for magnetic exchange

Table 4. Mössbauer Parameters for Sample 1

Temperature (K)	I.S.[a] (mm/sec)	Q.S.[b] (mm/sec)	Halfwidth (mm/sec)	Area[c]	χ_ν^2
298	0.62	0.76	0.56	1.45	1.04
	0.62	1.67	1.59	0.84	
80	0.73	0.74	0.44	1.56	1.27
	0.73	1.66	1.70	1.20	
5	0.74	0.76	0.37	1.63	1.07
	0.74	2.01	1.49	0.73	

[a] isomer shift (I.S.) is quoted relative to $Na_2Fe(CN)_5NO \cdot 2H_2O$
[b] quadrupole splitting [c] area is normalized to background
χ_ν^2 (chi-squared)/(number of degrees of freedom)

fit parameters supports a majority of Y-Y pairs. Previous studies of Fe-rich tourmalines indicated $\underline{J} \sim -6$ cm^{-1} (Tsang et al. 1971). The weakly interacting population ($\underline{J} = -1.25$ cm^{-1}, Table 3) was required to fit the low temperature region. It probably corresponds to interaction among Fe^{3+} ions with one intervening diamagnetic ion (e.g. in the helix). The non-interacting ions contribute a constant background to the observations which does not strongly constrain the relative percentages of non-interacting ferrous and ferric iron. However, the proportions of coupled versus non-interacting ions are well constrained.

Mössbauer Spectroscopy

The most striking feature of the Mössbauer spectrum of sample 1 is its unusual temperature dependence (Fig. 3). At 298 K the halfwidth of the doublet is similar to those of glasses (Kurkjian and Buchanan 1964), while at 5 K it is within the normal range for crystalline material. The area of this doublet is roughly constant with temperature. The overall broad, non-Lorentzian peak shape is similar to partially relaxed hyperfine structure (Wignall 1966) and complex compositional-structural intermediates (Dollase and Gustafson 1982). The major cause of these peak shapes can be discerned from the observed temperature dependence. Since the quadrupole splitting of ferric iron is normally independent of temperature, in contrast to Fe^{2+} (Greenwood and Gibb 1971), the coalescence of doublets from multiple environments is unlikely to produce the decreasing peak widths. The major cause of the broad non-Lorentzian shape, therefore, cannot be ascribed to compositional complexity. Relaxational processes can also affect the peak shape of Mössbauer absorption. Fe^{3+} may relax by spin-spin relaxation among Fe^{3+}

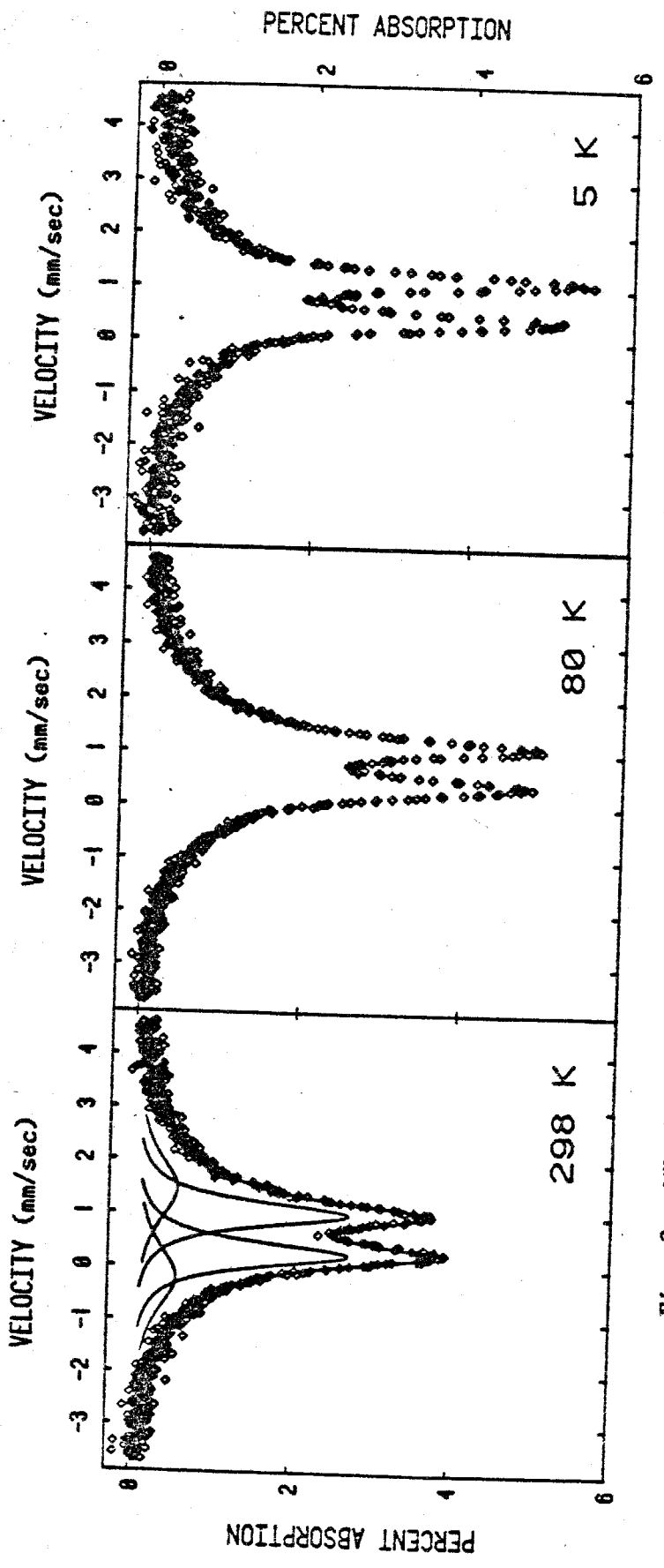

Fig. 3. Mössbauer spectra of sample 1 at various temperatures indicated to the lower right of each spectrum. Velocity is shown relative to sodium nitroprusside. A best-fit, 2 doublet calculated spectrum and components is shown for the 298 K spectrum.

groups or by cross relaxation with Fe^{2+} which in turn relaxes more rapidly by spin-lattice relaxation. The width of broad bands generated by spin-spin relaxation alone is independent of temperature (Wignall 1966). Therefore, we propose that the large decrease in width can be explained by cross relaxation enhanced by greater interaction among ferric and ferrous ions at lower temperatures. Supporting evidence for this is provided by increased intensity of Fe^{2+} optical absorption bands at low temperatures which are intensified by interaction with Fe^{3+} (Chapter 3).

These spectra were fit to symmetric lorentzian doublets to compare to previous data and to determine general absorption characteristics. The best fit parameters are presented in Table 4 and the calculated peaks are indicated for the 298 K spectrum in Fig. 3. The increase in isomer shift with temperature is in agreement with that expected from the second-order Doppler shift (Greenwood and Gibb 1971). These calculated doublets represent overlapping contributions from non-lorentzian peaks with broad tails due to relaxation effects, as well as Fe^{3+} in multiple sites and a small amount of Fe^{2+}. The isomer shift (IS) and quadrupole splitting (QS) of both doublets are consistent with ferric iron in an octahedral site.

The inner doublet accounts for most of the absorption. Its halfwidth at 5 K corresponds to that of a single, well-defined site and points to the preferential occupancy of either the Y or Z site. Its IS and QS are in reasonable agreement with an approximate fit to an oxidized Fe^{2+}-tourmaline (Gorelikova et al. 1976) and the general characteristics of Fe^{3+} in Fe^{2+}-rich tourmalines (Saegusa et al. 1979; Hermon et al. 1973; Gorelikova et al. 1976). The apparent discrepancy

of the IS with the major doublet in buergerite (Hermon et al. 1973) was not substantiated by an examination of the published spectrum, nor by independent data (IS = 0.61, QS = 1.12 mm/sec, RG Burns, personal communication). The outer doublet represents the non-lorentzian character of the inner doublet as well as the other components described above. This complexity is indicated by a halfwidth which is ~3.5 times greater than that generally observed for single components in crystalline phases. The maximum amount of Fe^{2+} estimated from the intensity in the wings of the 298 K spectrum at a position characteristic of Fe^{2+} in tourmaline and a typical halfwidth is 13 percent. The symmetry of these spectra about the Fe^{3+} isomer shift would argue against even this much Fe^{2+}. This compares to ~9% indicated by optical data.

A comparison of sample 1 to buergerite will be used to establish which site corresponds to the inner doublet. X-ray structure refinement has established that ~90% of the Fe^{3+} in buergerite is in the Y-site (Barton 1969). The isomer shift of the major doublet agrees with sample 1 within experimental error. The quadrupole splitting, however, is ~0.3 mm/sec larger in buergerite. Larger quadrupole splittings in Fe^{3+} compounds correspond to greater distortion and/or smaller sites. Since a structure refinement is not available for this sample, the buergerite structure will be compared to the Mg-tourmaline structure of Buerger et al. (1962). While the Fe^{3+} environment in sample 1 will not be precisely that of Mg, it should be intermediate between the Mg-site and the Fe^{3+}-site in buergerite. The Y-site in Mg-tourmaline is not only larger than in buergerite, it is also less distorted as measured by the range in Y-O bond lengths. Although the Z-site in Mg-tourmaline is

also less distorted, it is smaller than the Y-site in buergerite. These considerations suggest that Fe^{3+} prefers the Y-site in this sample. The maximum possible proportion of Fe^{2+} in the Z-site can be estimated from a doublet area corresponding to the height of the outer doublet at 5 K and a typical halfwidth. This calculation leads to a maximum Fe^{3+} in the Z-site of ~10% or 0.05 per formula unit.

Optical Spectroscopy

The optical spectrum of sample 1 is illustrated in Fig. 4 and is typical of samples 1-5. The broad bands at ~700 nm and ~1100 nm are produced by electronic transitions of ferrous ions and indicate ~0.30 wt% FeO for this sample (Chapter 3). Vibrational overtones of hydroxyl groups generate the weak, sharp bands between 1350 and 1500 nm. These features will not be discussed further. The other features of this spectrum have not been recognized in previous studies of tourmaline and cannot be assigned by analogy to other silicate minerals. The 425 nm band Manning (1969) assigned to Fe^{3+} is not evident and is more likely associated with Fe^{2+}-Ti^{4+} charge transfer (Chapter 4). The 485 nm ($E \perp c$) and 540 nm ($E \parallel c$) bands increase in intensity with increasing Fe^{3+} and are assigned to Fe^{3+}. The unusual red color of samples 1-5 results from the dominance of these Fe^{3+} transitions. Unlike most tourmalines, the iron in these samples is at least 90% ferric iron. These samples thus provide an ideal opportunity to observe the optical spectroscopy of Fe^{3+} in tourmaline.

Transitions among the electronic levels of Fe^{3+} generally produce 3 sets of bands in the visible and near infrared. Two of these are broad bands (halfwidth ~2500 cm^{-1}) in the regions 750-1000 nm and 550-700 nm

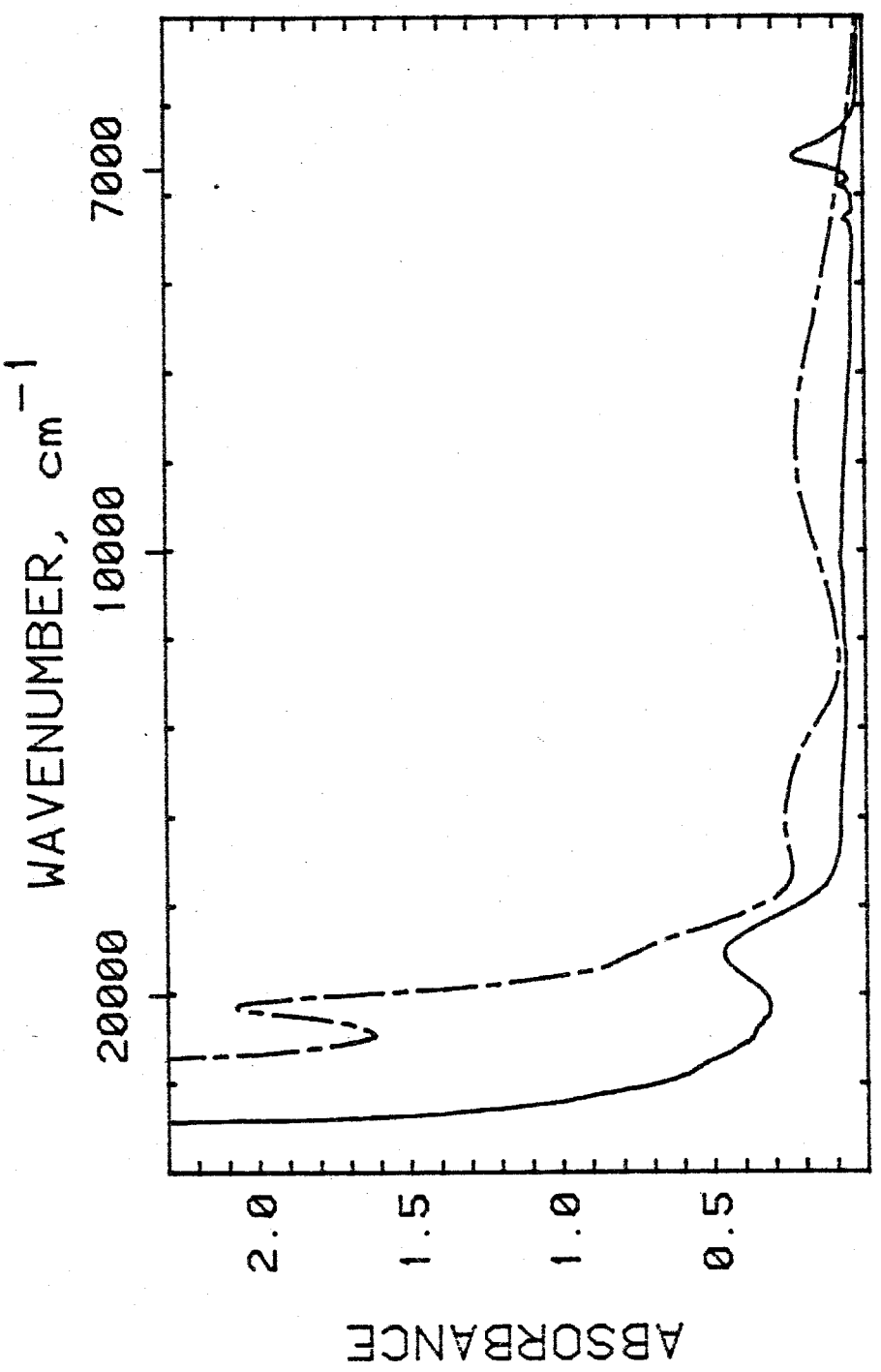

Fig. 4. Room temperature polarized absorption spectra of sample 1.

Broken line: $\mathbf{E} \perp \underline{c}$ Solid line: $\mathbf{E} \parallel \underline{c}$ Sample thickness: 0.311 mm

for octahedral coordination. The most distinctive Fe^{3+} feature is a sharp band or bands in the region 410-450 nm with a halfwidth of ~500 cm^{-1}. This typical pattern is not observed in any of these samples or in any published spectrum of tourmaline. In addition to unusual band positions and widths, the transitions observed are also much more intense than simple Fe^{3+} electronic transitions. Also, the intensities of the bands do not increase linearly with increasing Fe^{3+}, but with the proportion of Fe^{3+} having Fe^{3+} neighbors (Fig. 5). Thus, all of the optical features associated with Fe^{3+} in these tourmalines are assigned to simultaneous transitions of Fe^{3+} clusters which are antiferromagnetically coupled. Such transitions were first described for Mn^{2+} compounds which are isoelectronic with Fe^{3+} (Lohr and McClure 1968). These transitions occur at the same wavelength as those of isolated ions but with much higher intensities. The intensification occurs in the direction corresponding to the vector between the interacting cations. 'Ion-pair' transitions involving Fe^{3+} have been documented in sapphire (Krebs and Maisch 1971) and various sulfates (Rossman 1975, 1976a). Based upon the polarization of the bands observed in samples 1-5, ion-pairs within the trimer and those within the helix can be distinguished.

Fe^{3+}-Fe^{3+} pairs in the trimer

Ion-pair transitions among Fe^{3+} groups within the trimer are represented by the absorption bands at 485 nm and ~530 nm in the direction E⊥c. The assignment of these bands to Fe^{3+} is supported by decreasing intensity upon partial reduction of the iron in sample 1. No significant change in intensity was observed upon oxidation which removed the Fe^{2+} features at ~700 and 1100 nm. The assignment of these

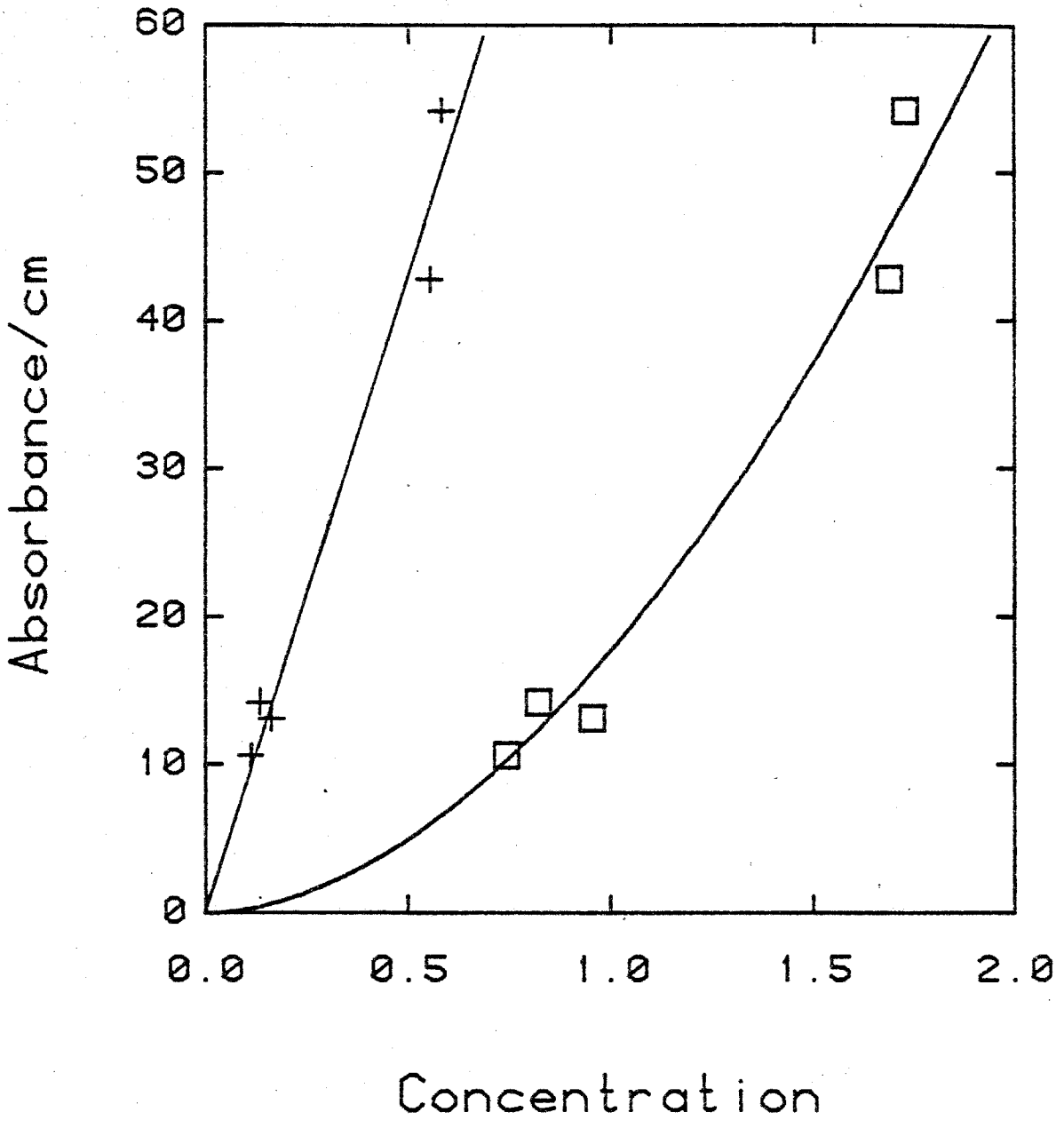

Fig. 5. Absorbance/cm of the 485 mn band (El_c) vs concentration in moles/liter of □: total Fe^{3+} and +: Fe^{3+} in Fe_2^{3+} X and Fe_3^{3+}. A Beer's law best fit is shown for interacting Fe^{3+}(+). The solid line associated with total Fe^{3+} approximates the deviation from Beer's law.

bands to Y-Y Fe^{3+} pairs was based upon their polarization along Fe^{3+}-Fe^{3+} vectors in $E \perp c$ and the dominance of Y-site occupancy indicated by the Mössbauer spectrum of sample 1. The 485 and 530 nm bands were also generated in Sample 6 upon complete oxidation. Sample 6, which is an Al-rich tourmaline originally containing predominantly Fe^{2+}, undoubtedly contains most of its iron in the trimer and shows only these features. The minimum molar absorptivity of the 485 nm band based on total Fe^{3+} which ranges from 14 to 31 $M^{-1}cm^{-1}$ is greater than an order of magnitude more intense than the analogous bands of isolated Fe^{3+} and points to the influence of exchange coupled groups. Molar absorptivities for samples 1-5 based on the amount of Fe^{3+} in 'dimers' and 'trimers' calculated assuming a random distribution within the Y-site yield a value of ~90 $M^{-1}cm^{-1}$. This fraction of Fe^{3+} adjacent to Fe^{3+} in Y-Y pairs based on optically determined Fe^{2+}/Fe^{3+} ratios is in close agreement with the distribution indicated by the magnetic data for sample 1. The molar absorptivity of these pairs (90 $M^{-1}cm^{-1}$) is in agreement with molar absorptivities found for antiferromagnetically-coupled Fe^{3+}, ~30-100 $M^{-1}cm^{-1}$ (Rossman 1975, 1976a, 1976b).

Samples 1-5 exhibit a red color which is similar to the color of minerals in which Fe^{2+}-Ti^{4+} charge transfer (CT) is the dominant optical feature, such as fassaite from ADOR (Mao et al. 1977). In tourmaline, Fe^{2+}-Ti^{4+} CT has been assigned to a broad band in the region 400-460 nm $E \perp c$ (Smith 1978; Faye et al. 1974). An assignment of Fe^{2+}-Ti^{4+} CT to the 485 nm band was rejected on the basis of 3 factors. The intensity does not correlate with Ti^{4+} and Fe^{2+} contents. The halfwidth (~1600 cm^{-1}) is much smaller than that of Fe^{2+}-Ti^{4+} CT in tourmaline (~8000 cm^{-1}, Chapter 4). The calculated maximum possible intensity

associated with Fe^{2+}-Ti^{4+} content is ~1 cm^{-1} or ~0.3 in Fig. 3 (Chapter 4). Thus, although Fe^{2+}-Ti^{4+} CT may contribute to the spectrum in this region, it will only raise the apparent background.

Additional electronic transitions occur at 360, 385, 400, and 440 nm at 296 K. Sample 4, which was also examined in this region, showed similar bands. These transitions can be distinguished from ligand to metal charge transfer bands because of their relatively low energy (Lehmann 1970). The differing temperature responses of these bands indicate different types of simultaneous transitions within Fe^{3+} groups. Simultaneous transitions in which electronic transitions occur in both ions have greater intensities at low temperatures and are known as 'cold' bands. These 2-exciton bands occur at the combined frequency of both electronic transitions. The 360 nm band can be assigned to a 'cold' band. It increases in intensity by a factor of ~3 at 80 K and is at an energy appropriate for the combination $({}^6\underline{A}_1 \rightarrow {}^4\underline{T}_1) + ({}^6\underline{A}_1 \rightarrow {}^4\underline{T}_2)$. The energy of these individual transitions are not precisely known, but the ~530 nm band $({}^6\underline{A}_1 \rightarrow {}^4\underline{T}_2)$ would require that the wavelength of the ${}^6\underline{A}_1 \rightarrow {}^4\underline{T}_1$ band be higher than 1000 nm. A weak, broad band at ~1000 nm is indicated in the spectra of the oxidized sample 6. The increase in intensity of the 360 nm band together with a shift of band maximum to lower energy and the shift of the 485 nm band to higher energy constitute the major changes illustrated in Fig. 6. Simultaneous transitions which involve an electronic transition for one atom and a spin-flip for another are termed exciton-magnon transitions. These bands are known as 'hot' bands because of their greater intensity at high temperatures (Murray 1974; Fujiwara et al. 1972). They occur at the same energy as the electronic transitions of isolated ions.

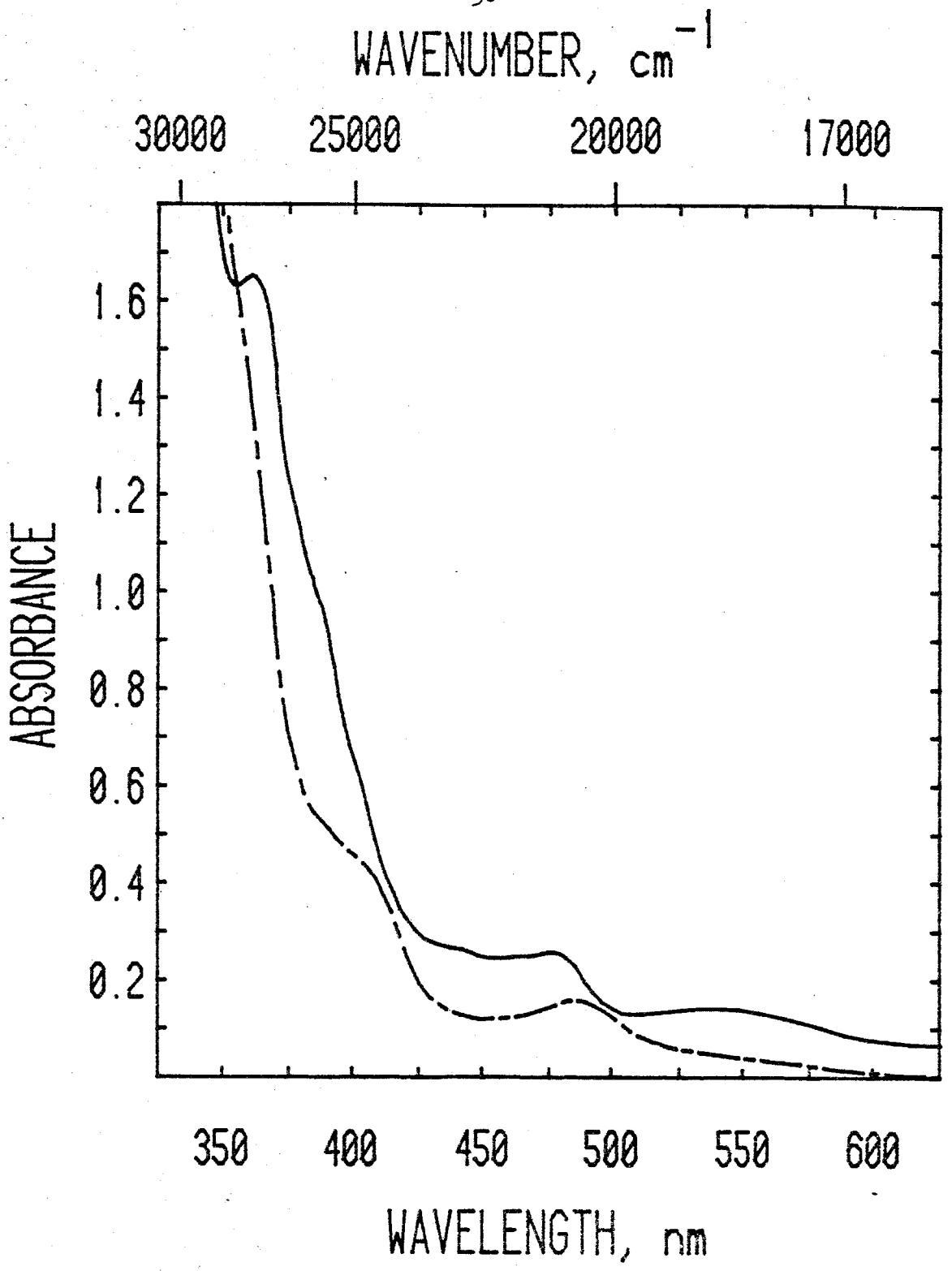

Fig. 6. E⊥c polarized absorption spectra of sample 1.

Broken line: 296 K Solid line: 83 K

Sample thickness: 0.021 mm

Although such considerations are complicated by energy shifts and splittings with temperature and contributions from Fe^{3+} pairs in the helix, the bands at 385, 400, 440 and 485 nm appear to be 'hot' bands. The band at 440 nm may also be a 'hot' band or it may be the $^6\underline{A}_1 \rightarrow (^4\underline{A}_1, ^4\underline{E})$ band of isolated Fe^{3+} .

Two factors which deserve further attention are noted here. First, the energy shift of the 360 nm and 485 nm bands are not typical of the limited data on other Fe^{3+} systems. Second, the general behavior of the Fe^{3+} pair transitions which is that the $^6\underline{A}_1 \rightarrow {}^4\underline{T}_1$ and $^6\underline{A}_1 \rightarrow (^4\underline{A}_1, ^4\underline{E})$ have the highest intensity of the three lowest energy bands is not observed. The $^6\underline{A}_1 \rightarrow {}^4\underline{A}_1$ transition Y-Y pairs in this case has a very low intensity and may not be intensified at all. An evaluation of the degree of noncompliance of these pairs requires a larger data base particularly in silicates and a more thorough theoretical description of environmental factors.

These considerations require the assignment of the 485 nm band to the $^6\underline{A}_1 \rightarrow (^4\underline{A}_1, ^4\underline{E})$ transition. This is an unusually low energy for this transition. It also exhibits a much broader width than normal. Low energies have been observed in epidote (Burns and Strens 1967) and appear to result from extreme distortion. The Y-site of tourmaline is only moderately distorted, however. There are a few other compounds which also exhibit such low energies. A relevant comparison is provided by the mineral coalingite, $Mg_{10}Fe^{3+}{}_2(OH)_{24}CO_3 \cdot 2H_2O$, in which the cations occupy edge-sharing octahedral sheets (Pastor-Rodriguez and Taylor 1971). The major Fe^{3+} transition is observed as a broad band at ~475 nm with a shoulder at ~409 nm (Fig. 7). Exchange interaction between large sites with edge-shared connections may produce the low energies observed

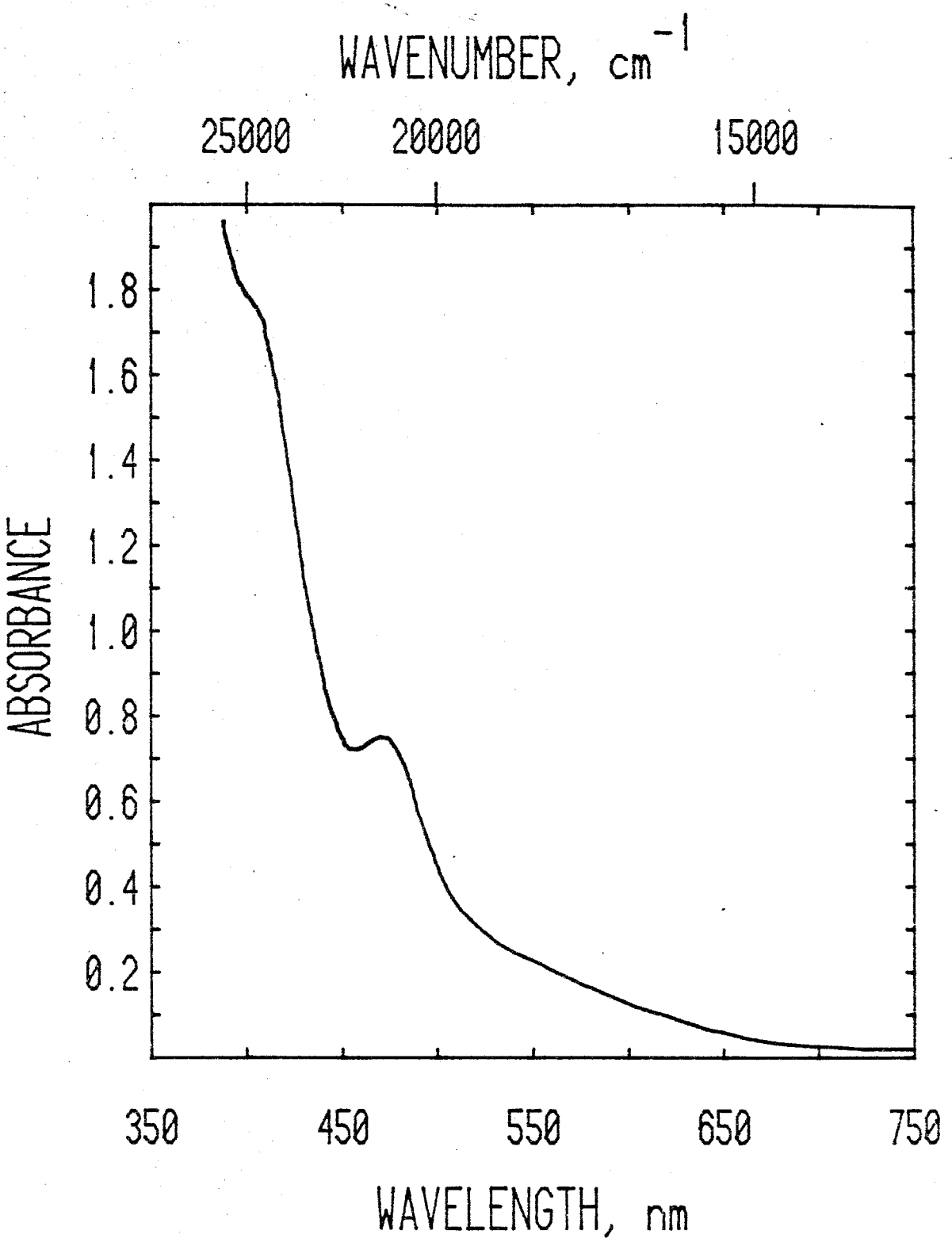

Fig. 7. Unpolarized room temperature absorption spectrum of coalingite (sample 12). The feature at 490 nm has a molar absorptivity of ~75 $M^{-1}cm^{-1}$ which is much higher than those of isolated Fe^{3+} ions and can thus be associated with ion-pair transitions. Sample thickness: 7.8 μm

in tourmaline and coalingite. This is also supported by a lowering by ~30 nm of the $^6\underline{A}_1 \rightarrow (^4\underline{A}_1, ^4\underline{E})$ transition for edge-shared units in the sulfate amarantite and the phosphates leucophosphite (Rossman 1976b) and pharmacosiderite (446 nm, Rossman unpublished results) as compared to isolated Fe^{3+} (Lehmann 1970). A contribution from tetrahedral Fe^{3+}, which also has bands in this region, can be discounted because of the lack of a Si-deficiency and the mismatch of the Mössbauer features with tetrahedral Fe^{3+} (Waychunas and Rossman 1983).

Fe^{3+}-Fe^{3+} pairs in the helix

Ion-pair transitions among Fe^{3+} groups within the helix are represented by the bands at 540 and 425 nm. These transitions are illustrated in Fig. 8 for the polarization $\mathbf{E} \parallel \underline{c}$ at 296 K and 83 K. The assignment of these features to Fe^{3+} is based upon their response to partial oxidation and reduction which was similar to the 485 nm ($\mathbf{E} \perp \underline{c}$) band. This behavior eliminates Fe^{2+}/Fe^{3+} charge transfer from the assignment possibilities. A significant contribution from Mn^{3+} at 540 nm can be dismissed because of the temperature response of these bands. Since the iron content of the helix and the degree of ordering is not known, the molar absorptivities of these bands cannot be evaluated. However, an upper limit of ~10% Fe^{3+} in the Z-site can be estimated from the 5 K Mössbauer spectrum assuming a halfwidth of 0.5 mm/sec. This leads to an estimate of the minimum value for the molar absorptivity of ~50 $M^{-1}cm^{-1}$ for the 540 nm band. This value is 2 orders of magnitude greater than that for Fe^{3+} bands of isolated ions and indicates the intensification associated with exchange coupled pairs. The intensity of these bands vary independently of the 485 nm band in $\mathbf{E} \perp \underline{c}$ associated with the trimer groups. These bands can be attributed to

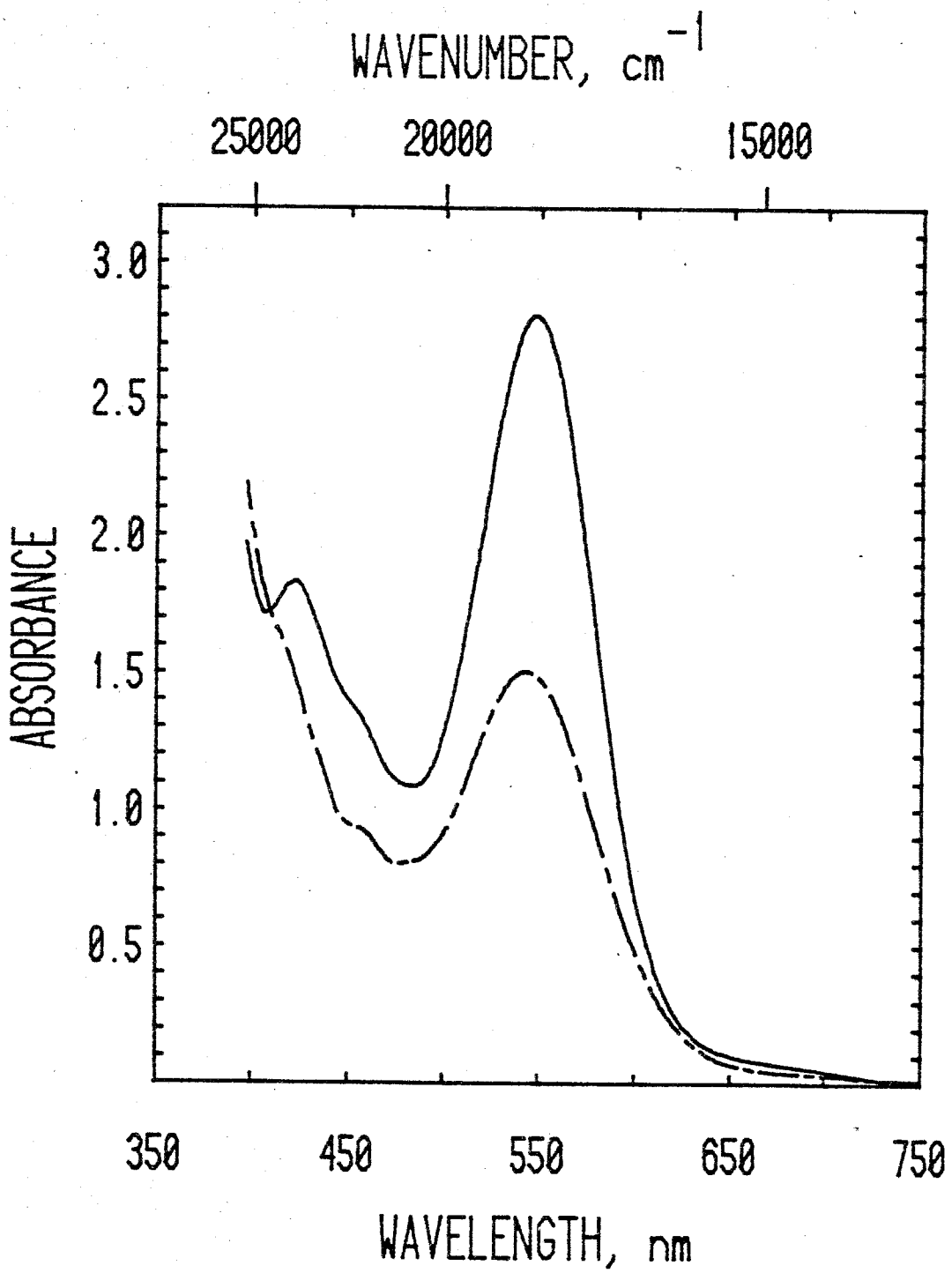

Fig. 8. E∥c polarized absorption spectrum of sample 1.

Broken line: 296 K Solid line: 83 K

Sample thickness: 1.11 mm

Fe^{3+} groups in the helix on the basis of intensity ratios among E∥c and E⊥c because the intensity is increased along the vector between the interacting cations. Vectors between adjacent cations in the helix lie 35° off the c-axis and thus have components in both polarizations. Specifically, the intensity ratio E⊥c/E∥c should be 0.49. This cannot be rigorously tested because of the interfering trimer feature in the same general wavelength. Using sample 6 to remove the trimer contribution in E⊥c, E⊥c/E∥c ratios of 0.4-0.6 were obtained for samples 1-4; in approximate agreement with the observed ratio within the uncertainty of this calculation. Sample 5 has an unusually low ratio of 0.1, but this could be related to low levels of other chromophores. The contribution in E⊥c is most easily seen by the increase in intensity at 540 nm at 83 K as shown in Fig. 6.

The temperature response of the 540 and 425 nm bands is not as simply explained as the trimer bands. The 540 nm band increases in integrated intensity by 60% from 296 K to 83 K. This behavior is typical of 'cold' bands and would indicate an assignment of 2 x ($^6A_1 \rightarrow {}^4T_1$). The 425 nm band maintains an intensity 0.2 times that of the 540 nm band. However, its energy does not correspond to a sum or combination of reasonable band positions. In addition, a weak band at ~800 nm is evident in the fully oxidized sample 1. This appears to be the $^6A_1 \rightarrow {}^4T_1$ transition and would contradict the assignment above. An alternate interpretation based on exciton-magnon bands is possible. The 425 and 540 nm bands have energies typical of Fe^{3+} transitions of the great majority of high-spin Fe^{3+} compounds. The typical effects of exchange coupling are large increases in intensity of the sharp band(s) between 410 and 450 nm and lesser increases for the broad band in the

region 750-1000 nm in exciton-magnon transitions. In this case, the band near 500 nm, which is generally little if at all affected, has the greatest intensity. The strength of magnetic exchange is affected by the geometry of the connection (Murray 1974). The unusual temperature response, therefore, may result from anisotropic contraction in the helix with decreasing temperature. This proposal must be tested by low temperature structure refinements.

Iron-rich tourmalines which are Al-deficient exhibit a Fe^{3+} feature at 410 nm (Fig. 9), as well as the transitions associated with pairs in the helix and trimer. Fe^{2+}-Fe^{3+} interactions (Smith 1978; Chapter 3) produce the dominant bands at ~700 and ~1100 nm. Fe^{3+} groups within the trimer produce the characteristic absorption band at 485 nm in $\mathbf{E} \perp \underline{c}$ as seen previously. Fe^{3+} groups within the helix are evident from the small band at ~540 nm in $\mathbf{E} \parallel \underline{c}$. A possible assignment of the 410 nm feature to the $^6\underline{A}_1 \rightarrow (^4\underline{A}_1, ^4\underline{E})$ band of Mn^{2+} which occurs at 414 nm in Li,Al-tourmalines (Reinitz and Rossman, in prep.) can be ruled out by the extremely low Mn content of these samples. The band at 410 nm in $\mathbf{E} \perp \underline{c}$ has an intensity nearly equal to the 485 nm band and can be assigned to ion-pairs between the trimer and helix. This assignment is supported by the polarization of this band. In addition, it is restricted to tourmalines in which substantial amounts of Fe^{3+} are incorporated into the helix due to Al-deficiencies. 410 nm is a very unusual wavelength for the $^6\underline{A}_1 \rightarrow (^4\underline{A}_1, ^4\underline{E})$ band of Fe^{3+} in silicates. The spectroscopy of non-interacting Fe^{3+} ions in tourmaline would ordinarily indicate the energy of pair transitions. An attempt to observe dilute ferric iron spectroscopically by heating Mg-tourmalines with <0.5% FeO at 850°C for 69 hours were unsuccessful despite an obvious decrease in Fe^{2+}.

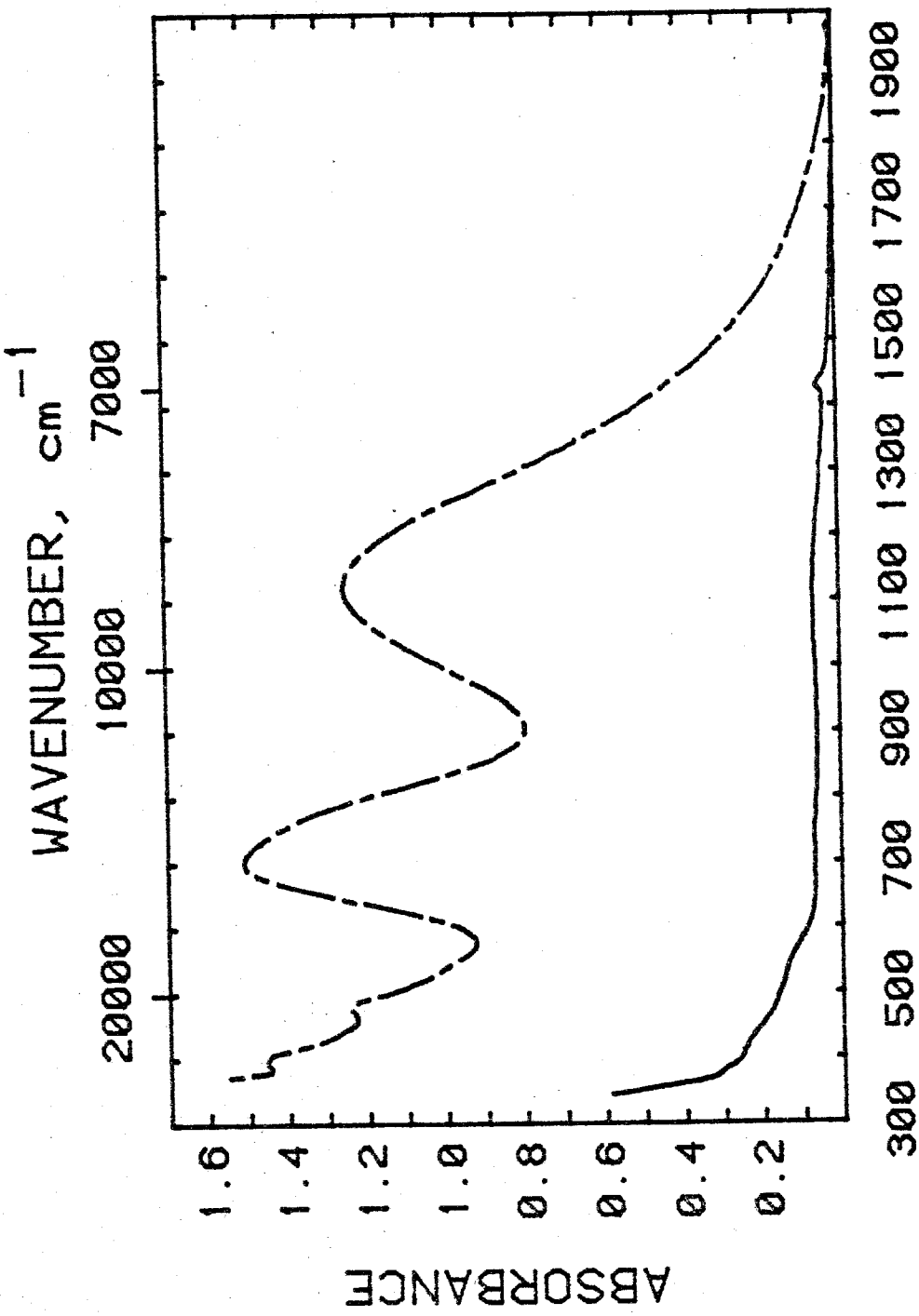

Fig. 9. Room temperature absorption spectra of sample 7. This is representative of samples 8-10. Sample thickness: 0.020 mm

Polarization directions E⊥c: broken line E∥c: solid line

However, the transitions associated with pairs in the helix and trimer can provide similar information given correct assignments. While it is generally believed that intensified pair transitions occur at the same wavelength as the corresponding transitions of isolated ions, these views are based on studies of pairs which are symmetric or nearly so. These Y-Z pairs are asymmetric and do not simply exhibit the transitions of the individual ions. An optical investigation of ferridravite, which is extremely Al deficient (Walenta and Dunn 1979), would help to fully establish this assignment

Structural Effects

Although the transitions related to Fe^{3+} discussed above are observed in tourmalines which span a large compositional range, their properties cannot be simply extended to the highest Fe^{3+} concentrations. Buergerite (Mason et al. 1964) has ~4 times the Fe^{3+} content of sample 1. Approximately 90% of this Fe^{3+} is located in the trimer (Hermon et al. 1973), but the optical spectrum is not dominated by a band at 485 nm. It consists of a shoulder at ~490 nm on a background of what appears to be Fe^{3+}–O CT (Fig. 10). The distance between cations within the trimer in buergerite is 317 pm (Barton 1969) as opposed to 304 pm in dravite (Buerger et al. 1962). This increased separation results in a decreased antiferromagnetic interaction among the Fe^{3+} ions and is evidenced by a coupling constant which is ~1/3 that found for sample 1 (Tsang et al. 1971). A correlation between molar absorptivity and coupling constant has been observed in a survey of antiferromagnetically coupled Fe^{3+} compounds (Rossman unpublished data). The weaker interaction is correspondingly seen as a lower absorptivity, ~7 $M^{-1}cm^{-1}$. A lower absorptivity at higher Fe^{3+}

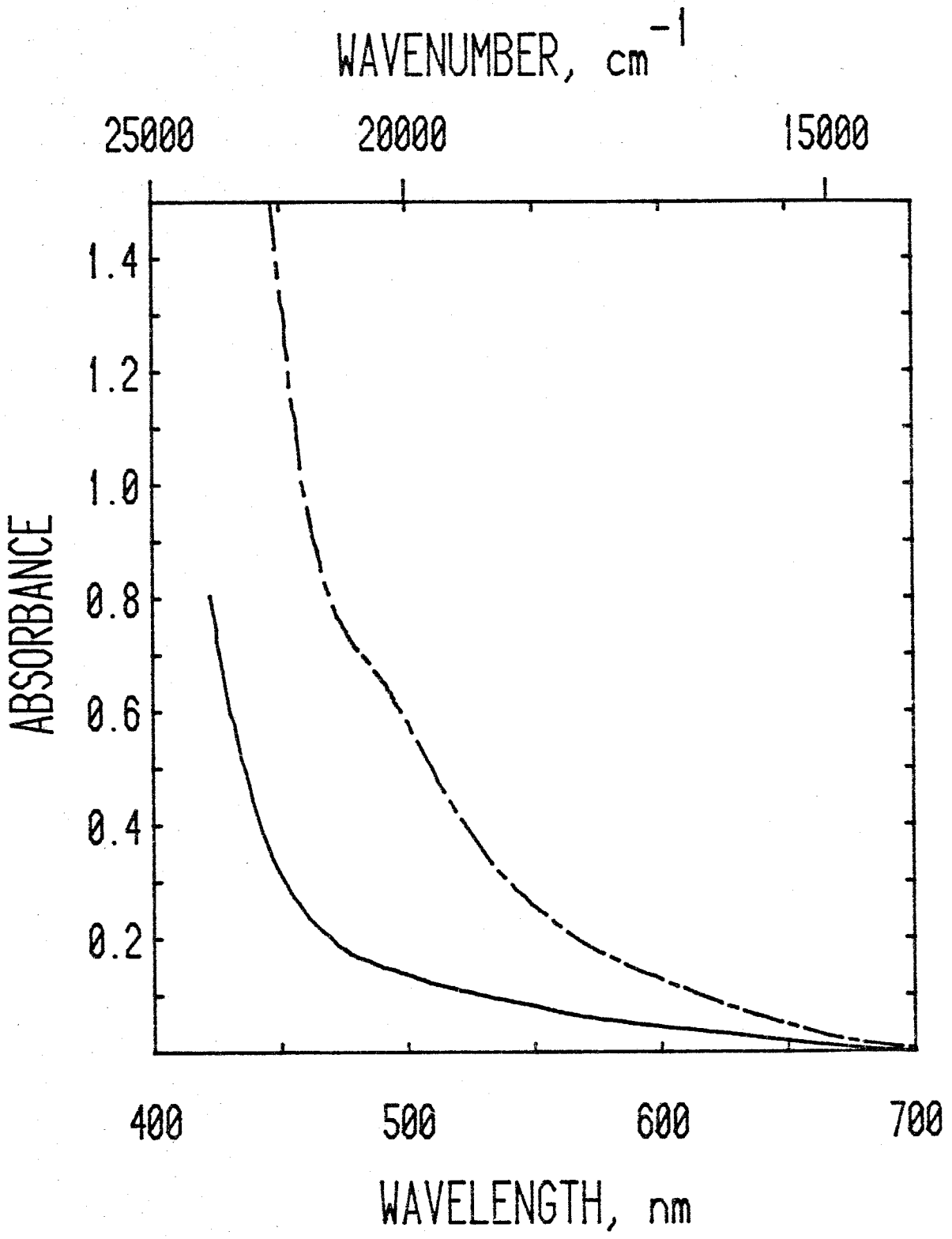

Fig. 10. Room temperature absorption spectra of buergerite (sample 11).

Polarization directions E⊥c: broken line E∥c: solid line

Sample thickness: ~16 µm

concentrations is also indicated by the iron-rich tourmaline, sample 6, which was completely oxidized. The Fe^{3+} content of this sample is ~80% of that in buergerite. The molar absorptivity of the 485 nm band based on calculated proportions of iron in 'dimers' and 'trimers' is 20 $M^{-1}cm^{-1}$ as compared to 90 $M^{-1}cm^{-1}$ for samples 1-5.

The Fe^{3+} transitions discussed above represent the optical features of Fe^{3+} in a wide range of tourmaline chemistries, but they are not apparent in oxidized tourmalines studied by Smith (1978). Smith observed bands at 524 and 463 nm in oxidized Fe-bearing tourmalines and attributed them to Fe^{3+}-pair transitions. These tourmalines were in the compositional series between Li,Al- and Fe^{2+}-tourmalines, whereas all tourmalines of this study were Mg,Fe-tourmalines. Small differences in the optical spectroscopy might thus be expected due to minor structural differences accompanying compositional differences. The 524 nm band was observed to occur in both polarizations and increase in intensity at low temperatures. It may correspond to the 540 nm band assigned to Fe^{3+} pairs in the helix in Mg,Fe^{2+}-tourmalines. In Smith's Mn-rich tourmalines, however, Mn^{3+} which absorbs at 520 nm (Manning 1969) may also contribute to this band. The 463 nm band does not correlate with the 524 nm band and is not consistently present in the oxidized samples. Since iron is known to prefer the trimer, the 524 nm band should not dominate the Fe^{3+} features in these samples. These assignments therefore, cannot be confirmed by this study and await the synthesis of Fe^{3+}-bearing Li,Al-tourmalines.

Summary

Interactions among various cations are very pronounced in tourmaline. In the ferric-rich tourmalines of this study these interactions are evident in magnetic and spectroscopic properties. Antiferromagnetic exchange among Fe^{3+} ions is indicated by decreasing magnetic moment at lower temperatures and by intense optical transitions. Three types of Fe^{3+}-pairs involving different site combinations can be distinguished by their optical characteristics. These characteristics have been established in ferric-rich tourmalines which contain low levels of other chromophoric ions. These observations have permitted the distinction of Fe^{3+} transitions in more complex members of the tourmaline group. In the absence of a large Fe^{2+} content, Fe^{3+} bands at 485 nm ($E \perp c$) and 540 nm ($E \parallel c$) dominate the visible region and give rise to a red or yellow color. The high intensities of these Fe^{3+} transitions are one indication that they result from ion-pair interactions. The transitions of isolated Fe^{3+} which were tentatively identified in sample 1 are not generally present in Fe^{3+}-bearing tourmalines. This is somewhat puzzling and suggests that the interactions with Fe^{2+} which are so prevalent in tourmaline may cause Fe^{3+} to lose its single ion identity. The transitions of Fe^{3+}-Fe^{3+} pairs in the trimer of the tourmaline structure (485 nm $E \perp c$) occur at unusually low energies. These low energies were proposed to result from interaction in the highly constrained, edge-shared sites of the trimer. Optical evidence of Fe^{3+} is particularly useful in minerals which are zoned or otherwise unamenable to bulk techniques such as Mössbauer spectroscopy. Because Fe^{3+} Mössbauer features are often obscured by Fe^{2+} in tourmaline, the Mössbauer spectra of the Kenyan

tourmaline provides the first clear standard for tourmalines of typical compositions. The temperature dependence of the Mössbauer spectrum of this dravite has not been observed in other tourmalines, or in other minerals, and may be related to Fe^{2+}-Fe^{3+} interactions.

REFERENCES

Amthauer, G, Annersten, H, and Hafner, SS (1976) The Mössbauer spectrum of ^{57}Fe in silicate garnets. Z Kristallogr 143:14-55

Amthauer, G and Rossman, GR (1984) Mixed valence of iron in minerals with cation clusters. Phys Chem Minerals, in press

Bank, H (1974) Rote Turmaline mit hoher Licht- und Doppelbrechung aus Kenya. Z Dtsch Gemmol Ges 23:89-92

Barton, R Jr. (1969) Refinement of the crystal structure of buergerite and the absolute orientation of tourmalines. Acta Crystallogr B25:1524-1533

Bence, AE and Albee, AL (1968) Empirical correction factors for electron microanalysis of silicates and oxides. J Geol 76:382-403

Buerger, MJ, Burnham, CW, and Peacor, DR (1962) Assessment of the several structures proposed for tourmaline. Acta Crystallogr 15:583-590

Burns, RG and Strens, RGJ (1967) Structural interpretation of polarized absorption spectra of the Al-Fe-Mn-Cr epidotes. Mineral Mag 36:204-226

Dollase, WA and Gustafson, WI (1982) ^{57}Fe Mössbauer spectral analysis of the sodic clinopyroxenes. Am Mineral 67:311-327

Donnay, G., Ingamells, CO and Moser, B (1966) Buergerite, a new species of tourmaline. Am Mineral 51:198-199

Dunn, PJ, Arem, JE and Saul, J (1975) Red dravite from Kenya. J Gemmol 14:386-387

Earnshaw, A, Figgis, BN, and Lewis, J (1966) Chemistry of polynuclear compounds. Part VI. Magnetic properties of trimeric chromium and iron carboxylates. J Chem Soc A 1966:1656-1663

Faye, GH, Manning, PG, Gosselin, JR and Tremblay, RJ (1974) The optical absorption spectra of tourmaline: Importance of charge transfer processes. Can Mineral 12:370-380

Fortier, S and Donnay, G (1975) Schorl refinement showing the composition dependence of the tourmaline structure. Can Mineral 13:173-177.

Fujiwara, T, Gebhardt, W, Petanides, K, and Tanabe, Y (1972) Temperature dependent oscillator strengths of optical absorptions in MnF_2 and $RbMnF_3$. J Phys Soc Japan 33:39-48

Gorelikova, NV, Perfil'yev, Yu D, and Bubeshkin, A M (1976) Mössbauer data on distribution of Fe ions in tourmaline. Zap Vses Mineral O-va 4: 418-427 (transl. Int Geol Rev 20:982-990, 1978)

Greenwood, NN and Gibb, TC (1971) Mössbauer spectroscopy. Chapman and Hall Ltd, London.

Hermon, E, Simkin, DJ, Donnay, G, and Muir, WB (1973) The distribution of Fe^{2+} and Fe^{3+} in iron-bearing tourmalines: a Mössbauer study. Tschermaks Mineral Petrogr Mitt 19:124-132

König, E (1966) Magnetic properties of coordination and organometallic transition metal compounds. In KH Hellwege and AM Hellwege, Ed., Landolt-Börnstein Numerical Data and Functional Relationships in Science and Technology, New Series II, 2:2-114

Krebs, JJ and Maisch, WG (1971) Exchange effects in the optical-absorption spectrum of Fe^{3+} in Al_2O_3. Phys Rev B: Solid State 4:757-769

Kurkjian, CR and Buchanan, DNE (1964) Mössbauer absorption of ^{57}Fe in inorganic glasses. Phys Chem Glasses 5:63-70

Lehmann, G (1970) Ligand field and charge transfer spectra of Fe(III)-O complexes. Z Phys Chem (Wiesbaden) 72:279-297

Lohr, LL Jr. and McClure, DS (1968) Optical spectra of divalent manganese salts. II. The effect of interionic coupling on absorption strength. J Chem Phys 49:3516-3521

Long, GJ, Robinson, WT, Tappmeyer, WP, and Bridges, DL (1973) The magnetic, electronic, and Mössbauer spectral properties of several trinuclear iron(III) carboxylate complexes. J Chem Soc, Dalton Trans 1973:573-579

Mao, HK, Bell, PM and Virgo, D (1977) Crystal-field spectra of fassaite from the Angra dos Reis meteorite. Earth Planet Sci Lett 35:352-356

Manning, PG (1969) Optical absorption spectra of chromium-bearing tourmaline, black tourmaline, and buergerite. Can Mineral 10:57-70

Mason, B, Donnay, G and Hardie, LA (1964) Ferric tourmaline from Mexico. Science (Washington DC) 144:71-73

Murray, KS (1974) Binuclear oxo-bridged iron(III) complexes. Coord Chem Rev 12:1-35

O'Connor, CJ (1982) Magnetochemistry--Advances in theory and experimentation. Prog Inorg Chem 29:203-283

Pastor-Rodriguez, J and Taylor, HFW (1971) Crystal structure of coalingite. Mineral Mag 38:286-294

Rossman, GR (1975) Spectroscopic and magnetic studies of ferric iron hydroxy sulfates: intensification of color in ferric iron clusters bridged by a single hydroxide ion. Am Mineral 60:698-704

Rossman, GR (1976a) Spectroscopic and magnetic studies of ferric iron hydroxy sulfates: the series $Fe(OH)SO_4 \cdot nH_2O$ and the jarosites. Am Mineral 61:398-404

Rossman, GR (1976b) The optical spectroscopic comparison of ferric iron tetrameric clusters in amarantite and leucophosphite. Am Mineral 61:933-938

Saegusa, N, Price, DC, and Smith, G (1979) Analysis of the Mössbauer spectra of several iron-rich tourmalines (schorls). J Phys (Paris) 40:C2,456-C2,459

Schugar, HJ, Rossman, GR, and Gray, HB (1969) A dihydroxo-bridged ferric dimer. J Am Chem Soc 91:4564-4566

Smith, G (1978) A reassessment of the role of iron in the 5,000-30,000 cm^{-1} region of the electronic absorption spectra of tourmaline. Phys Chem Minerals 3:343-373

Tsang, T, Thorpe, AN, Donnay, G, and Senftle, FE (1971) Magnetic susceptibility and triangular exchange coupling in the tourmaline mineral group. J Phys Chem Solids 32:1441-1448

Walenta, K and Dunn, PJ (1979) Ferridravite, a new member of the tourmaline group from Bolivia. Am Mineral 64:945-948

Waychunas, GA and Rossman, GR (1983) Spectroscopic standard for tetrahedrally coordinated ferric iron: $\gamma LiAlO_2:Fe^{3+}$. Phys Chem Minerals 9:212-215

Wignall, JWG (1966) Mössbauer line broadening in trivalent iron compounds. J Chem Phys 44:2462-2467

Wilkins, RWT, Farrell, EF, and Naiman, CS (1969) The crystal field spectra and dichroism of tourmaline. J Phys Chem Solids 30:43-56

Wu, CS, Rossman, GR, Gray, HB, Hammond, GS, and Schugar, HJ (1972) Chelates of β-diketones. VI. Synthesis and characterization of dimeric dialkoxo-bridged iron(III) complexes with acetylacetone and 2,2,6,6-tetramethylheptane-3,5-dione (HDPM). Inorg Chem 11:990-994

Chapter 3

Fe^{2+} - Fe^{3+} Interactions in Tourmaline

Introduction

A review of tourmaline chemistries (e.g. Deer et al. 1962) illustrates the lack of correlation between intensity of color and iron content in green, blue and black tourmalines. This behavior is similar to many compounds in which transition metals of multiple and variable oxidation states occupy adjacent sites. The intense colors of mixed-valence systems have been ascribed to optically induced charge transfer between adjacent cations. However, the optical spectroscopy of iron-bearing tourmalines is not typical of mixed valence systems. A study of green and blue tourmalines (Smith 1978a) revealed a previously unknown effect of the interaction among mixed valence cations -- an intensification of the characteristic absorption of individual cations. The intensification of Fe^{2+} transitions by neighboring Fe^{3+}, first demonstrated in tourmaline and biotite (Smith 1978b), has since been suggested for MgO:Fe (Smith 1980) and the protein hemerythrin (Loehr et al. 1980). Quantitative absorption intensities are of interest because they can be used to determine the concentration and site occupancy of Fe^{2+} in minerals such as olivine (Burns 1970) and pyroxene (Goldman and Rossman 1979). These determinations depend on a linear correlation between absorption intensity and concentration and would be corrupted by a strong interaction among adjacent cations. Although previous studies have demonstrated the existence of intensified Fe^{2+} absorption in Fe^{2+}-Fe^{3+} compounds, the

quantitative magnitude of the intensification of Fe^{2+} by Fe^{3+} neighbors has not been determined. This paper presents a systematic study of Fe^{2+}-Fe^{3+} interactions in a broad range of tourmaline chemistries directed toward a quantitative characterization of intensified Fe^{2+} transitions.

The wide range of chemistries and colors of the tourmaline group have prompted many optical investigations. These studies have generally encompassed a small range of chemistries from gem-bearing pegmatites and produced many conflicting assignments. Smith (1978a) reviewed these assignments for iron-bearing tourmalines. Mössbauer data on a few of these Li,Al-tourmalines have shown very low or undetectable Fe^{3+} (Burns 1972; Simon 1973; Faye et al. 1974). Most Mössbauer studies have been focused on black Fe,Mg-tourmalines and have detected much larger and quite variable Fe^{3+} contents (Hermon et al. 1973; Gorelikova et al. 1976; Saegusa et al. 1979). Because of the greater abundance of Fe^{3+} in black tourmalines, they will be emphasized in this study of Fe^{2+}-Fe^{3+} interactions. Optical spectra of a few black tourmalines have been qualitatively examined by Manning (1969, 1973), Faye et al. (1974) and Wilkins et al. (1969) but without regard to intensified Fe^{2+} transitions.

Tourmalines can generally be grouped into 2 solid solution series. The detailed spectroscopic behaviors of these groups are distinct and will be discussed in addition to the larger variations indicated above. These series will

be differentiated using the sample nomenclature described below. The major chemical variations in tourmaline occur in the X-, Y- and Z-sites as defined by the general formula $XY_3Z_6Si_6O_{18}(BO_3)_3(OH,O,F)_4$. The Z-site is predominantly Al in common compositions. In addition to extensive substitutions in the Y-site, transition elements generally occur at lower concentrations in the Z-site. Previous optical studies have emphasized the elbaite-schorl series in which X = Na and Y = Li, Al for the elbaite end member and X = Na and Y = Fe^{2+} for the schorl end member. This group is dominated by chemistries closer to elbaite than schorl. Greater chemical variation is found in the dravite-uvite-schorl series. The dravite end member chemistry is X = Na and Y = Mg. The uvite end member differs in X = Ca and Z = Al, Mg. The spectroscopic properties of the transition elements are not affected by changes in composition in the uvite-dravite series. The major substitutions of interest include the Mg, Fe^{2+} variations between these end members and schorl and the incorporation of Fe^{3+}. Substantial amounts of Fe^{3+} can occur in both the Y- and Z-sites but do not commonly approach the level of Fe^{3+} in the end members discussed in chapter 2. The dravite-uvite-schorl series will be emphasized in this paper and will be designated Fe,Mg-tourmalines.

Experimental

Sample localities are presented in Table 1. Chemical analyses were obtained using a MAC5-SA5 electron microprobe and are presented in Tables 2 and 3. Data reduction was accomplished using the methods of Bence and Albee (1968). Semiquantitative (±20%) analyses of samples M1 and Z31 were obtained using a Kevex 0700 EDS XRF system. The fluorescence of polished crystal slabs was calibrated against visually homogeneous tourmalines which were analyzed by microprobe. Differentiation of the elbaite-schorl series from Fe,Mg-tourmalines was based on Mg content and characteristic OH vibrations (Appendix).

Optical spectra were obtained in a manner similar to that described in Rossman (1975). The spectra of thin samples (0.005-0.030 mm) were generally measured while attached to a glass slide with epoxy. The thickness of these samples was determined using a microscope micrometer on polished, perpendicular sections. Many of the samples were extremely inhomogeneous in color. Zones of uniform color were selected, and the same area was analyzed by electron microprobe. Low temperature spectra were obtained by placing the sample on a coldfinger immersed in liquid nitrogen in a quartz dewar. Temperatures were monitored using a copper-constantan thermocouple placed sightly above the sample. Temperature variation during a spectrum was limited to 80 to 86 K. Room temperature spectra were measured in the same apparatus without moving the sample to

Table 1 Sample Descriptions

Sample	Color	Locality	Archival Code
S2	blue*	White Queen Mine, Pala, CA	GRR# 3/13/78
S3	b=brown* g=green*	Newry, ME	CIT# 1372
S4	b=blue* c&g=green*	Cecil Co., MD	CIT# 3575
S5	b=blue* g=green*	Anza Borrego, CA	GRR# 3/16/83
S6	brown*	Portland, CT	CIT# 1087
S7	green*	Santa Cruz, Sonora Mexico	NMNH# R15504
S8	green*	Pierrepont, NY	NMNH# 81511
S9	brown*	Madagascar	Harvard# 108796
S10	a=blue* b=blue* c=green*	Minas Gerais, Brazil	
S11	blue*	Cahuilla Mt., Riverside Co., CA	CIT# 13763
S12	brown*	Syndenham, Ontario	CIT# 2884
D1	brown	Yinnietharra, Australia	CIT# 12683
D2	brown	Bryant Lake, NY	CIT# 12684
D7	red	Minas Gerais, Brazil	NMNH# 137101
T22	blue*	Blue Lady Mine, San Diego Co., CA	GRR# 8/10/83
EB1	blue	Afghanistan	GRR# 1/27/80
EB2	light blue	Afghanistan	GRR# 1/27/80
EB3	blue	Afghanistan	GRR# 1/27/80

Table 1 cont.

Sample	Color	Locality	Archival Code
EG3	green	Afghanistan	GRR# 1/27/80
EG4	dark green	Afghanistan	GRR# 1/27/80
EG1#4	blue*	Stewart Lithia Mine Pala, CA	GRR# 5/27/77
EG5	light green	Himalaya Mine, Mesa Grande, CA	GRR# 6/7/84
T15	green	Zambia	GRR# 2/11/83 #16
Z31	blue-green	Zambia	GRR# 2/11/83 #31
M1	blue	Mozambique	GRR# 9/6/82B

* E⊥c color in thin section

Table 2 Electron Microprobe Analyses of Fe,Mg-tourmalines

Sample	Na_2O	CaO	K_2O	MgO	FeO	MnO	TiO_2	Al_2O_3	SiO_2	F
S2	2.03	0.03	0.04	0.09	13.5	0.95	0.08	35.2	34.7	0.6
S3b	1.69	0.43	0.02	4.87	8.45	0.07	0.35	34.7	35.3	BDL
S3g	1.88	0.85	0.04	6.25	6.88	0.03	1.01	34.2	34.7	BDL
S4b	2.26	0.72	0.02	8.01	7.79	0.06	0.28	30.9	35.6	0.6
S4g	2.39	0.61	0.01	7.78	6.93	0.05	0.53	31.9	35.6	0.3
S4c	2.43	0.61	0.02	7.91	8.38	0.04	0.36	30.3	36.1	0.2
S5b	1.68	0.34	0.04	3.11	9.16	0.28	0.34	36.6	34.8	0.2
S5g	1.78	0.41	0.04	5.04	6.82	0.15	0.31	36.1	35.4	0.4
S6	2.31	0.43	0.06	3.56	11.6	0.14	1.03	32.5	34.7	1.2
S7	1.86	1.98	0.05	6.48	18.1	0.05	1.18	22.2	34.0	0.5
S8	1.44	2.92	0.05	10.8	8.23	BDL	0.55	26.3	35.2	1.6
S9	1.67	2.42	0.08	8.58	13.4	0.01	1.69	23.6	34.4	1.1
S10a	1.67	0.06	0.05	2.80	11.0	0.15	0.15	34.8	35.4	0.2
S10b	1.72	0.07	0.01	2.94	10.8	0.14	0.23	34.9	35.4	0.2
S10c	1.94	0.11	0.05	2.99	10.8	0.16	0.40	34.5	35.2	0.2
S11	1.34	0.06	0.04	0.48	13.3	0.28	0.05	35.4	35.4	BDL
S12	1.58	2.61	0.04	10.9	7.84	BDL	0.72	26.5	35.3	1.6
D1	2.93	0.37	0.02	11.6	0.46	BDL	1.09	32.0	37.2	0.1
D2	0.77	4.25	0.10	14.3	0.38	BDL	0.58	28.7	36.5	0.3
D7	1.77	1.64	0.11	10.1	4.46	0.22	0.22	31.0	36.1	0.1

BDL -- below detection limit

Table 3 Electron Microprobe Analyses of Elbaites

Sample	Na_2O	CaO	MgO	FeO	MnO	TiO_2	Al_2O_3	ZnO	SiO_2	F
T15	2.45	0.47	0.21	2.10	1.06	0.05	39.4	NA	37.3	0.3
T22	2.01	0.06	BDL	12.2	0.89	0.04	35.0	0.59	35.2	1.4
EG3	2.50	0.26	BDL	2.49	1.51	0.02	39.8	0.09	37.5	1.4
EG4	2.74	0.18	BDL	4.32	1.67	0.04	37.8	0.41	37.4	1.6
EG5	1.70	1.20	BDL	0.42	0.51	0.02	42.4	0.06	38.0	1.2
EB1	2.90	0.17	BDL	5.34	1.10	BDL	37.7	0.14	36.4	1.4
EB2	2.45	0.43	BDL	0.91	3.17	BDL	39.5	0.04	37.1	1.5
EB3	2.39	0.25	BDL	1.62	1.71	BDL	40.0	0.06	36.9	0.3
EG1#4	2.66	0.16	0.08	4.61	2.74	BDL	38.4	NA	36.9	1.4

BDL -- below detection limit NA -- not analyzed

insure quantitative comparisons.

Samples EB3, M1 and Z31 were subject to radiation from a ^{137}Cs source which emits 0.462, 1.01, and 1.436 MeV gamma rays and was producing doses of ~1.3 Mrads/day.

Mössbauer spectra (fitted and raw data) were provided for samples S7, S8 and S9 by Roger Burns (MIT) and by Glen Waychunas (Stanford) for samples S2 and S6. Three doublet fits were used to estimate Fe^{2+} concentrations in the Y- and Z-sites and Fe^{3+} concentrations. Z-site occupancy of Fe^{3+} was estimated by charge balance requirements in the absence of H-defects. With the exception of D2, these results were used to calculate the fraction of Fe^{2+} with Fe^{3+} neighbors assuming a random distribution. The same calculation for D2 was accomplished using correlated ESR and optical data. ESR spectra were obtained on powdered samples of D2 before and after partial oxidation using a Varian E-line X-band spectrometer at ~9.2 GHz.

Results and Discussion

The basic characteristics of Fe^{2+} absorption in tourmaline are illustrated in Fig. 1. At very low iron contents and low Fe^{3+}/Fe^{2+} ratios the spectroscopy of non-interacting Fe^{2+} can be seen (Fig. 1a). The broad bands at 720 and 1250 nm can be assigned to components of the $^5\underline{T}_2 \rightarrow {}^5\underline{E}$ Fe^{2+} transition split by the non-cubic crystal field (Smith 1978a). Unlike the previously published spectra and most of my tourmaline spectra, the intensity of these

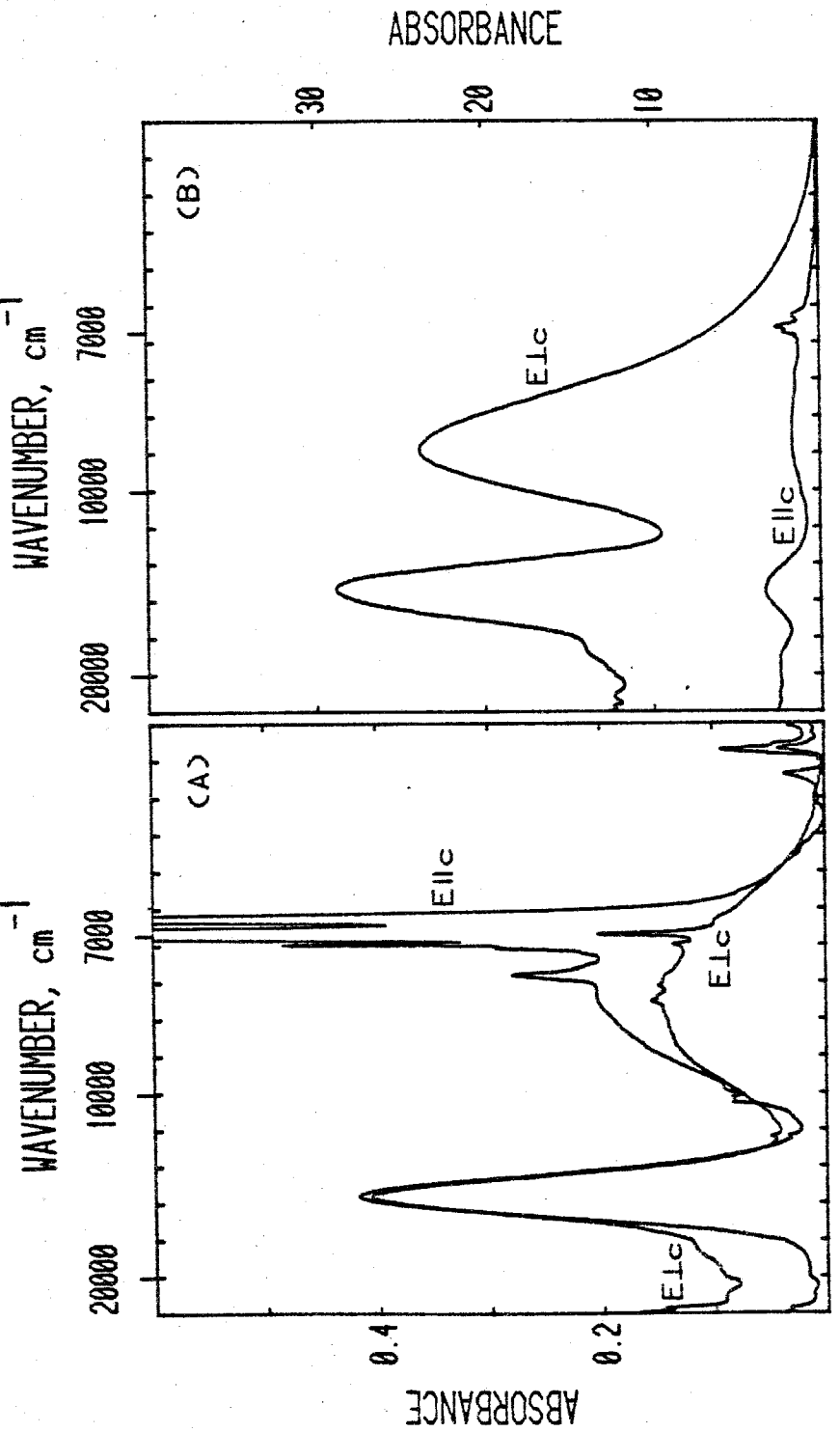

Fig. 1. Room temperature absorption spectra of elbaites normalized to a thickness of 2.461 mm.
A) Sample EB2, absorbance scale left B) Sample EG1#4, absorbance scale right

transitions in E⊥c does not exceed that in E∥c. The sharp bands between 1300 and 1500 nm are vibrational transitions which will not be discussed in this chapter. A comparison of this spectrum to that of a more typical tourmaline (Fig. 1b) shows the basic features of Fe^{2+}–Fe^{3+} interactions in tourmaline. Absorption intensity in E∥c has increased linearly with iron content. This behavior is typical of transition element absorption in most environments. The same transitions in E⊥c have increased ~10 times over the increase in Fe content. This added intensity in E⊥c can be attributed to Fe^{3+} as has been demonstrated by partial oxidation of natural samples (Smith 1978a; Wilkins et al. 1969). Fe^{2+}–Fe^{3+} charge transfer, the expected signature of Fe^{2+}–Fe^{3+} interactions, has been assigned to the comparatively weak feature at 550 nm (Smith 1978a; Faye et al. 1974; Townsend 1970). These spectra are representative of the gemmy, low Fe^{3+}/Fe^{2+} elbaites which have been preferentially studied but which do not exhibit the greatest Fe^{2+}–Fe^{3+} effects.

Figure 2 illustrates the spectrum of a Fe,Mg-tourmaline particularly rich in Fe^{3+} as evidenced by the Fe^{3+} band at 485 nm (Chapter 2). In most Fe^{2+}–Fe^{3+} compounds this large change in the relative amount of Fe^{3+} would be accompanied by a large change in the optical spectrum. In particular, a greater contribution from Fe^{2+}–Fe^{3+} charge transfer would be expected. However, excluding the Fe^{3+} feature at 485 nm and Fe^{2+}–Ti^{4+} charge transfer at 420 nm (Chapter 4),

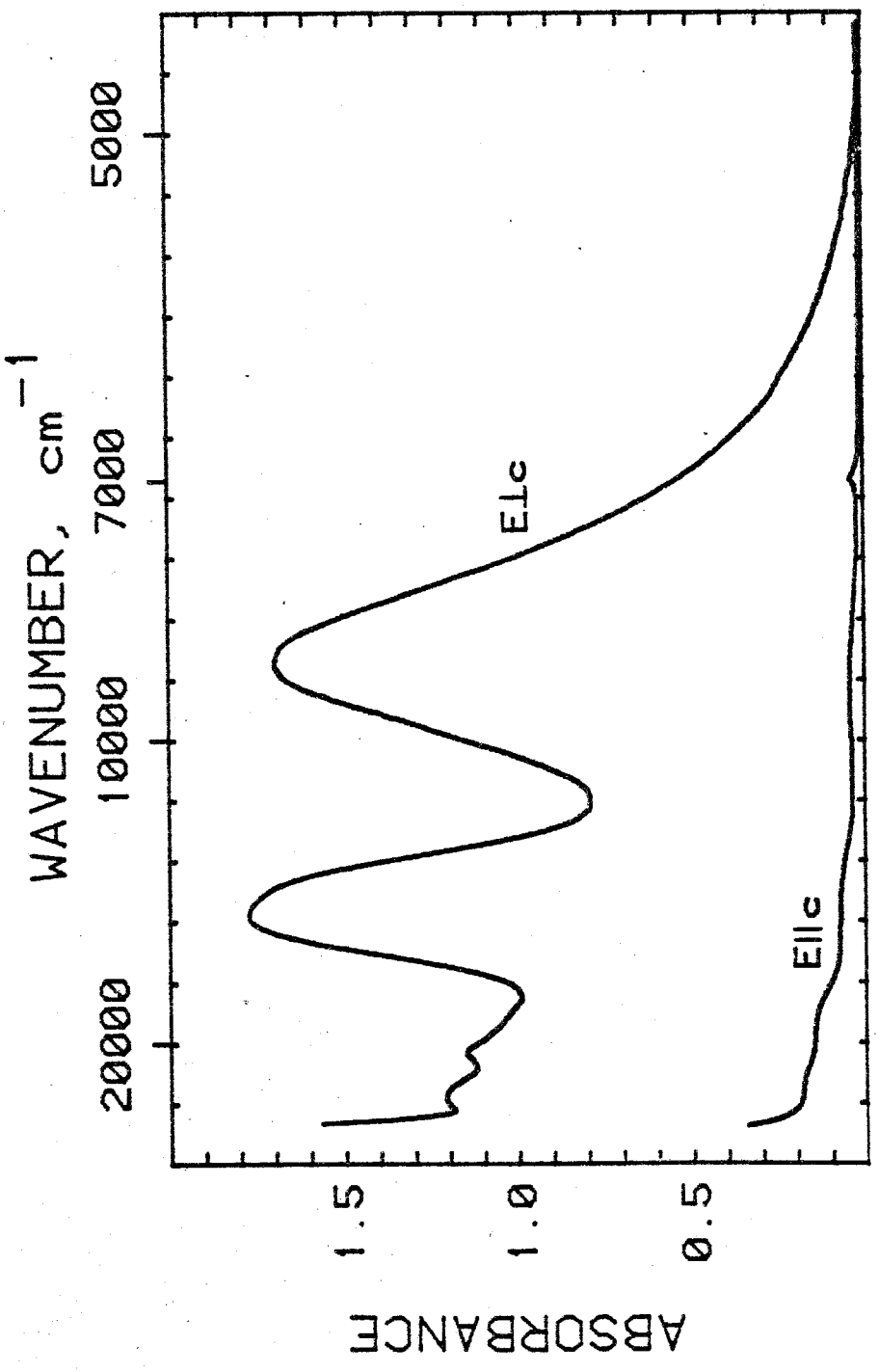

Fig. 2. Room temperature absorption spectra of sample S4c.

Sample thickness: 0.024 mm

this spectrum shows the same features as those of Fig. 1. The major difference lies in the much larger E⊥c/E∥c ratio of the Fe^{2+} bands. Although Fe^{2+}–Fe^{3+} charge transfer may contribute to absorption in E⊥c, it is not the dominant expression of Fe^{2+}–Fe^{3+} interactions in tourmaline as it is in most Fe^{2+}–Fe^{3+} compounds. Fe^{2+}–Fe^{3+} tourmalines thus provide a rare opportunity to fully characterize a second effect of Fe^{2+}–Fe^{3+} interactions--intensified Fe^{2+} transitions.

The qualitative relationship of enhanced intensity of Fe^{2+} transitions to Fe^{3+} can be simply demonstrated by partial oxidation of tourmaline as illustrated in Fig. 3. Oxidation of Fe^{2+} in tourmaline by heating in air has been established by Mössbauer studies (Gorelikova et al. 1976; Faye et al. 1974). This is accurately reflected in E∥c (Fig. 3b) by a decrease in intensity of the 1100 nm Fe^{2+} transition in an Fe,Mg-tourmaline. However, the intensity of this feature in E⊥c has increased, despite a decrease in Fe^{2+}. In addition a Fe^{3+} band at 485 nm has appeared. With the exception of the Fe^{3+} band at 485 nm, similar changes have been observed in elbaites (Smith 1978a; Wilkins et al. 1969). These results indicate a higher intensity for Fe^{2+} in Fe^{2+}–Fe^{3+} pairs as compared to non-interacting Fe^{2+}.

The restriction of anomalous intensity to E⊥c is further evidence that this effect can be attributed to ion-pair interactions. The polarization of ion-pair transitions along intercation vectors is a familiar aspect of charge

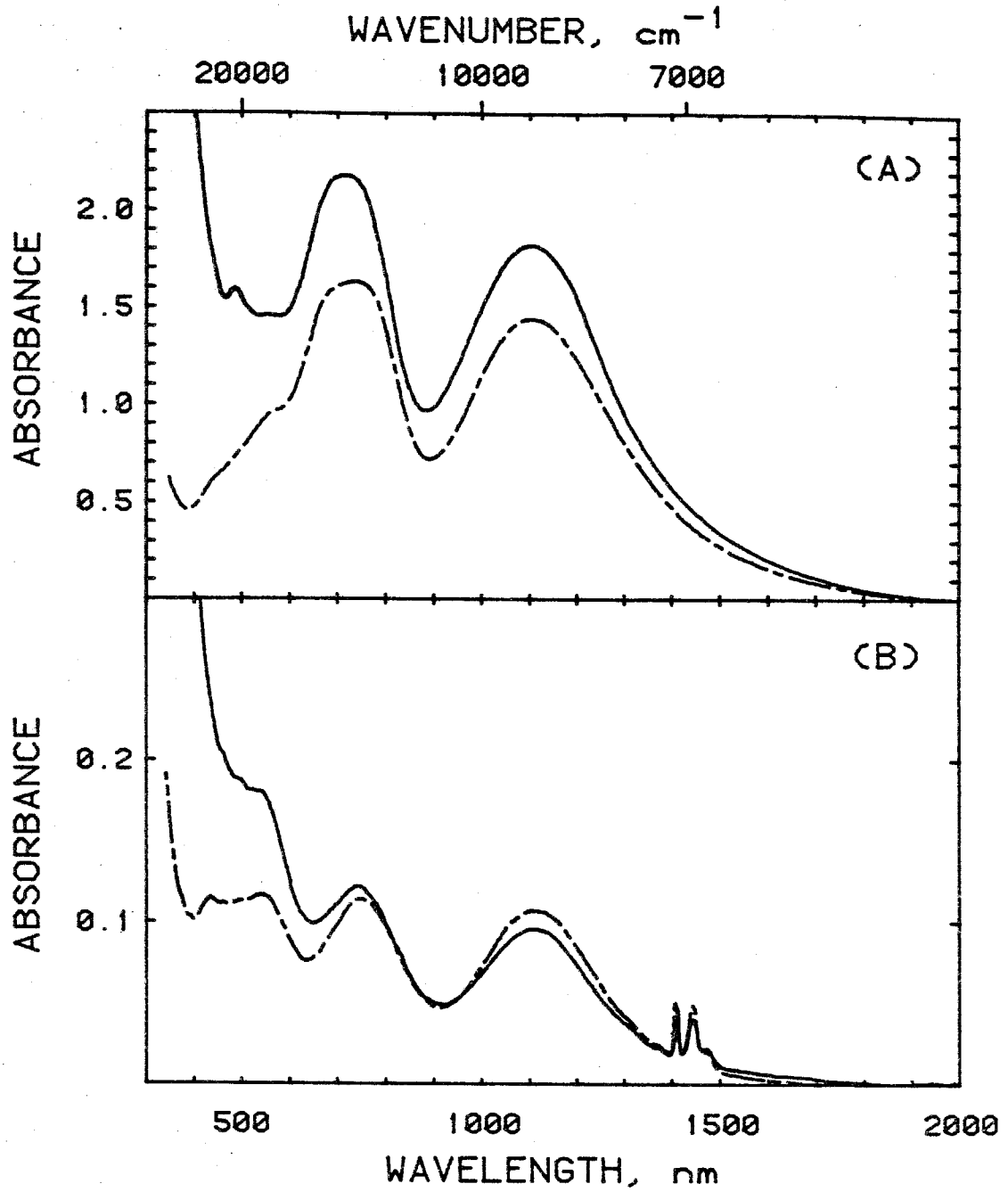

Fig. 3. Room temperature absorption spectra of untreated (broken line) and oxidized (solid line) sample S11. Sample thickness: 0.045 mm A) E⊥c polarization B) E∥c polarization

transfer transitions and the intensified spin-forbidden transitions of Chapter 2. The dominant distribution of Fe^{2+}-Fe^{3+} pairs in tourmaline are in site combinations with vectors perpendicular to the c-axis. As was indicated in the introduction, transition elements occur in the Y- and Z-sites in tourmaline but generally prefer the Y-site. Ion-pairs within the Y-site trimer and those between the trimer and the Z-site helix are oriented perpendicular to the c-axis (Buerger et al. 1962). Either of these ion-pairs are consistent with the observed polarization. Ion-pairs can also occur within the Z-site helix but are oriented at ~35° to the c-axis.

Intensity of Fe^{2+} absorption in Fe^{2+}-Fe^{3+} groups

Extreme variations in Fe^{2+} molar absorptivities from compound to compound have made it difficult to differentiate intensified from unperturbed Fe^{2+} transitions without systematic studies of a range of compositions. Goldman and Rossman (in prep.) have shown, however, that absorption intensity can be estimated from structural parameters. The variation of molar absorptivity with iron-oxygen distance (in the absence of Fe^{3+}) is shown in Fig. 4. The average distances for the Y- and Z-sites of elbaite (Donnay and Barton 1972), dravite (Buerger et al. 1962), and schorl (Fortier and Donnay 1975) are included in the crosshatched regions. This approximate correlation indicates that Fe^{2+} molar absorptivities for tourmalines should be ~4-15

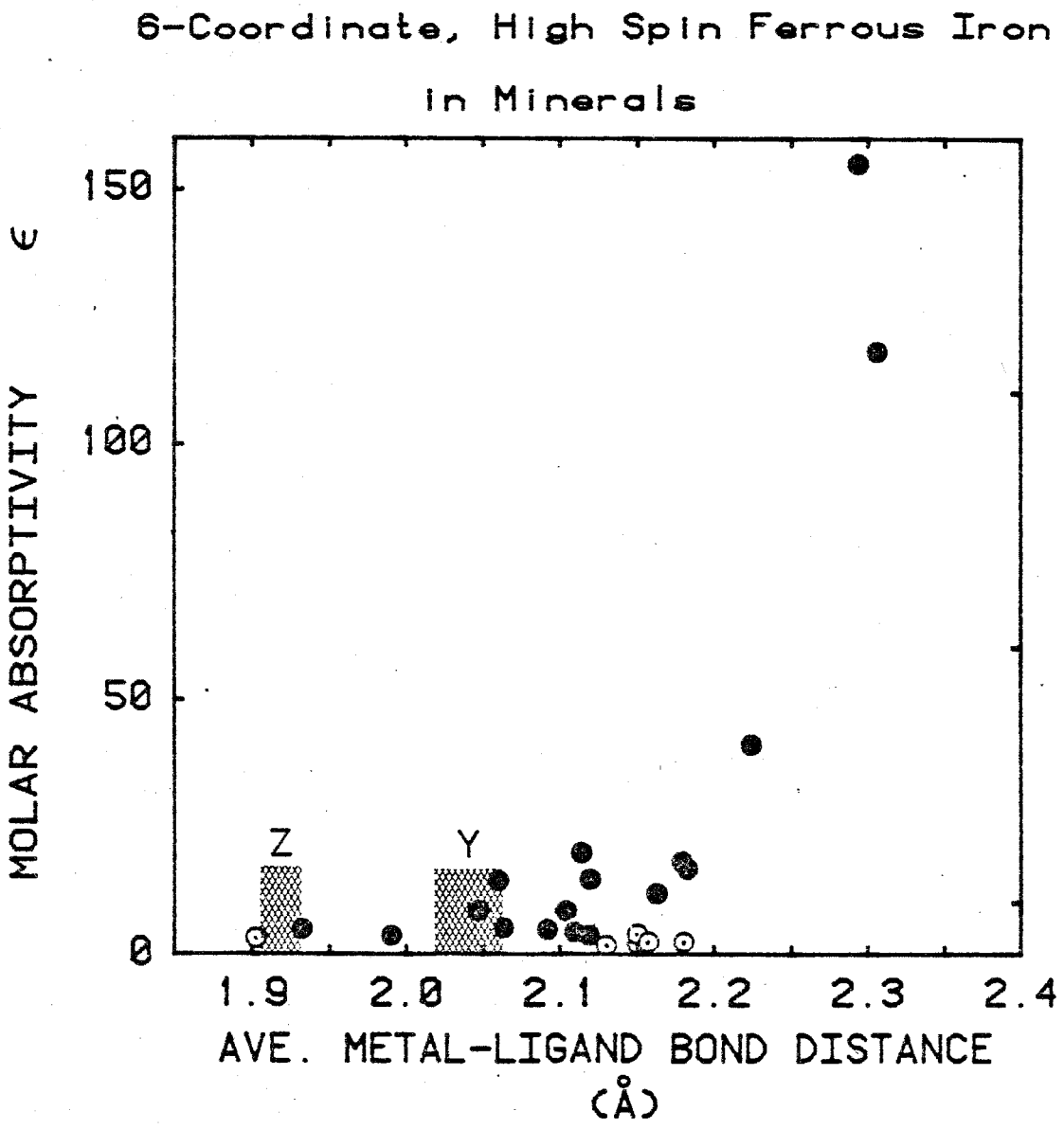

Fig. 4. Variation of Fe^{2+} molar absorptivity with average Fe-O distance (taken from Goldman and Rossman, in prep.). The average Y-O and Z-O distances of tourmaline end members are included within the labelled, hatchured regions.

$M^{-1}cm^{-1}$. These values can be contrasted with minimum molar absorptivities for the 1100 nm band based on total Fe content (Fig. 5). Fe^{2+} absorptivities in E∥c (indicated by the solid symbols) vary from 3-5 $M^{-1}cm^{-1}$ with a few exceptions. Higher absorptivities are characteristic of samples with large Al deficiencies which permit a small number of Fe^{2+}-Fe^{3+} pairs in Z-Z combinations. Most of the apparent variation in E∥c absorptivity can be related to errors introduced by normalizing absorbance to Fe_{total} instead of Fe^{2+}. Molar absorptivities for samples S6 and S2 based on Mössbauer measurements of Fe^{2+} are 4.4 and 5.2 $M^{-1}cm^{-1}$. This discrepancy may reflect a small difference in the Y- and Z-site absorptivities. The molar absorptivity of the 720 nm band in elbaites (E∥c) is somewhat smaller (3.2 $M^{-1}cm^{-1}$, Smith 1978a Fig. 4a) in accord with smaller sites. In contrast to E∥c, absorptivities in E⊥c approach the predicted values only in elbaites and at low iron contents in Fe,Mg-tourmalines and vary by more than an order of magnitude. These variations indicate two or more Fe^{2+} species with very different absorptivities. Predicted absorptivities for the Y- and Z-sites (Fig. 4) are not large enough or different enough to produce the observed variations. As was indicated by partial oxidation in Fig. 3a and will be demonstrated below, Fe^{2+}-Fe^{3+} pairs are the intensely absorbing species.

The magnitude of the variations in the minimum E⊥c absorptivities indicate a potential of at least an order of

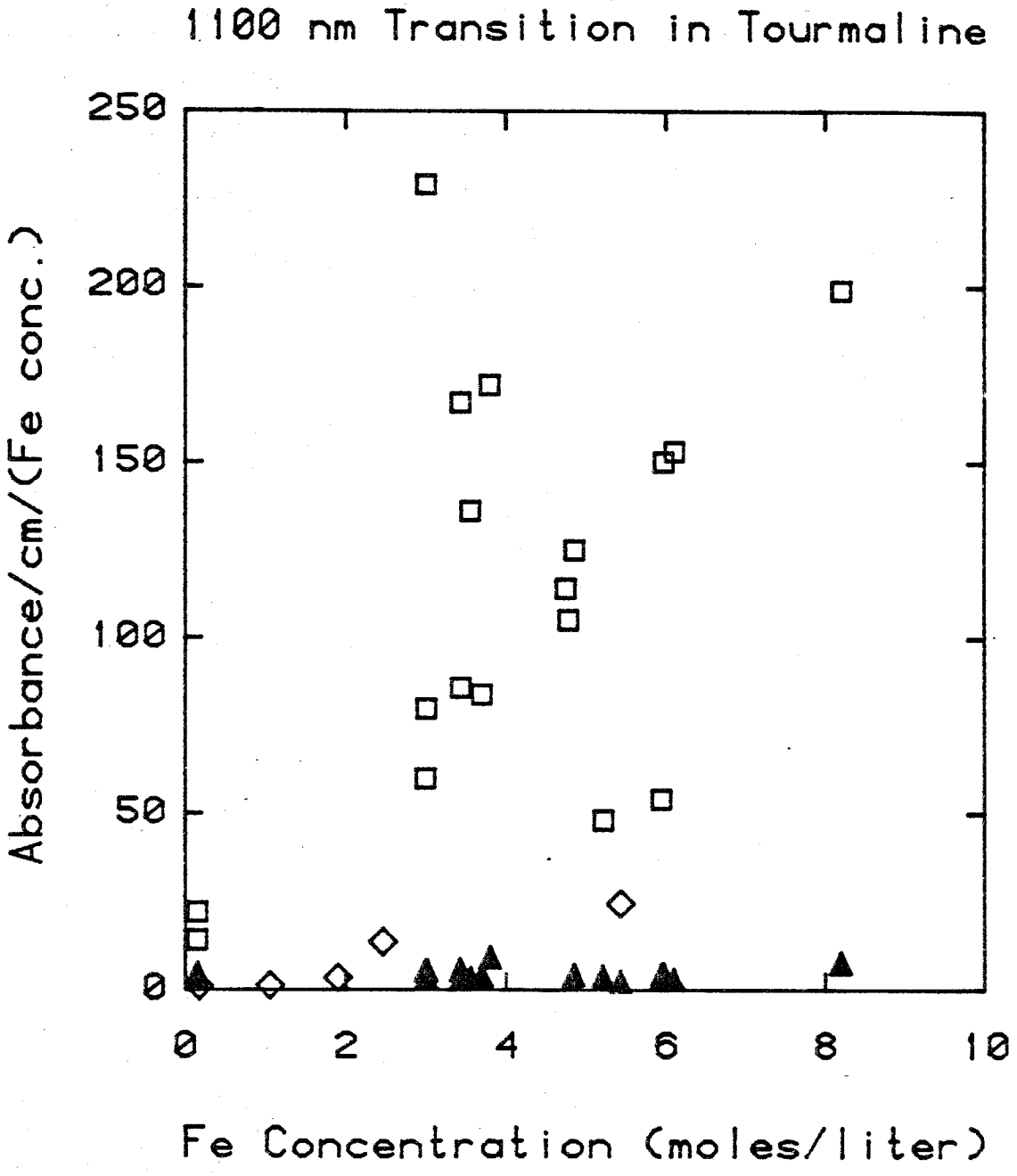

Fig. 5. Minimum molar absorptivities of the 1100 nm Fe^{2+} band of tourmalines. □: E⊥c Fe,Mg-tourmalines ◇: E⊥c elbaite-schorls ▲: E∥c Fe,Mg-tourmalines

magnitude increase in Fe^{2+} absorption intensity in the presence of Fe^{3+}. In order to refine the magnitude of the intensity increase and demonstrate its relationship to Fe^{3+} independent measures of Fe^{2+} and Fe^{3+} were acquired. The intensity of Fe^{2+} absorption in Fe^{2+}-Fe^{3+} pairs can be seen by relating molar absorptivity to the fraction of Fe^{2+} with Fe^{3+} neighbors (Fig. 6). The fraction of Fe^{2+} with Fe^{3+} neighbors was calculated with Fe^{2+} and Fe^{3+} site occupancies assuming a random distribution. Details of this calculation are given in the experimental section. A direct correlation of Fe^{3+} with increasing intensity is shown in Fig. 6. Several complicating factors make it difficult to judge the exact form of the relationship between absorptivity and the fraction of Fe^{2+}-Fe^{3+}. However, the average absorptivity of Fe^{2+} in Fe^{2+}-Fe^{3+} pairs can be estimated by a linear fit to these points extrapolated to 100% Fe^{2+} with Fe^{3+}. This value, ~1200 $M^{-1}cm^{-1}$ is 2 orders of magnitude greater than the absorptivity of non-interacting Fe^{2+} (~$E \| \underline{c}$ molar absorptivity) and ~10 times greater than the large absorptivities associated with extremely distorted sites (Fig. 4). Both components of the $^5\underline{T} \rightarrow {}^5\underline{E}$ transition exhibit similar intensifications as indicated by an approximately constant intensity ratio at ~700 and 1100 nm ($E \perp \underline{c}$ in Fe,Mg-tourmalines). The magnitude of this effect points to the extreme caution which must be excercised when interpreting optical intensities quantitatively. Together with another intense ion-pair transition (Fe^{2+}-Ti^{4+} charge transfer) this

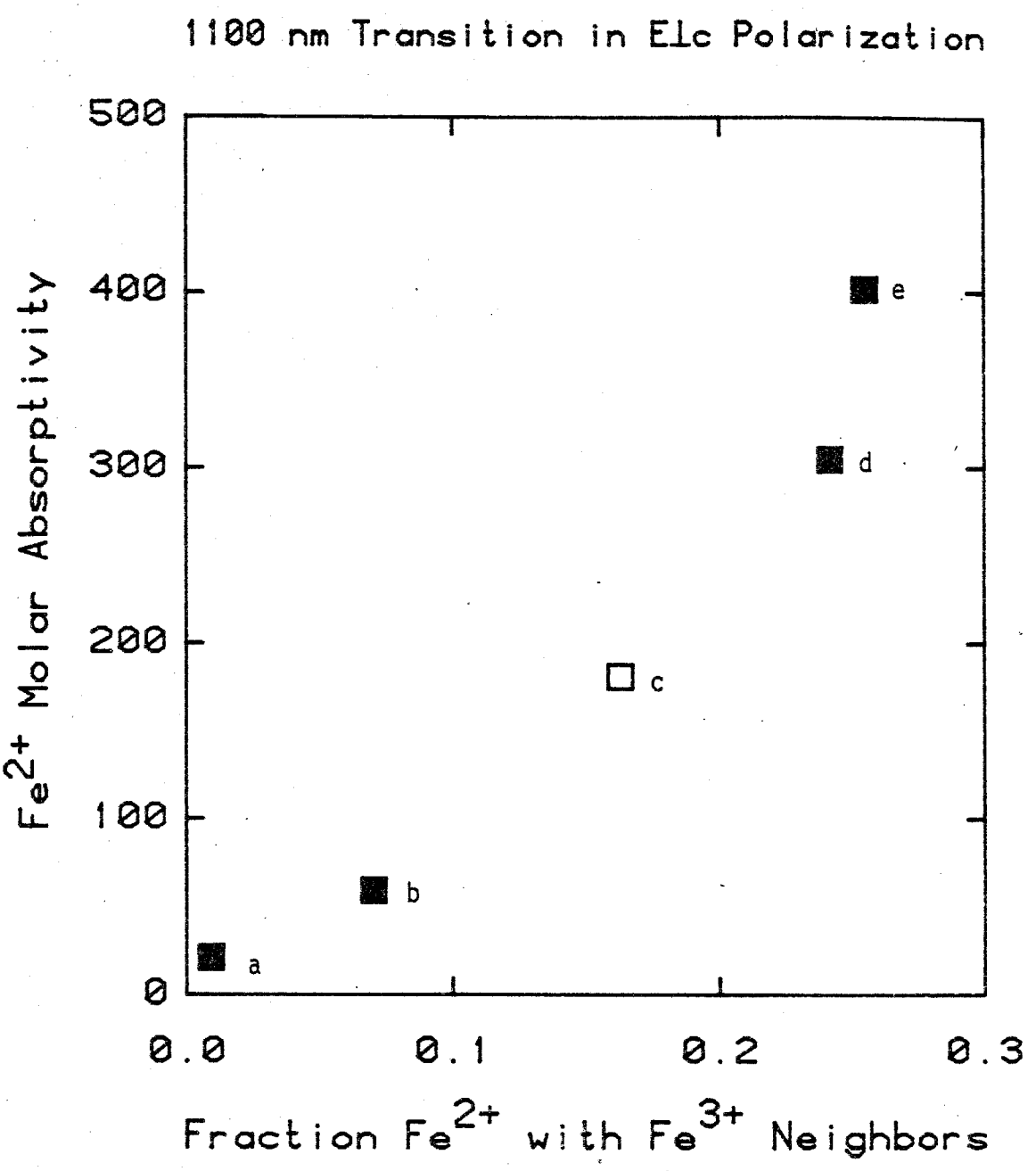

Fig. 6. Variation of Fe^{2+} molar absorptivity with the ratio of Fe^{2+}-Fe^{3+} groups to total Fe^{2+}. Data represented by open symbols differ from the other data because of uncertainty arising from poor Mössbauer data. Included samples: a = D2, b = S6, c = S2, d = S9, e = S7.

effect produces one of the most familiar properties of tourmaline, its visible pleochroism.

Errors in this assessment of the molar absorptivity of Fe^{2+}-Fe^{3+} pairs could be introduced by 3 non-experimental uncertainties which could not be reduced. Two of these are related to the effect of different Fe^{2+}-Fe^{3+} clusters, various numbers of Fe^{3+} neighbors as well as different site involvements. Deviations from a random distribution are also possible. Experimental uncertainties were reduced by selecting visually homogeneous samples to insure the correlation of Mössbauer and optical data. The slightly concave shape of the correlation of Fig. 6 is undoubtedly related to deviations from the calculational assumptions. Both an increase in absorptivity with greater numbers of Fe^{3+} neighbors and the preferential avoidance of Fe^{2+} and Fe^{3+} could produce a similar correlation. A preferential avoidance of Fe^{2+} and Fe^{3+} is indicated by several Fe^{3+}-rich tourmalines (D4, D7 and T21) which have the lowest observed $E \perp \underline{c}/E \parallel \underline{c}$ ratios of Fe,Mg-tourmalines. The effect of different Fe^{2+}-Fe^{3+} pairs cannot be assessed without a more extensive study using correlated Mössbauer and optical data.

Diagnostic Attributes of Intensified Fe^{2+} Transitions

The characteristics of intensified transitions which are shared by their parent unperturbed transitions, namely energy and width, have made this effect of ion-pair

interactions difficult to distinguish in individual cases. Intensified Fe^{2+} transitions, however, do possess characteristics which can be used diagnostically. The restriction of intensity increases to the vector between the interacting cations can be useful with known structures. In these cases it can also be used to determine the sites involved. A more generally useful characteristic is the response of these transitions to temperature variation. Unperturbed d-d transitions maintain a constant integrated intensity with varying temperature or decrease in intensity with decreasing temperature. This behavior can be seen in E$\parallel\underline{c}$ in tourmalines (Fig. 7; Smith 1978a) and for non-interacting Fe^{2+} in E$\perp\underline{c}$ (Fig. 8). Fe^{2+} bands in E$\perp\underline{c}$ of most tourmalines exhibit large intensity increases with decreasing temperature. Smith's study of elbaites found increases in integrated intensity of 20-50% from 293 K to 10 K at 1100 nm. Both Fe^{2+} bands in elbaites (725 and 1100 nm) in E$\perp\underline{c}$ show this behavior. Fe,Mg-tourmalines exhibit 2 bands at 765 and 670 nm which maintain similar intensities as well as a band at 1100 nm (Fig. 9). Increases in integrated intensity for Fe,Mg-tourmalines with temperature decreasing from 296 K to 77 K ranged from 0 to 50% at 1100 nm. No change in intensity was observed only in samples with a E$\perp\underline{c}$/E$\parallel\underline{c}$ intensity ratio less than 4. However, above 10% change in intensity there is no correlation of the amount of intensity increase to the degree of intensification as indicated by the E$\perp\underline{c}$/E$\parallel\underline{c}$ ratio. These variations

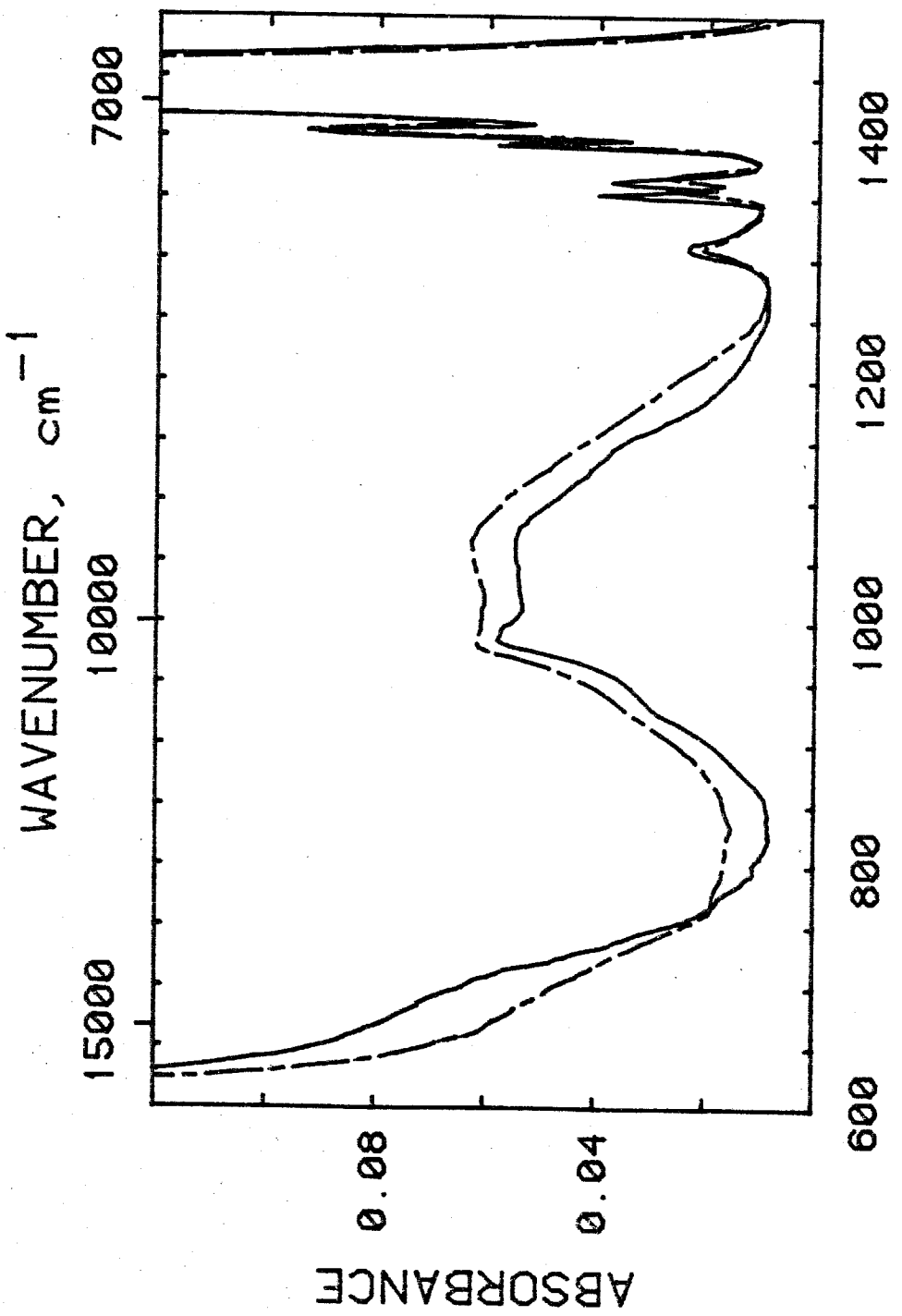

Fig. 7. E⊥c polarized absorption spectra of sample D7 illustrating the consistent behavior of Fe^{2+} transitions in this polarization. Sample thickness = 0.616 mm. Temperatures are indicated by line type: solid = 296 K broken = 83 K

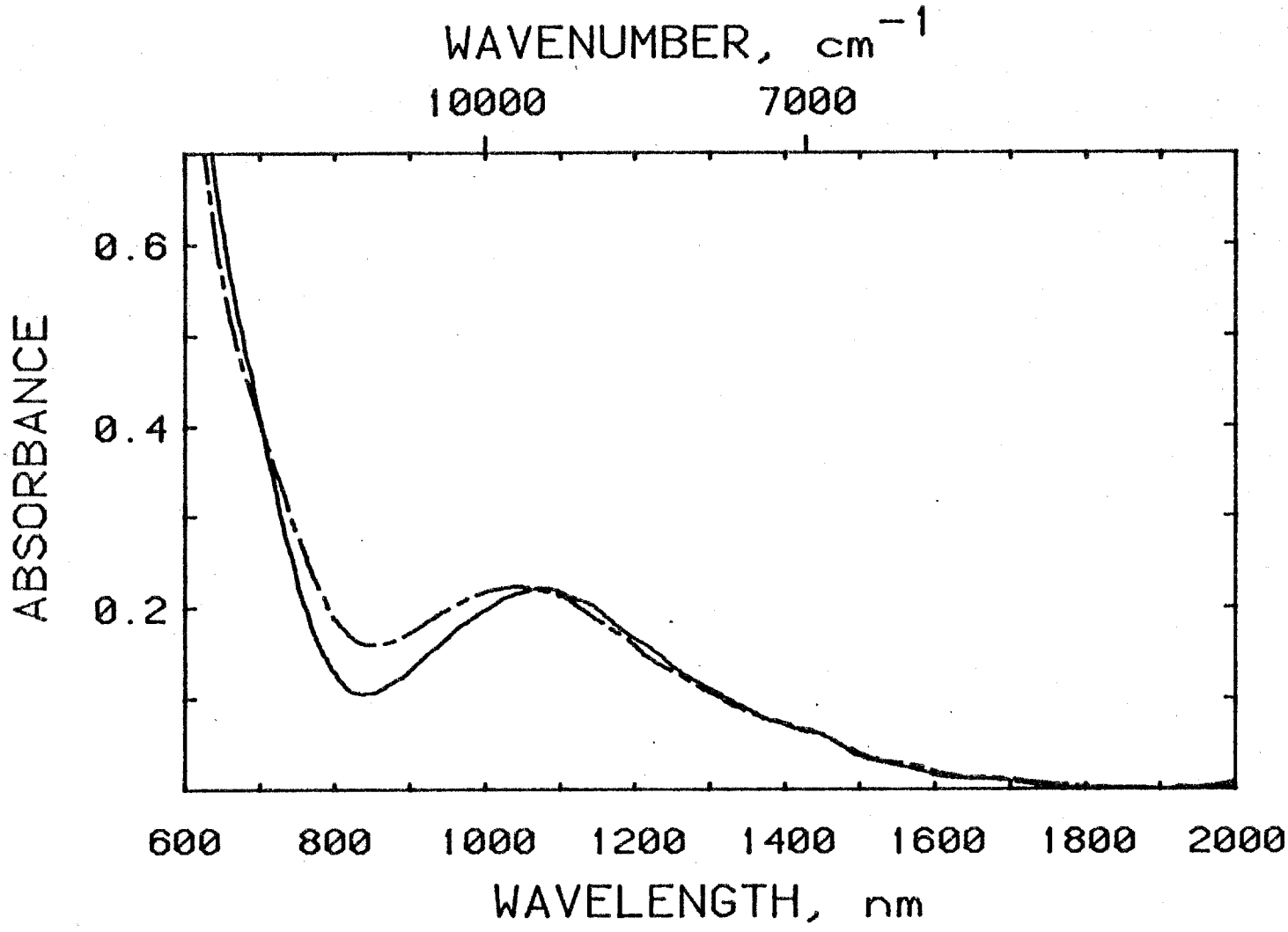

Fig. 8. E⊥c polarized absorption spectra of sample D7 illustrating the behavior of non-interacting Fe^{2+} in Fe,Mg-tourmalines. Sample thickness = 0.616 mm.
Temperatures: broken line = 296 K solid line = 83 K

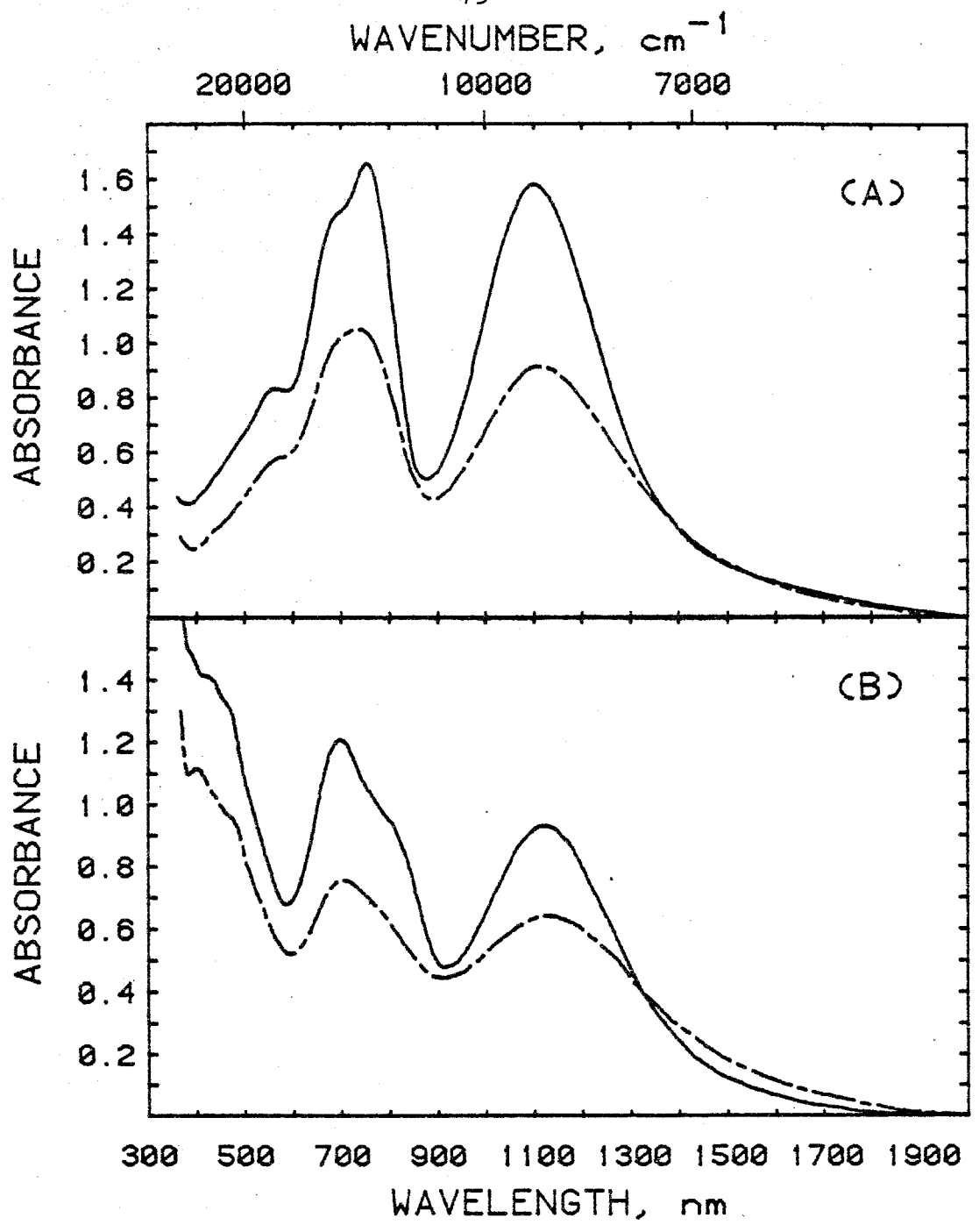

Fig. 9. E⊥c polarized absorption spectra of Fe,Mg-tourmalines illustrating the response of intensified Fe^{2+} transitions to temperature variation. Temperatures: broken line = 296 K solid line = 83 K (A) Sample S2, thickness = 0.0098 mm (B) Sample S9, thickness = 0.0074 mm

bring into doubt the reliability of intensity increases at low temperature to distinguish intensified transitions in other compounds. Experimental investigations of other Fe^{2+}-Fe^{3+} compounds as well as a theoretical treatment of intensified transitions are required to assess the certainty of low temperature intensity increases.

Fe^{2+}-Fe^{3+} Charge Transfer in Tourmaline

Fe^{2+}-Fe^{3+} charge transfer has previously been assigned to a transition between 530 and 570 nm (Smith 1978a; Smith and Strens 1976; Faye et al. 1974; Townsend 1970). These assignments were based predominantly on studies of the response of a few samples to partial oxidation. The application of this assignment to untreated tourmalines is complicated by the fact that there are several transitions which occur in this region. Ferric-rich Fe,Mg-tourmalines exhibit a transition at 535-545 nm in both E⊥c and E∥c which can be attributed to a Fe^{3+}-Fe^{3+} ion-pair transition (Chapter 2). Mn^{3+} in elbaites has a transition at 520 nm in E⊥c (Manning 1969b). I have also found, in agreement with Faye et al. (1968), weak, spin-forbidden transitions of Fe^{2+} in elbaites at 497 (sharp) and 550 nm. The comparatively large width of charge transfer transitions (Smith and Strens 1976) should permit the differentiation of Fe^{2+}-Fe^{3+} charge transfer from d-d transitions in the same wavelength region. In addition, Fe^{2+}-Fe^{3+} charge transfer should be more intense in those tourmalines with highly intensified Fe^{2+}

transitions. A transition at 575 nm in E⊥c is clearly shown in black Fe,Mg-tourmalines with little Ti (Fig. 9a). This is a relatively minor feature, however, and is frequently obscured by more intense Fe^{2+}-Ti^{4+} charge transfer (Chapter 4). The general presence of the 575 nm band was indicated by fits of gaussian bands to Ti-containing samples. The ~4500 cm^{-1} halfwidth of this transition and its ~50% increase in integrated intensity at low temperature are consistent with Fe^{2+}-Fe^{3+} charge transfer. The polarization of the 575 nm band (E⊥c>>E∥c) agrees with the major Y-site occupancy of iron. Amthauer and Rossman (1984) found molar absorptivities of Fe^{2+}-Fe^{3+} charge transfer transitions to vary from 60 to 210 $M^{-1}cm^{-1}$. The lack of a prominent role for Fe^{2+}-Fe^{3+} charge transfer in tourmaline is consistent with a comparison of these values to the estimate of the absorptivity of Fe^{2+} in Fe^{2+}-Fe^{3+} pairs (~1200 $M^{-1}cm^{-1}$).

The presence of an additional band at ~700 nm in Fe,Mg-tourmalines as compared to elbaites might indicate Fe^{2+}-Fe^{3+} charge transfer in another of the 2 site combinations which produce E⊥c polarization. However, the 80 K halfwidths of the 670 and 765 nm bands are similar (~2100 cm^{-1}) and comparable to the ~2500 cm^{-1} halfwidth of the 1100 nm band. These values are distinctly lower than the observed range of halfwidths of Fe^{2+}-Fe^{3+} charge transfer, 3500-6000 cm^{-1} (Chapter 5). I have therefore assigned the transitions at 670, 765 and 1100 nm in E⊥c to intensified Fe^{2+} d-d transitions.

Site Assignments of Fe^{2+} Absorption

The most significant difference illustrated thus far between elbaites and Fe,Mg-tourmalines is the number of intensified transitions. The 670, 765 and 1100 nm bands of Fe,Mg-tourmalines are present at all Fe concentration levels. Because charge transfer can be ruled out and 6-coordinate Fe^{2+} exhibits at most 2 transitions in this region, these bands must reflect Fe^{2+} in different sites. This is supported by the lack of a correlation between the proportion of the 670 and 765 nm bands and Fe^{2+} concentration or the amount of Fe^{3+}. The 2 tourmalines presented in Fig. 9 show the extremes of variation in the ratio of the 670 and 765 nm bands. Assignment of the 765 nm band to Fe^{2+} in the Y site and the 670 nm band to Fe^{2+} in the Z site with both sites absorbing at 1100 nm is based on the correlation of Fe-O distance and the average energy of the $^5T_2 \rightarrow {}^5E$ transition (Faye 1972). In the absence of independent data on the site distribution of Fe^{2+}, approximate Y- and Z-site occupancies can be obtained from compositional data. A rough correlation between the 670 nm band and Z-site occupancy of Fe^{2+} as indicated by the substitution $Na^+ + Al^{3+} = Ca^{2+} + Mg^{2+}(Fe^{2+})$ supports this assignment. In addition, comparison of Fe,Mg-tourmalines and elbaites provides further support of this assignment. Using the correlation presented by Faye (1972), Fe^{2+} in the larger sites of Fe,Mg-tourmalines would be expected to

absorb at lower energy than in elbaites. The 720 nm band of elbaites can thus be associated with the 765 nm band of Fe,Mg-tourmalines. A Y-site assignment is indicated by the general restriction of Fe^{2+} to the Y-site in elbaites (Burns 1972; Faye et al. 1974).

The assignments presented above conflict with Smith's assignments in elbaites. Three Fe^{2+} transitions are also present in elbaites, but it is the low energy band which is degenerate. At low temperatures the Fe^{2+} band at ~1200 nm in E$\parallel$c is resolved into 2 components at 1080 and 1300 nm (Fig. 10b). Smith (1978a) proposed that Fe^{2+} in the Y site absorbed at 720 and 1300 nm and Fe^{2+} in the Z site at 720 and 1080 nm. This would require a much larger absorptivity for Fe^{2+} in the Z site as compared to the Y site because of the predominance of Y-site occupancy in elbaites. Such a difference is inconsistent with the sizes of the sites (Fig. 4). In addition, the relative proportion of the 1080 and 1300 nm bands show an approximate correlation with Fe content. An increasing proportion of the 1080 band with increasing Fe content is indicated in Fig. 1. Above 1.5 Fe atoms per formula, Li-bearing tourmalines show a spectroscopy similar the Fe,Mg-tourmalines (Fig. 11). Fig. 10a illustrates another difference between elbaites and Fe,Mg-tourmalines. At very low Fe^{3+} contents, both 1080 and 1300 nm bands can be seen in E$\perp$c. However, only the 1080 nm band is intensified. At higher Fe^{3+} contents there is no indication of the 1300 nm bands in E$\perp$c (Smith 1978a). If

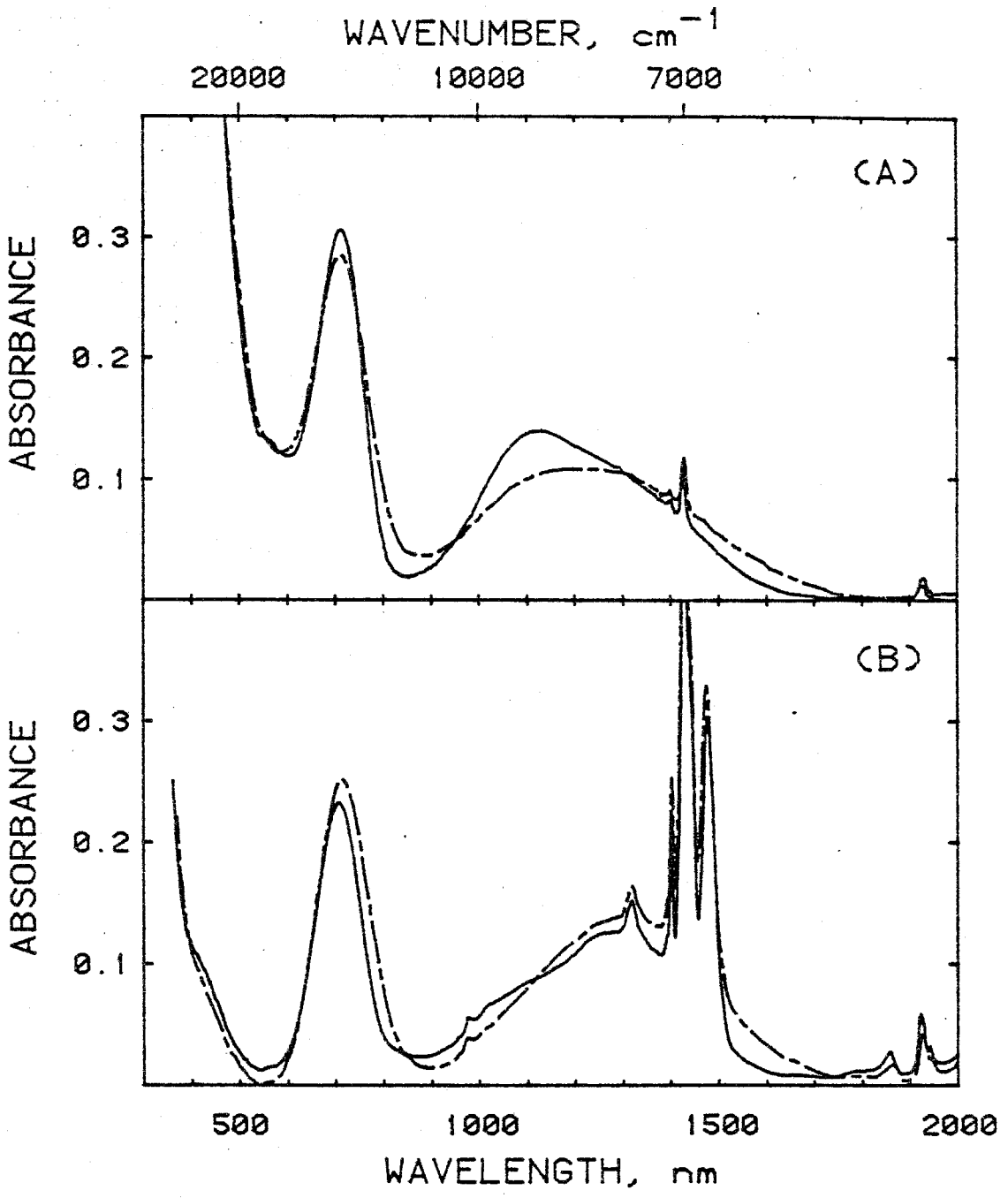

Fig. 10 Absorption spectra of sample T15 at 296 K (broken line) and 83 K (solid line). Sample thickness = 0.873 mm. (A) E⊥c polarization (B) E∥c polarization

the 1080 and 1300 nm bands represent different sites, these results suggest that Fe^{2+} can be intensified in only one site. This directly contradicts the behavior of Fe,Mg-tourmalines. These large differences between the optical properties of Fe,Mg-tourmalines and elbaites are not expected from the slight structural differences between the end members of the tourmaline group.

My preferred assignments to the 1080 and 1300 nm bands are that they both represent Fe^{2+} in the Y site but with differing degrees of distortion. At low iron contents, the Li and Al neighbors of Fe^{2+} in elbaites are smaller and may permit minor enlarging of the site for Fe^{2+} producing a lowering of the energy of the optical transition. Neighbors such as Fe^{2+} and Mg are similar in size and would not permit such adjustments. A shoulder on the 720 nm band is evident at high Fe contents in Li-bearing tourmalines (Fig. 11) and can be assigned to Fe^{2+} in the Z site.

Application to Radiation Effects

The extremely large absorption intensities of Fe^{2+} in association with Fe^{3+} suggests that optical spectra of tourmalines should provide a sensitive probe of Fe^{3+}. This is illustrated below for radiation induced changes. The effects of ionizing radiation are diverse and often difficult to specify. γ-irradiation of Mn-bearing elbaites oxidizes Mn^{2+} to Mn^{3+} (Reinitz and Rossman, in prep.). A large variability in the accompanying color

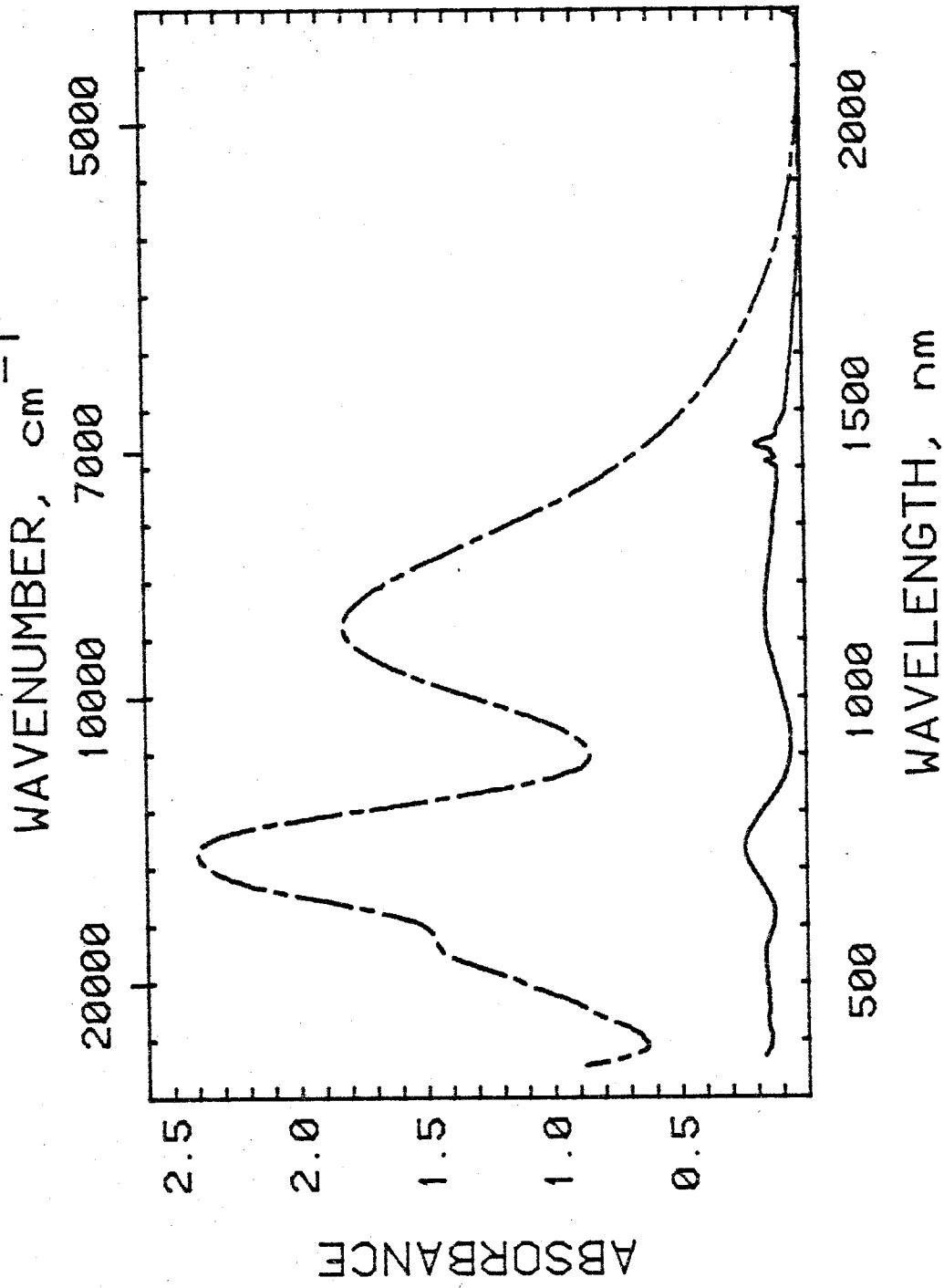

Fig. 11 296 K absorption spectra of sample T22 (a schorl in the elbaite-schorl series). Sample thickness = 0.128 mm Polarizations: solid line = E$\parallel$c broken line = E$\perp$c

change (Nassau 1975), however, indicates the complexity of this process. In order to assess the influence of iron, several blue elbaites containing 2-4% FeO and MnO were subject to γ-irradiation. These samples showed no evidence of the conversion of Mn^{2+} to Mn^{3+} at doses as high as 52 Mrads. Instead, small changes in Fe^{2+} absorption were noted (Fig. 12). The oxidation of Fe^{2+} to Fe^{3+} is indicated by increasing absorption at 720 and 1100nm in E$\perp$c. These bands exhibit no discernible change in E$\parallel$c. Similar behavior was also observed in samples EB3 and M1 which have similar FeO contents. The conversion of Mn^{2+} to Mn^{3+} was seen in sample EB2 with FeO ~1%. These observations suggest that neighboring cations can strongly affect the response of ions to irradiation. Voskresenskaya et al. (1979) also observed changes in the oxidation state of Fe upon γ-irradiation using Mössbauer spectroscopy but observed reduction of Fe^{3+} below 0.35 Grads and oxidation above 0.35 Grads. The changes illustrated in Fig. 12 correspond to very small increases in Fe^{3+} which would not be resolved in Mössbauer spectra.

The utility of Fe^{2+} absorption in tourmaline to monitor radiation dose has also been noted for neutron irradiation. Vargas and Tupinamba (1962) observed increasing absorption at ~700 and ~1100 nm with neutron irradiation and noted a linear relation of neutron dose to the log of the change in absorbance.

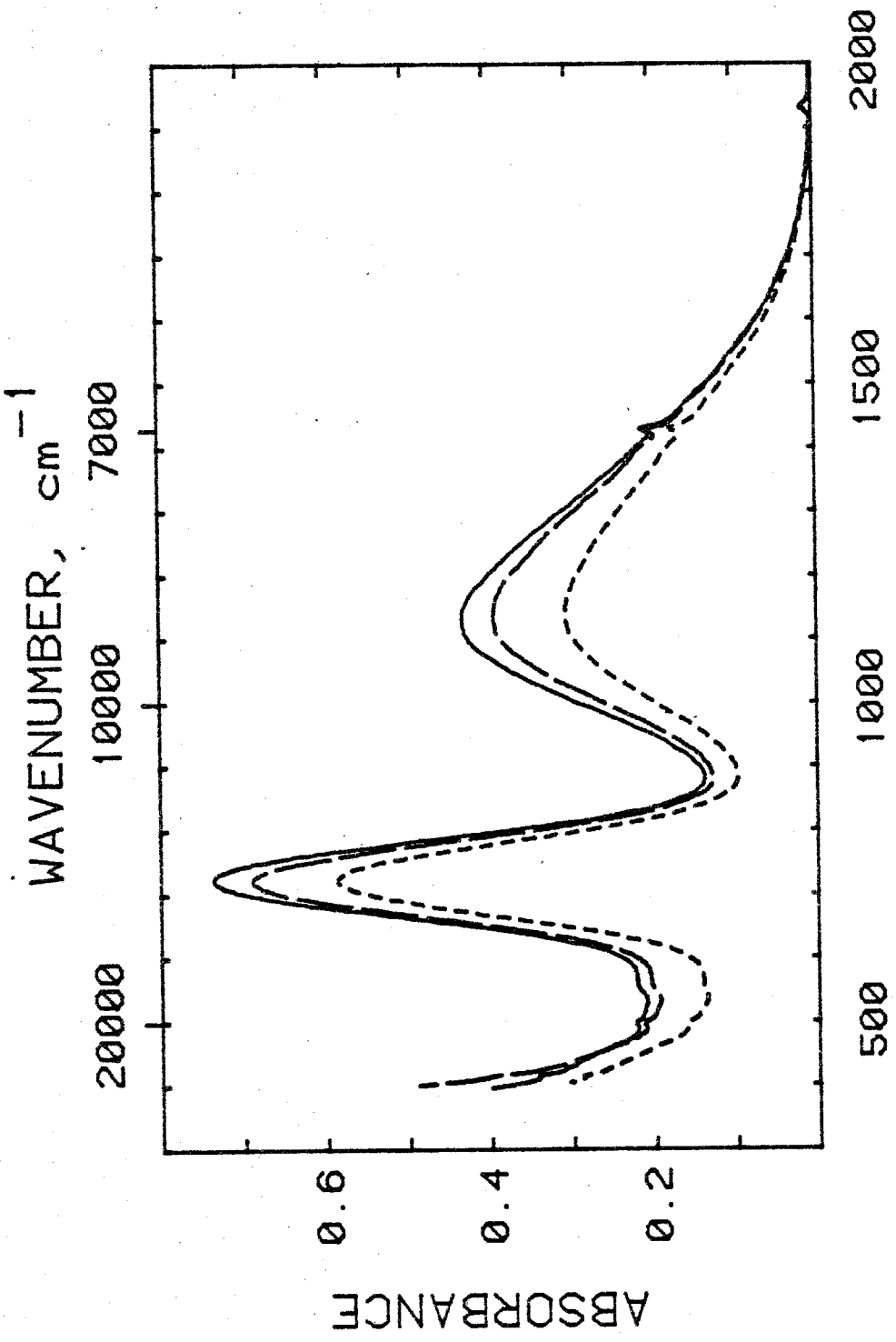

Fig. 12 E⊥c polarized absorption spectra of sample Z31 at various radiation doses.
Sample thickness = 0.778 mm Solid line: 40.8 Mrads + natural irradiation
Long dashed line: 51.4 Mrads after bleaching at 873 K
Short dashed line: 0 effective Mrads, bleached at 873 K

Summary

Tourmalines provide one of the most pronounced examples of a recently discovered aspect of Fe^{2+}-Fe^{3+} interaction--intensified Fe^{2+} transitions. Although the more familiar aspect of Fe^{2+}-Fe^{3+} interactions, Fe^{2+}-Fe^{3+} charge transfer, is also present, intensified Fe^{2+} transitions are the dominant effect at all Fe^{3+} concentrations. Fe^{3+} next to Fe^{2+} was observed to increase the absorptivity of Fe^{2+} bands to ~1200 $M^{-1}cm^{-1}$ from ~5 $M^{-1}cm^{-1}$ for non-interacting Fe^{2+}. Approximately equal degrees of intensification were observed for both components of the ${}^5\underline{T}_2 \rightarrow {}^5\underline{E}$ Fe^{2+} transition as well as for Fe^{2+} in two different crystallographic sites. As with other ion-pair transitions, this effect is restricted to the vector between the interacting cations. Significant differences between the optical spectroscopy of Fe,Mg tourmalines and elbaites have been related to structural and compositional factors. The basic characteristics of Fe^{2+}-Fe^{3+} interactions, however, are constant within the tourmaline group.

This extremely large change in absorption intensity implies that optical measurements of Fe^{3+} cannot be relied upon. However, because this effect is polarized, there may be useful unaffected polarizations such as $E \parallel \underline{c}$ in tourmaline. In addition, increases in intensity with decreasing temperature which occur in tourmaline may prove to be a consistent characteristic which can be used to detect intensified absorption bands. In itself, this effect

is a very sensitive probe of Fe^{3+} in tourmaline. Its general utility must be assessed by similar studies in other materials. The predictability of intensfied Fe^{2+} transitions will require the development of a theoretical understanding.

REFERENCES

Amthauer, G and Rossman, GR (1984) Mixed valence of iron in minerals with cation clusters. Phys Chem Minerals 11:37-51

Bence, AE and Albee, AL (1968) Empirical correction factors for electron microanalysis of silicates and oxides. J Geol 76:382-403

Buerger, MJ, Burnham, CW and Peacor, DR (1962) Assessment of the several structures proposed for tourmaline. Acta Crystallogr 15:583-590

Burns, RG (1970) Crystal field spectra and evidence of cation ordering in olivine minerals. Am Mineral 55:1608-1632

Burns, RG (1972) Mixed valencies and site occupancies of iron in silicate minerals from Mössbauer spectroscopy. Can J Spectr 17:51-59

Deer, WA, Howie, RA, and Zussman, J (1962) Rock-forming minerals Vol. 1 Ortho- and ring silicates, J Wiley & Sons, New York

Donnay, G and Barton, R Jr (1972) Refinement of the crystal structure of elbaite and the mechanism of tourmaline solid solution. Tschermaks Mineral Petrogr Mitt 18:273-286

Faye , GH (1972) Relationship between crystal-field splitting parameter, " Δ_{v_1}", and M_{host}-O bond distance as an aid in the interpretation of absorption spectra of Fe^{2+}-bearing materials. Can Mineral 11:473-487

Faye, GH, Manning, PG and Nickel, EH (1968) The polarized optical absorption spectra of tourmaline, cordierite, chloritoid and vivianite: Ferrous-ferric electronic interaction as a source of pleochroism. Am Mineral 53: 1174-1201

Faye, GH, Manning, PG, Gosselin, JR and Tremblay, RJ (1974) The optical absorption spectra of tourmaline: Importance of charge-transfer processes. Can Mineral 12:370-380

Fortier, S and Donnay, G (1975) Schorl refinement showing composition dependence of the tourmaline structure. Can Mineral 13:173-177

Goldman, DG and Rossman, GR (1979) Determination of quantitative cation distribution in orthopyroxenes from electronic absorption spectra. Phys Chem Minerals 4:43-53

Gorelikova, NV, Perfil'yev, YuD and Bubeshkin, AM (1976) Mössbauer data on distribution of Fe ions in tourmaline. Zap Vses Mineral O-va 4:418-427 (transl. Int Geol Rev 20:982-990, 1978)

Hermon, E, Simkin, DJ, Donnay, G and Muir, WB (1973) The distribution of Fe^{2+} and Fe^{3+} in iron-bearing tourmalines: A Mössbauer study. Tschermaks Mineral Petrogr Mitt 19:124-132

Loehr, JS, Loehr, TM, Mauk, AG and Gray, HB (1980) An electronic spectroscopic study of iron coordination in hemerythrin. J Am Chem Soc 102:6992-6996

Manning, PG (1969b) An optical absorption study of the origin of colour and pleochroism in pink and brown tourmalines. Can Mineral 9:678-690

Manning, PG (1969a) Optical absorption spectra of chromium-bearing tourmaline, black tourmaline and buergerite. Can Mineral 10:57-70

Manning, PG (1973) Effect of second-nearest-neighbour interaction on Mn^{3+} absorption in pink and black tourmalines. Can Mineral 11:971-977

Nassau, K (1975) Gamma ray irradiation induced changes in the color of tourmalines. Am Mineral 60:710-713

Rossman, GR (1975) Spectroscopic and magnetic studies of ferric iron hydroxy sulfates: intensification of color in ferric iron clusters bridged by a single hydroxide ion. Am Mineral 60:698-704

Saegusa, N, Price, DC and Smith, G (1979) Mössbauer spectra of several iron-rich tourmalines (schorls). J Phys (Paris) 40:C2/456-C2/459

Simon, HF (1973) Near-infrared and Mössbauer study of cation site occupancies in tourmalines. Unpublished MS Thesis MIT

Smith, G (1978a) A reassessment of the role of iron in the 5000-30000 cm-1 region of the electronic absorption spectra of tourmaline. Phys Chem Minerals 3:343-373

Smith, G (1978b) Evidence for absorption by exchange-coupled Fe^{2+}-Fe^{3+} pairs in the near infra-red spectra of minerals. Phys Chem Minerals 3:375-383

Smith, G (1980) Evidence for optical absorption by Fe^{2+}-Fe^{3+} interactions in MgO:Fe. Phys Stat Sol A 61:K191-K195

Smith, G and Strens, RGJ (1976) Intervalence-transfer absorption in some silicate, oxide, and phosphate minerals. In RGJ Strens, ed., The Physics and Chemistry of Minerals and Rocks, J Wiley & Sons, New York, pp 583-612

Townsend, MG (1970) On the dichroism of tourmaline. J Phys Chem Solids 31:2481-2488

Vargas, JI and Tupinamba, GAC (1962) Tourmaline as a new thermal neutron dosimeter. Inter-Am. Symp. Peaceful Appl. Nucl. Energy 4th Mexico City 1, 67.

Voskresenskaya, IE, Korovushkin, VV, Moiseev, BM and Shipko, MN (1979) Mössbauer investigation of γ-irradiated ferriferrous elbaites. Kristallogr 24:835-837 (transl. Sov Phys Crystallogr 244:480-481, (1979)

Wilkins, RWT, Farrell, EF and Naiman, CS (1969) The crystal field spectra and dichroism of tourmaline. J Phys Chem Solids 30:43-56

Chapter 4

Heteronuclear Charge Transfer in Minerals

Introduction

Mixed valence ion-pairs of transition elements are often present in minerals. Homonuclear ion-pairs which consist of a single element in different oxidation states have been studied extensively, particularly with regard to the intense optical transitions which correspond to charge transfer between the cations (Robin and Day 1967; Creutz 1983). The complex chemistries of natural materials suggests that ion-pairs consisting of dissimilar elements should be as common in minerals as homonuclear ion-pairs. Heteronuclear ion-pairs, such as Pd^{2+}-Pt^{4+} and Ag^{+}-Au^{3+} ion-pairs (Allen and Hush 1967), have been studied in chemical systems to a much lesser extent and have consisted of mineralogically rare combinations. The observation of charge transfer transitions in minerals has been hampered by multiple, overlapping transitions and complex compositions in which several charge transfer transitions are possible. Fe^{2+}-Ti^{4+} charge transfer should be a frequent component of mineral spectra, but the spectra of minerals such as biotite (Robbins and Strens 1972) and Ti-pyroxenes (Burns et al. 1976) exemplify these difficulties. Most assignments of more distinct transitions, such as those of blue sapphire (Burns 1981), are complicated by low concentrations of the cations involved and the presence of other transition element cations at similar concentrations. Transitions assigned to Fe^{2+}-Ti^{4+} charge transfer have encompassed large variations in wavelength (400-900 nm) and bandwidth (Burns

1981). Increasing intensity with decreasing temperature has been utilized as the major criterion for identification. Very few unambiguous examples of Fe^{2+}–Ti^{4+} charge transfer are available to aid in the determination of these assignments.

Charge transfer transitions are potentially useful as sensitive probes not only of specific ions, but also of their site occupancies and the extent of cation ordering. These applications require the correct identification of specific transitions and a quantitative understanding of the relationship between intensity and concentration. Minerals containing the cations of interest in stoichiometric concentrations and edge- or face-sharing pair sites should provide reliable qualitative and quantitative characteristics of charge transfer transitions. These phases have not been studied previously because of experimental difficulties associated with the large intensities of charge transfer transitions. Similar data, however, can only be obtained from more dilute examples which span a large compositional range. This study will emphasize both concentrated Fe,Ti-minerals and a series of tourmalines containing large variations in Fe and Ti content to determine the characteristics of Fe^{2+}–Ti^{4+} charge transfer transitions. Mn^{2+}–Ti^{4+} charge transfer in tourmaline will also be characterized.

Experimental

The stoichiometric Fe,Ti-minerals which were selected include taramellite (CIT# 6848) and traskite (CIT# 7302) from Rush Creek, Fresno Co., CA and neptunite (GRR# 7/4/74) from San Benito Co., CA. The tourmaline samples are described in Table 3. Labels specifying zones of uniform color are indicated in Table 3 with the color descriptors. Differentiation of the elbaite-schorl series from Fe,Mg-tourmalines was based on Mg content and characteristic OH vibrations (Appendix). Chemical analyses were obtained using a MAC5-SA5 electron microprobe and are presented in Tables 1 and 2. Data reduction was accomplished using the methods of Bence and Albee (1968).

Optical spectra were obtained in a manner similar to that described in Rossman (1975). The spectra of thin samples (0.005-0.030 mm) were generally measured while attached to a glass slide with epoxy. The thickness of these samples was determined using a microscope micrometer on polished, perpendicular sections. Low temperature spectra were obtained by placing the sample on a coldfinger immersed in liquid nitrogen in a quartz dewar. Temperatures were monitored using a copper-constantan thermocouple placed sightly above the sample. Temperature variation during a spectrum was limited to 80 to 86 K. Room temperature spectra were measured in the same apparatus without moving the sample to insure quantitative comparisons.

Table 1 Electron Microprobe Analyses of Fe,Ti-minerals

Sample	weight % oxides									
	Na_2O	CaO	BaO	FeO	MgO	MnO	TiO_2	SiO_2	Cl	F
Taramellite	0	0	39.3	6.70	1.13	0.40	11.6	33.0	1.95	0
Traskite	0.14	0.50	48.2	5.77	0.16	1.28	7.12	26.1	4.23	0.5

	Na_2O	K_2O	FeO	MgO	MnO	TiO_2	SiO_2
Neptunite light zone	7.38	4.94	11.0	2.08	1.38	17.5	53.9

Table 2 Electron Microprobe Analyses of Tourmalines

Sample	Na_2O	CaO	MgO	FeO	MnO	TiO_2	Al_2O_3	ZnO	SiO_2	F
T10	2.61	0.26	BDL	BDL	6.85	0.33	37.8	NA	36.2	0.4
NP1	2.24	1.22	BDL	0.13	5.74	0.46	39.0	0.03	35.1	1.5
NP2	2.51	0.81	BDL	1.46	5.10	0.26	38.2	BDL	35.8	1.6
NP3	2.37	0.78	BDL	4.79	3.58	0.78	37.3	0.23	35.4	1.2
EG3	2.50	0.26	BDL	2.49	1.51	0.02	39.8	0.09	37.5	1.4
EG4	2.74	0.18	BDL	4.32	1.67	0.04	37.8	0.41	37.4	1.6
S2	2.03	0.03	0.09	13.5	0.95	0.08	35.2	NA	34.7	0.6
S3b	1.69	0.43	4.87	8.45	0.07	0.35	34.7	NA	35.3	BDL
S3g	1.88	0.85	6.25	6.88	0.03	1.01	34.2	NA	34.7	BDL
S4b	2.26	0.72	8.01	7.79	0.06	0.28	30.9	NA	35.6	0.6
S4g	2.39	0.61	7.78	6.93	0.05	0.53	31.9	NA	35.6	0.3
S5b	1.68	0.34	3.11	9.16	0.28	0.34	36.6	NA	34.8	0.2
S5g	1.78	0.41	5.04	6.82	0.15	0.31	36.1	NA	35.4	0.4
S6	2.31	0.43	3.56	11.6	0.14	1.03	32.5	NA	34.7	12
S10c	1.94	0.11	2.99	10.8	0.16	0.40	34.5	NA	35.2	0.2
D1	2.93	0.37	11.6	0.46	BDL	1.09	32.0	NA	37.2	0.1
D2	0.77	4.25	14.3	0.38	BDL	0.58	28.7	NA	36.5	0.3
D3	1.99	1.10	10.1	0.08	0.01	0.69	35.2	NA	36.5	0.2

BDL -- below detection limits NA -- not analyzed

Results

Taramellite

High Fe and Ti concentrations in taramellite, $Ba_4(Fe,Ti)_4B_2Si_8O_{29}Cl_x$, and its structure indicate the potential to unambiguously assign Fe^{2+}–Ti^{4+} charge transfer. Fe and Ti occur in edge-sharing octahedral chains which lie along [100] and in which the nearest neighbor cations are 339 and 360 pm apart (Mazzi and Rossi 1980). The polarization of charge transfer transitions along the vector between the interacting cations would thus predict that Fe^{2+}–Ti^{4+} charge transfer should have intensity along this direction only. Figure 1 illustrates the optical spectrum of taramellite. There are several transitions which are predominantly polarized along [100]. The chemistry of this sample (Table 2) indicates that transitions due to Fe and Ti should be the major contributors to this spectrum. An approximate oxidation state distribution of 72% Fe^{2+} and 28% Fe^{3+} is indicated by analyses by Alfors and Pabst (1984) on taramellites from this locality. Thus Fe^{2+}–Fe^{3+} charge transfer and intensified Fe^{2+} transitions could also contribute to this spectrum. The transitions at 900 and 1150 nm have energies typical of crystal field transitions of Fe^{2+}. A possible assignment to Fe^{2+} intensified transitions (Chapter 3) is implied by their great intensity in [100]. Although it is not possible to predict precisely the energy of Fe^{2+}–Fe^{3+} charge transfer, the normal range of Fe^{2+}–Fe^{3+} charge transfer energies encompasses the 700 nm

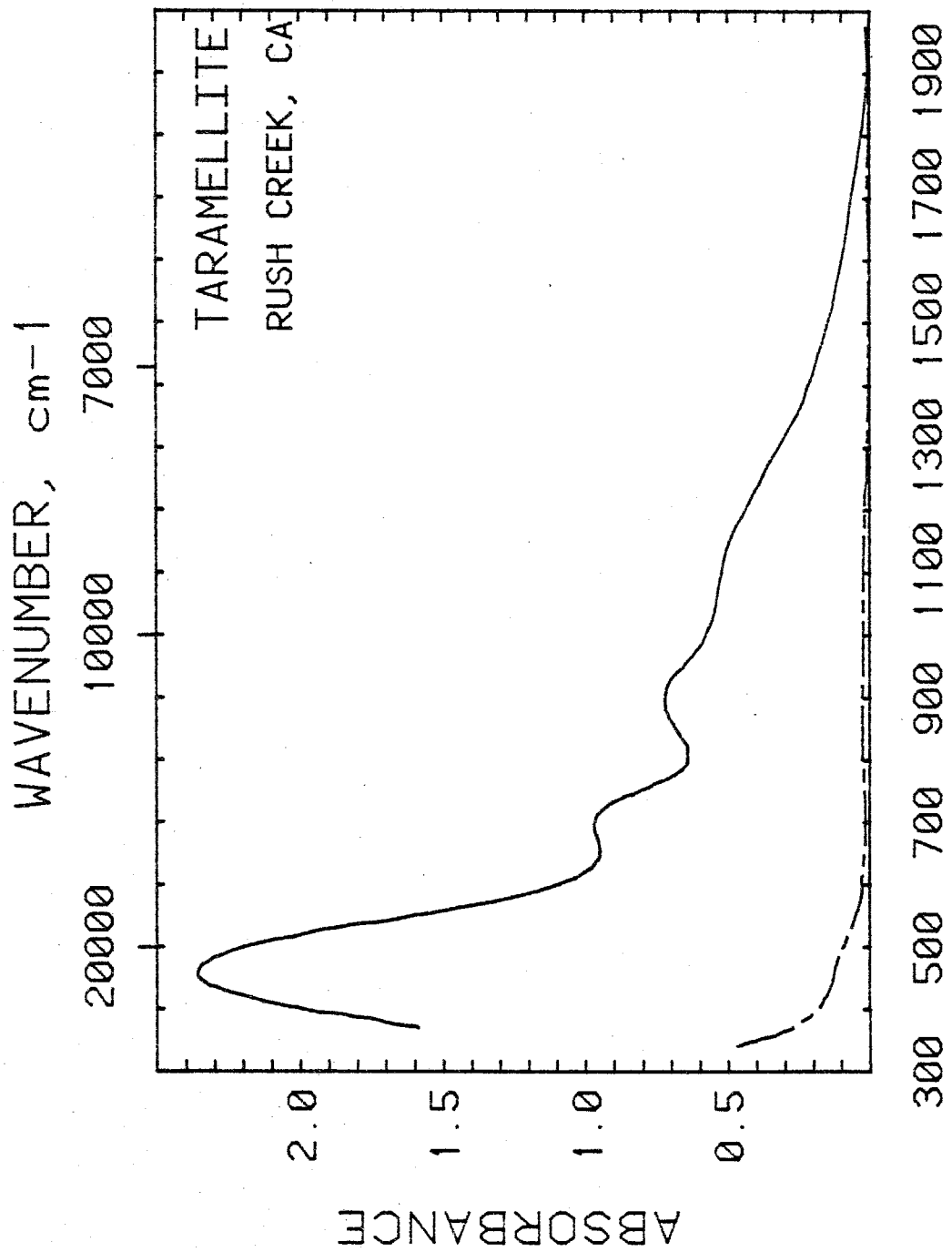

Fig. 1 296 K polarized absorption spectra of taramellite. Sample thickness = 0.009 mm
Polarizations: E∥Z -- solid line E⊥ (=E∥Y) -- broken line

band and excludes the 460 nm band (Chapter 5). Fe^{2+}–Ti^{4+} charge transfer can thus be assigned to the 460 nm band.

In addition to energy, the temperature response and width of transitions can be used as diagnostic criteria. Figure 2 illustrates the [100] spectrum of taramellite at 296 K and 83 K. Charge transfer transitions are generally expected to increase in intensity with decreasing temperature (Smith and Strens 1976). The 460 nm band, however, shows little if any increase at 83 K. In contrast, the 700 nm band, which has been assigned to Fe^{2+}–Fe^{3+} charge transfer, shows a large increase in intensity. Smith (1977) also noted larger intensity increases in Fe^{2+}–Fe^{3+} charge transfer than Fe^{2+}–Ti^{4+} charge transfer in more ambiguous examples of charge transfer. A potentially more useful characteristic of Fe^{2+}–Ti^{4+} charge transfer is the large width of the 460 nm band (~9000 cm^{-1}). This is distinctly larger than the width generally observed for Fe^{2+}–Fe^{3+} charge transfer (Chapter 5) and much larger than that of crystal field transitions (Smith and Strens 1976).

A quantitative characterization of this transition reveals a large relative intensity. A molar absorptivity of ~1300 $M^{-1}cm^{-1}$ was calculated assuming a random distribution within the octahedral chains. A molar absorptivity of ~450 $M^{-1}cm^{-1}$ would be valid if each Fe^{2+} were in contact with two Ti^{4+}. However, this would require an ordered distribution of cations within the octahedral chain. No distinction between individual octahedra was determined by the structure

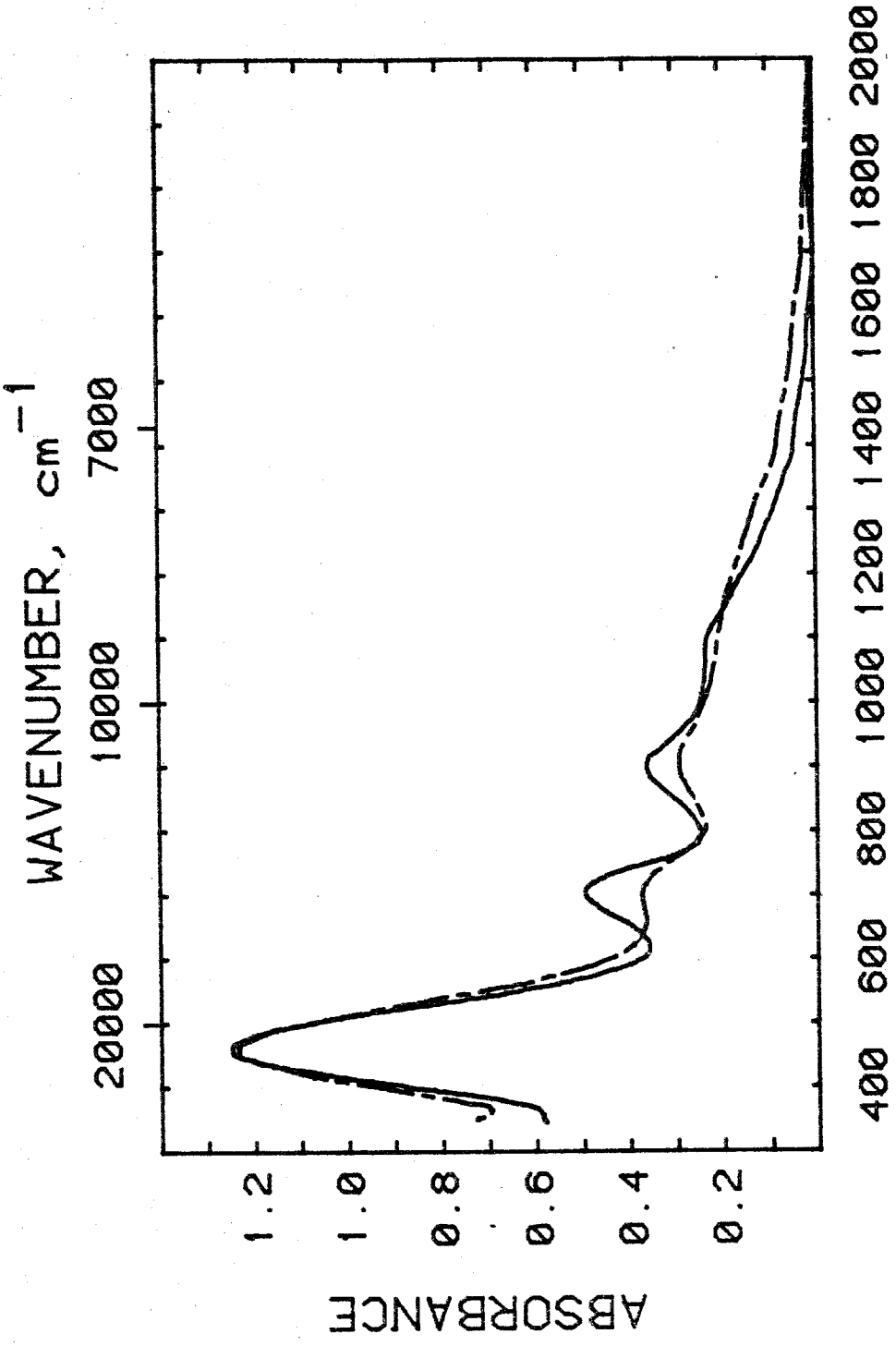

Fig. 2 E⊥Z polarized absorption spectra of taramellite. Sample thickness = 0.005 mm
Temperatures: 296 K -- broken line 83 K -- solid line

refinement (Mazzi and Rossi 1980). The absorptivity of Fe^{2+}–Ti^{4+} charge transfer in taramellite can be compared with absorptivities of Fe^{2+}–Fe^{3+} charge transfer in minerals which range between 60 and 210 $M^{-1}cm^{-1}$ (Amthauer and Rossman 1984).

Neptunite

Fe^{2+}–Ti^{4+} charge transfer is also an expected feature of the optical spectrum of neptunite, $KNa_2LiFe_2Ti_2Si_8O_{24}$. Fe and Ti occur in two edge-sharing octahedral chains along [110] and [1$\bar{1}$0] (Canillo et al. 1966; Borisov et al. 1965). These chains are interconnected through shared corners. The nearest cations within the chains are 314–328 pm apart, and the intercation vectors have substantial components in all optical directions. An ordered arrangement within the chains such that Fe^{2+} and Mn^{2+} alternate with Ti^{4+} was proposed to account for the piezoelectricity of neptunite (Canillo et al. 1966). Figure 3 illustrates the spectrum of neptunite in the visible region. The 415 nm transition can be unequivocally assigned to Fe^{2+}–Ti^{4+} charge transfer. The simplicity of this spectrum as opposed to that of taramellite can be related to the absence of Fe^{3+} (Bancroft et al. 1967). Relatively weak Fe^{2+} transitions at 860 and 1270 nm (Rossman unpublished results) provide the only other features in the visible–near infrared region. The width and intensity of this feature confirm this assignment. The width at half-height of the 415 nm transition is ~9000 cm^{-1} in agreement with taramellite. The molar absorptivity is

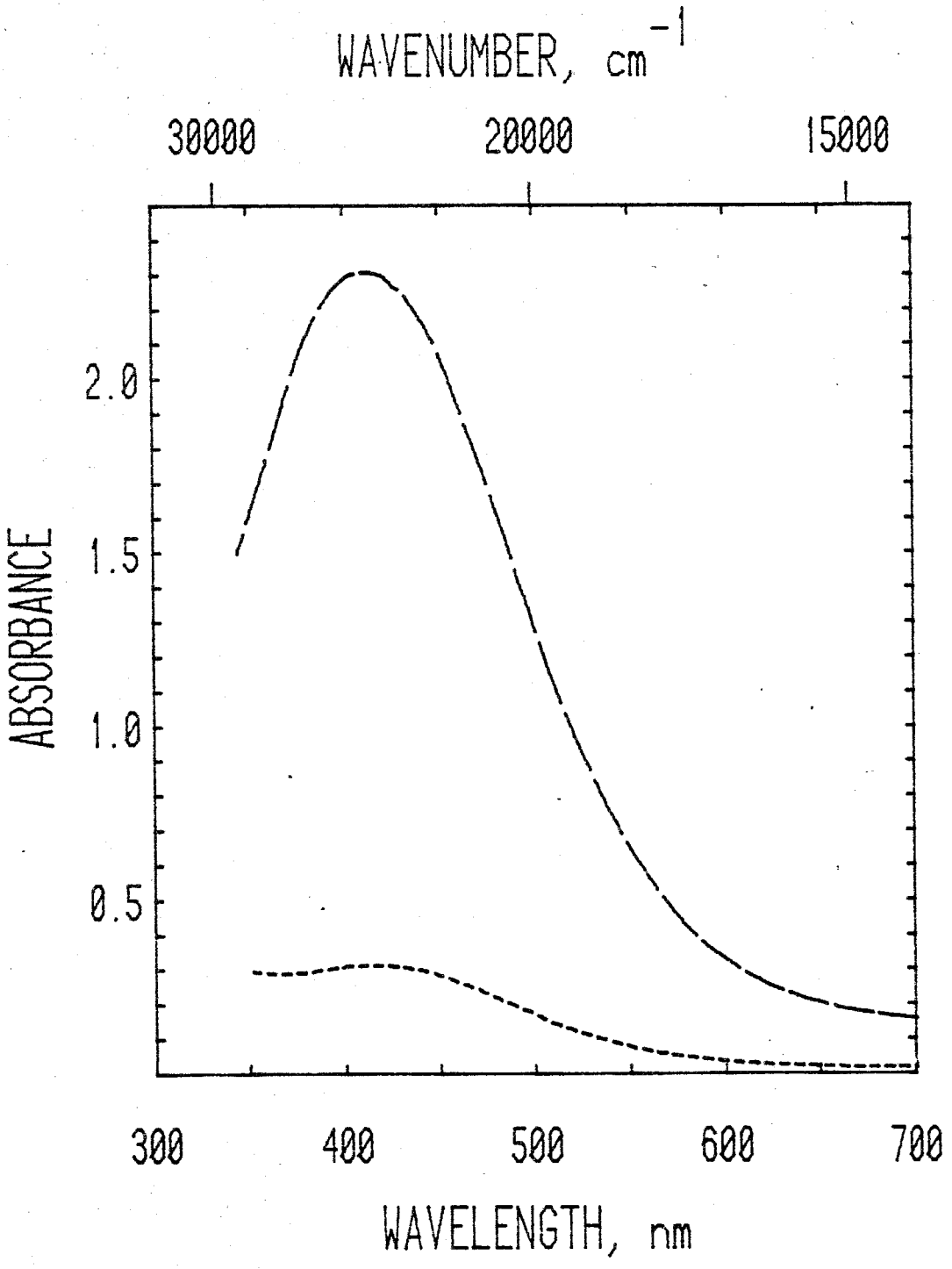

Fig. 3 296 K polarized absorption spectra of neptunite (a light brown zone).
Sample thickness = 0.010 mm Polarizations: E∥X -- short dash E∥Y -- long dash

~225 $M^{-1}cm^{-1}$ (calculated assuming each Fe has 2 Ti neighbors).

The observed intensity distribution provides the only inconsistency of this assignment. Due to experimental difficulties, gamma polarization is not shown. However, roughly equal intensities in gamma and beta polarizations were indicated. This intensity distribution is inconsistent with the structure of neptunite and the polarization of charge transfer transition along intercation vectors. The average orientation of the intercation vectors within the octahedral chain in alpha:beta:gamma is 1.3:1:1.2. The only intercation vector which agrees with the observed intensity ratios is that between the chains in the corner-shared pairs which are 393 pm apart and have the ratio 1:16:14. Although there is insufficient data on corner-sharing pairs to exclude the possibility of charge transfer from this ion-pair, charge transfer from the larger number of edge-sharing pairs should predominate. This intensity distribution is confirmed by the pleochroic behavior of neptunite (Ford 1909).

Traskite

The pleochroism and chemistry of traskite, $Ba_9Fe_2Ti_2(SiO_3)_{12}(OH,Cl,F)_6 \cdot 6H_2O$, indicated another potential example of Fe^{2+}-Ti^{4+} charge transfer. The E⊥c spectrum of traskite is shown in Figure 4. The E∥c spectrum was not available, but this direction is nearly colorless. The transitions at 850 and 950 can be assigned to Fe^{2+}

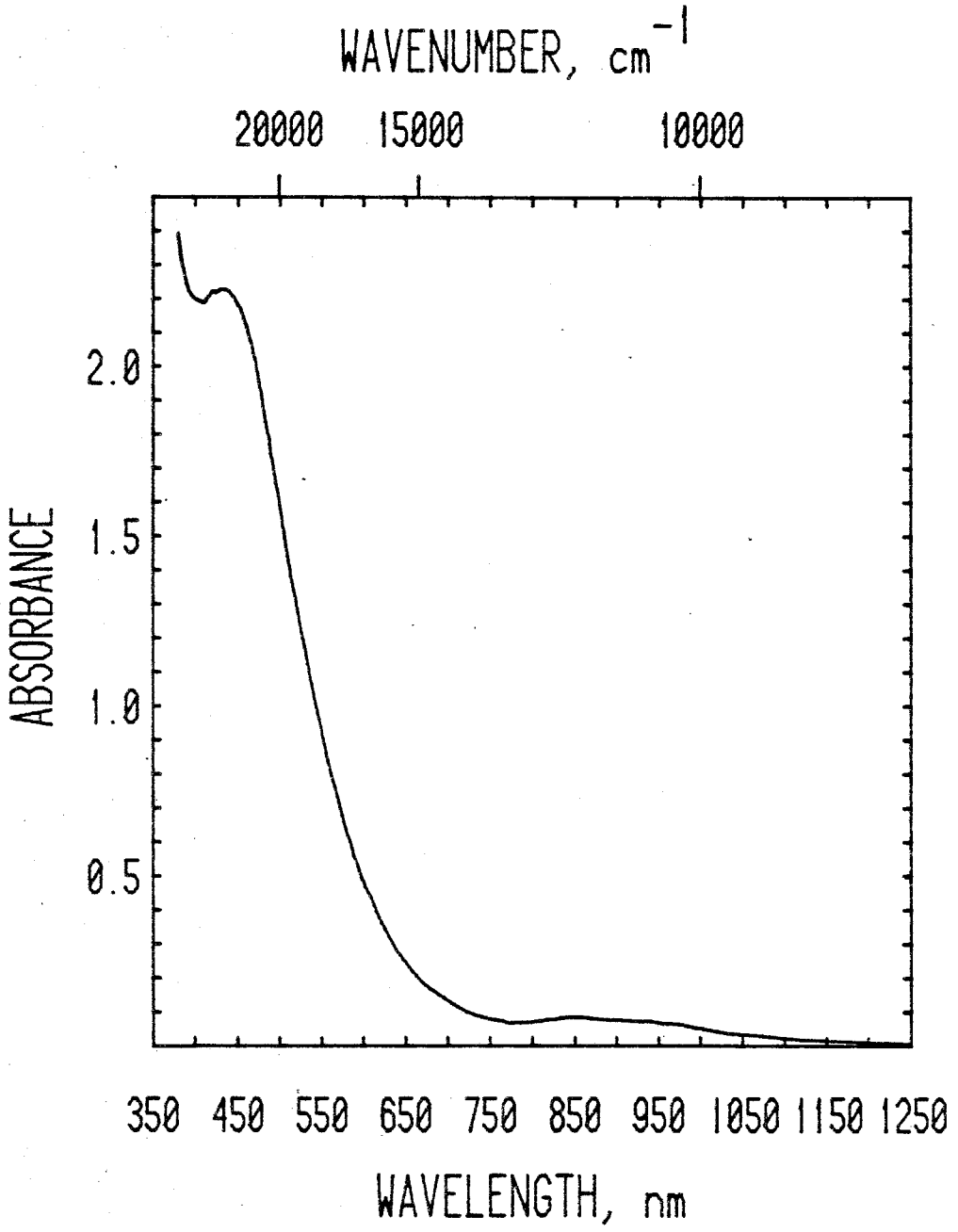

Fig. 4 E⊥c polarized absorption spectrum of traskite.

Sample thickness = 0.075 mm Temperature = 296 K

transitions. The remaining feature at 440 nm can therefore be assigned to Fe^{2+}-Ti^{4+} charge transfer. The ~7000 cm^{-1} width of this band is comparable to Fe^{2+}-Ti^{4+} in taramellite and neptunite. Malinovskii et al. (1976) have proposed a structure in which Fe and Ti occupy octahedra 3/4 of which are in corner-sharing pairs which are oriented perpendicular to the c-axis. They have suggested the formula $Ba_{24}A_2B_2CD_{12}Si_{12}O_{36}(Si_2O_7)_6(O,OH)_{30}Cl_6 \cdot 14H_2O$ where A, B, C, and D are positions occupied by Ti, Fe, Mn, Ca, Sr, Mg, and Al atoms. The determination of this structure was heavily biased by the Ba sites. It is difficult to reconcile a previous analysis of traskite (Alfors and Putman 1965) and the microprobe analysis of this sample with this formula. This structure has therefore not been used to calculate the molar absorptivity. A minimum value of ~75 $M^{-1}cm^{-1}$ is based on the assumptions that all Fe is Fe^{2+} and that every Fe is in contact with one Ti.

Tourmaline

Faye et al. (1974) and Smith (1978) have suggested that a broad transition in the region 400-450 nm (Fig. 5) in tourmaline could be assigned to Fe^{2+}-Ti^{4+} charge transfer. This assignment could not be confirmed by a correlation between Fe and Ti content and intensity. Tourmaline has the general formula $XY_3Z_6Si_6O_{18}(BO_3)_3(OH,O,F)_4$ where X is Na or Ca, Y is Mg, Fe or Li-Al, and Z is generally Al. Unlike the phases discussed above, it does not contain stoichiometric amounts of Ti, and in most gemmy tourmalines Ti concentra-

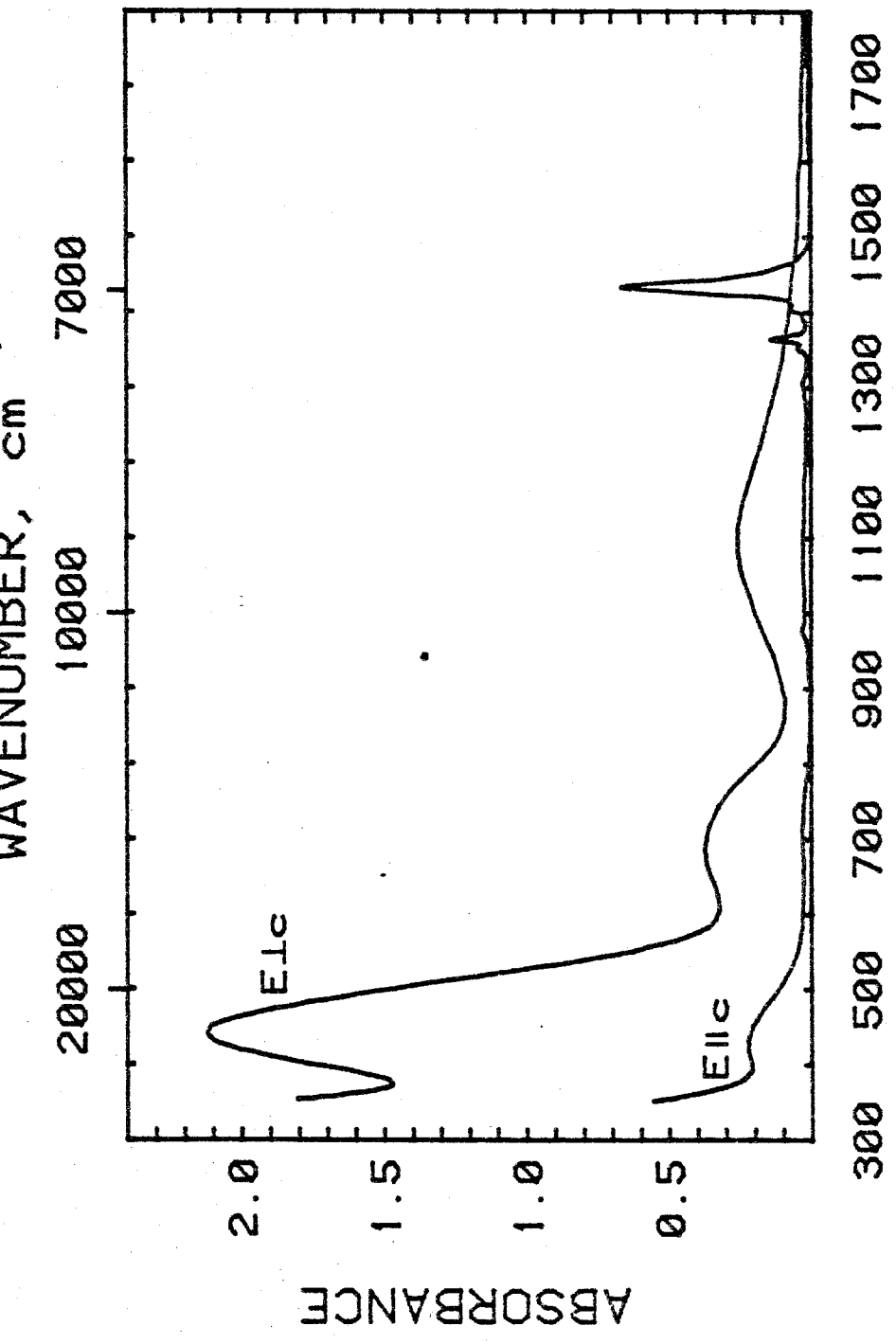

Fig. 5 296 K polarized absorption spectra of tourmaline D1.

Sample thickness = 0.680 mm

tions do not exceed 0.10 % TiO_2. Such low Ti concentrations are near the detection limits of electron microprobe analyses and are subject to large uncertainties. Fe,Mg-tourmalines generally possess higher Ti concentrations. The relationship between intensity of the 440 nm band and the concentration of Fe,Ti-pairs in a series of Fe,Mg-tourmalines was examined and is shown in Fig. 6. The localities and compositions of these samples are shown in Table 3 and Table 2. This correlation justifies the assignment to Fe^{2+}-Ti^{4+} charge transfer. A molar absorptivity of ~4000 $M^{-1}cm^{-1}$ is indicated by the illustrated least squares fit to these data. The concentrations of Fe^{2+}-Ti^{4+} pairs were calculated assuming a random distribution of Fe and Ti within the Y-trimer (Buerger et al. 1962). Although transition elements also occur in the Z site, Y-site occupancy predominates. This site preference is evident in the restriction of charge transfer intensity to the $E \perp c$ polarization. Y-Y and Y-Z ion pairs are oriented perpendicular to the c-axis, and Z-Z ion-pairs are oriented at 35° to the c-axis (Buerger et al 1962).

Minor differences characterize Fe^{2+}-Ti^{4+} charge transfer in the two basic compositional series of tourmaline. Elbaites (Li,Al-tourmalines) may have a lower molar absorptivity (possibly as low as 40% of that stated above) as indicated by one sample with sufficient Fe and Ti to compare to Fe,Mg-tourmalines (solid symbol Fig. 6).

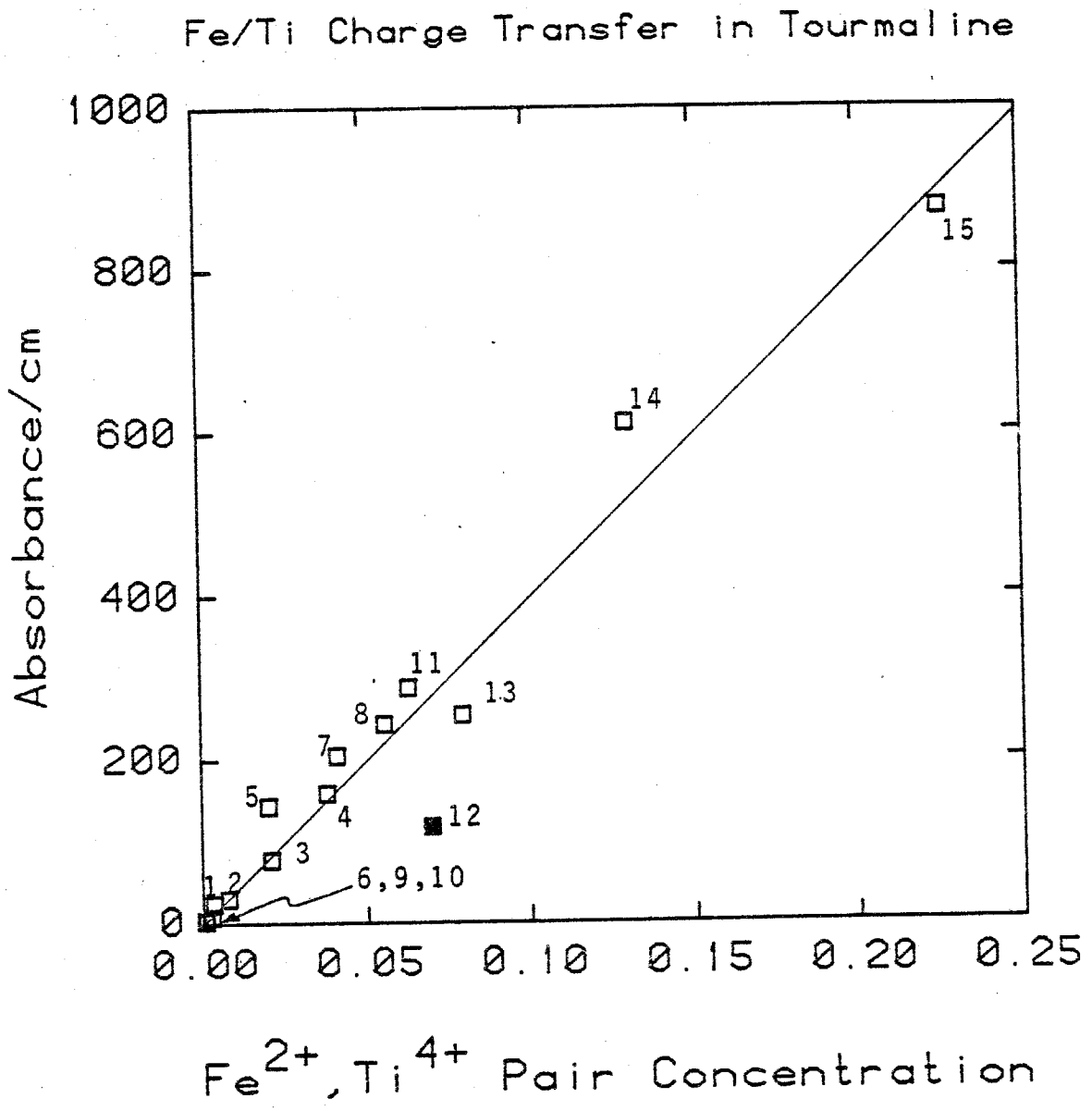

Fig. 6 Intensity of the 440 nm band in Fe,Mg-tourmalines (open squares) and the 420 nm band in elbaites (filled square) vs Fe,Ti pair concentration in moles/liter. See Table 3 for sample key.

Table 3 Tourmaline Sample Descriptions

Sample	Color	Locality	Fig. 6 Code	Archival Code
S2	blue*	White Queen Mine, Pala, CA	3	GRR# 3/13/78
S3	b=brown* g=green*	Newry, ME	14 8	CIT# 1372
S4	b=blue* g=green*	Cecil Co., MD	7 11	CIT# 3575
S5	b=blue* g=green*	Anza Borrego, CA	5 4	GRR# 3/16/83
S6	brown*	Portland, CT	15	CIT# 1087
S10c	green*	Minas Gerais, Brazil	13	
D1	brown	Yinnietharra, Australia	2	CIT# 12683
D2	brown	Bryant Lake, NY	1	CIT# 12684
D3	yellow	East Africa	10	GRR# 5/3/82
EG3	green	Afghanistan	6	GRR# 1/27/80
EG4	dark green	Afghanistan	9	GRR# 1/27/80
T10	yellow-green	Zambia		GRR# 11/8/82
NP	1=yellow 2=light brown 3=dark brown	Nepal	 12	GRR# 2/2/80

* E⊥c color in thin section

Fe^{2+}–Ti^{4+} charge transfer also occurs at a higher energy (415 nm) in elbaites. Fe^{2+}–Ti^{4+} charge transfer in both groups increases in integrated intensity by 15% on going from 295 K to 83 K (Fig. 7). Smith (1977) observed an increase in intensity of ~25% at 5 K as compared to 293 K. The halfwidth of this transition is 8000–9000 cm^{-1} for both elbaites and Fe,Mg-tourmalines.

Mn^{2+}–Ti^{4+} Charge Transfer

Two unusual yellow elbaites with relatively high concentrations of Mn and Ti and extremely low concentrations of Fe afforded the opportunity to examine Mn^{2+}–Ti^{4+} charge transfer. Figure 8 illustrates the spectra of an elbaite which is zoned in Mn and Fe. An Fe rich zone exhibits Fe^{2+}–Ti^{4+} charge transfer at 415 nm. A second transition is evident in a zone with an Fe:Mn ratio of 1:4. Mn^{2+}–Ti^{4+} charge transfer at 325 nm is clearly shown in a zone with trace amounts of Fe. Charge transfer energies can be related to the ionization potential of the donor ion and the electron affinity of the acceptor ion. Although such considerations are difficult to apply to individual examples, the higher energy of Mn^{2+}–Ti^{4+} charge transfer as compared to Fe^{2+}–Ti^{4+} charge transfer can be correlated with a higher third ionization potential for Mn than Fe. This relationship was also observed in a reflectance study of Fe and Mn doped $MgTiO_3$ (Blasse 1981). The molar absorptivity of the 325 nm band, ~450 $M^{-1}cm^{-1}$, is much lower than that of Fe^{2+}–Ti^{4+} charge transfer in tourmaline. The width and

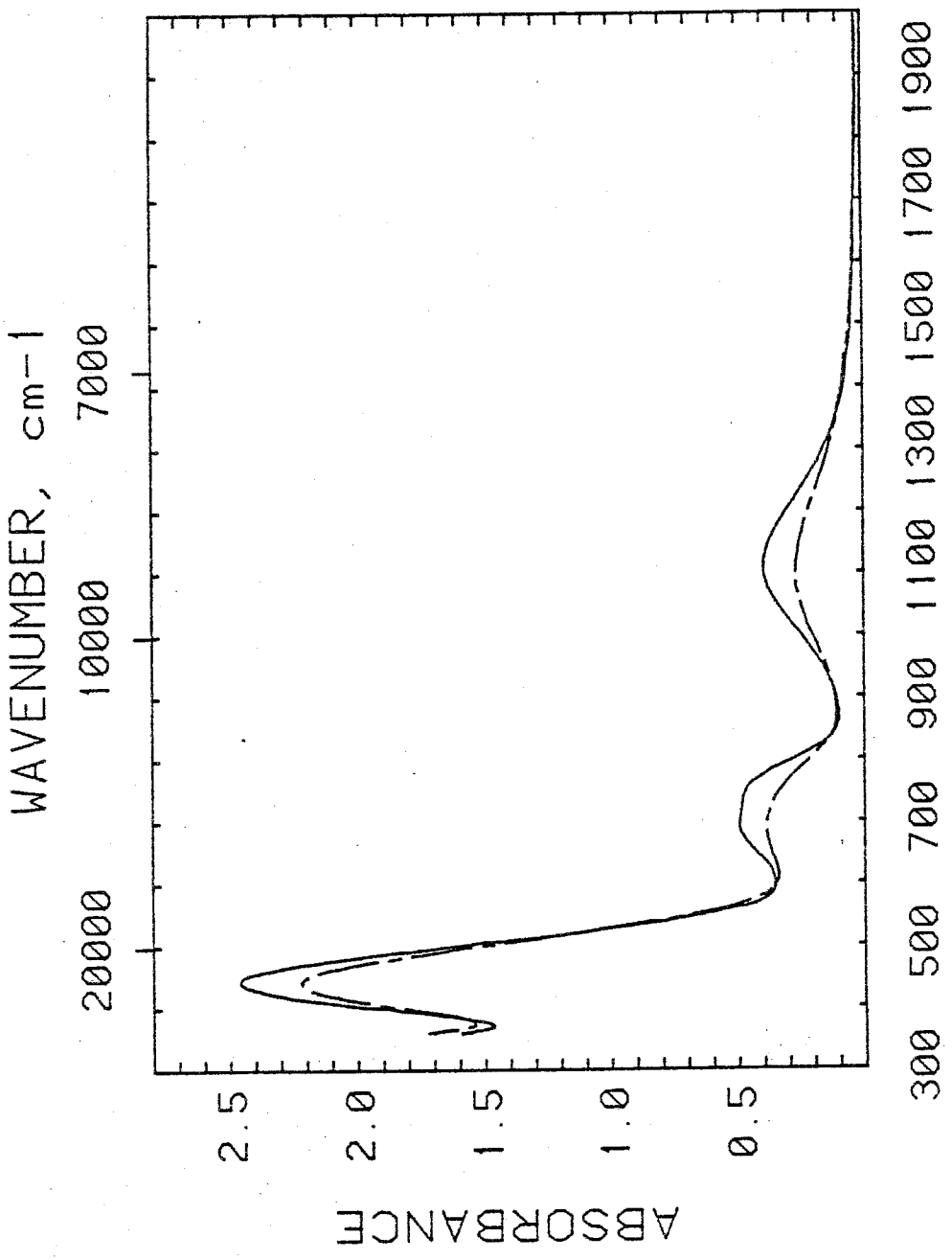

Fig. 7 E⊥c polarized absorption spectra of tourmaline D1. Sample thickness = 0.680 mm
Temperatures: 296 K -- broken line 83 K -- solid line

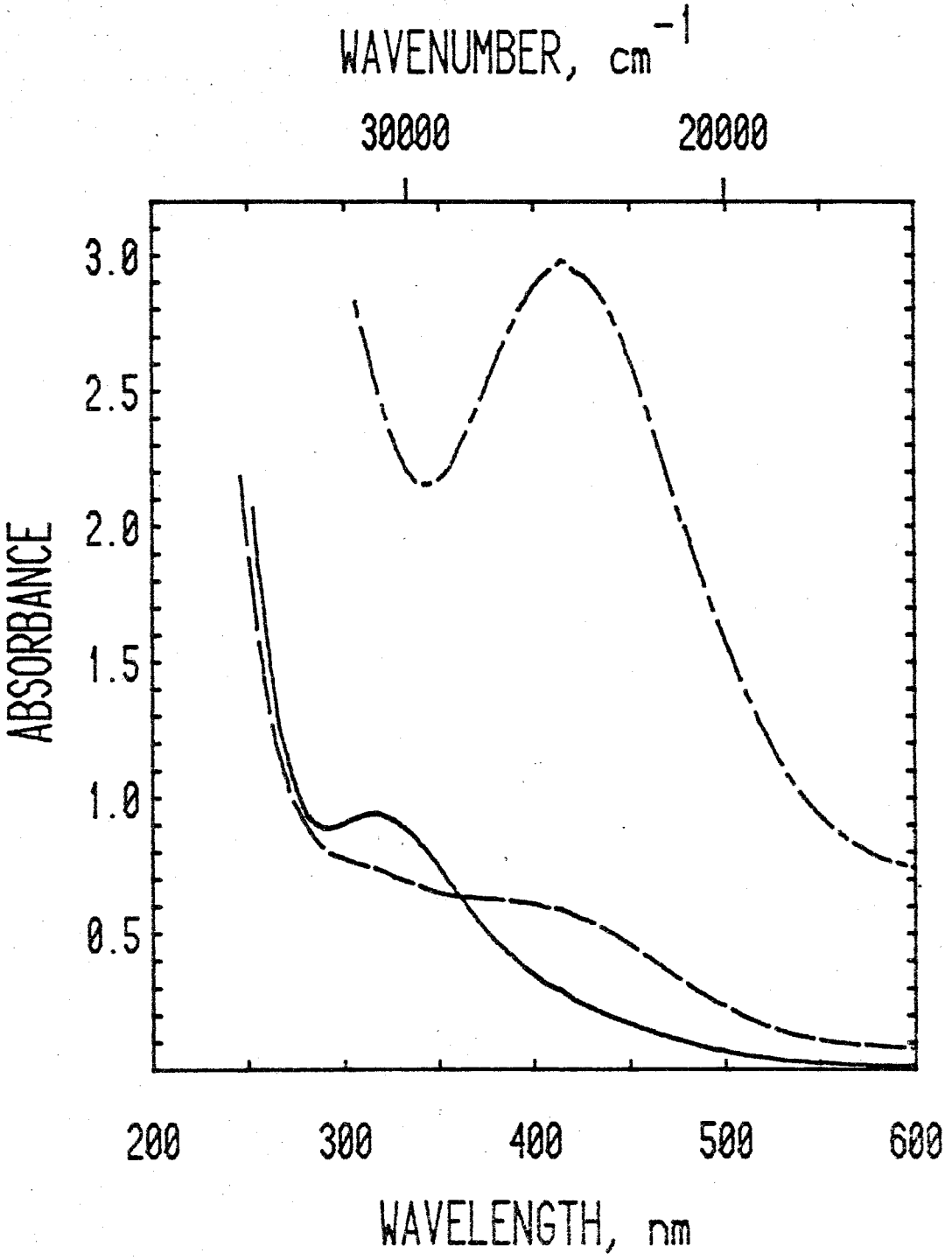

Fig. 8 E⊥c polarized absorption spectra of tourmaline NP. Sample thickness = 0.150 mm
yellow zone (NP1) -- solid line light brown zone (NP2) -- long dash line
dark brown zone (NP3) -- long & short dash line

temperature dependence of Fe^{2+}–Ti^{4+} charge transfer and Mn^{2+}–Ti^{4+} charge transfer, however, are similar. A small increase in intensity of Mn^{2+}–Ti^{4+} at low temperature is shown in Fig. 9. The halfwidth of the 325 nm band is ~7000 cm^{-1}. Both charge transfer transitions are also polarized in E⊥c.

Discussion

With the exception of intensity, Fe^{2+}–Ti^{4+} charge transfer transitions in taramellite, traskite, neptunite, and tourmaline exhibit similar characteristics. The energy of these transitions fall within a fairly narrow range, 400–460 nm, which is distinctly separated from the energy range of Fe^{2+}–Fe^{3+} charge transfer (Chapter 5). The 7000–9000 cm^{-1} halfwidths are also distinctly larger than Fe^{2+}–Fe^{3+} charge transfer as well as crystal field transitions which may occur in the same energy region. Minor or imperceptible increases in intensity with decreasing temperature were observed. Energy and halfwidth thus appear to be the most useful diagnostic characteristics for Fe^{2+}–Ti^{4+} charge transfer. Molar absorptivities varied between ~100 and ~4000 $M^{-1}cm^{-1}$. These values are generally larger than or equal to those of Fe^{2+}–Fe^{3+} charge transfer in minerals (Amthauer and Rossman 1984) and larger than those of crystal field transitions. Thus the presence of Fe and Ti should generally have a large influence on color. The large variation in molar absorptivity among different phases

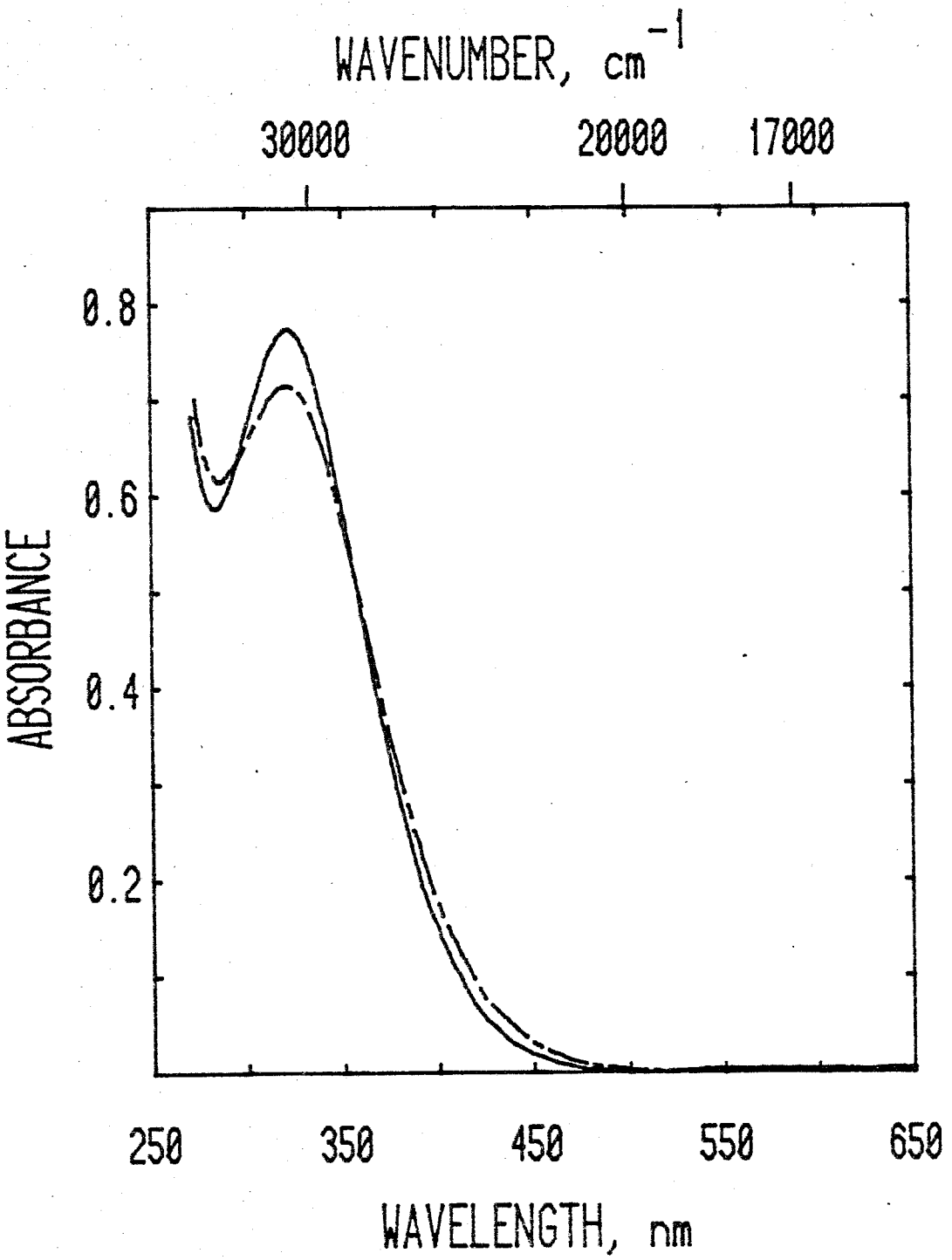

Fig. 9 E⊥c polarized absorption spectra of tourmaline T10. Sample thickness = 0.159 mm
Temperature: 296 K -- broken line 83 K -- solid line

suggests that the quantitative use of these transitions will be limited to phases in which intensity can be calibrated against concentration.

There are few unambiguous examples of Fe^{2+}-Ti^{4+} charge transfer to which the above data can be compared. Optical spectra of fassaite from the Angra dos Reis meteorite have been studied extensively (Mao et al. 1977). Composition, polarization and pressure variations were used to assign a transition at 500 nm to Fe^{2+}-Ti^{4+} charge transfer. This wavelength and a halfwidth of ~9000 cm^{-1} are consistent with the characteristics stated above. The most frequently cited mineral containing Fe^{2+}-Ti^{4+} charge transfer is corundum. Blue or green corundums have been prepared solely by simultaneously doping Fe and Ti into Al_2O_3. Transitions at 560-590 nm, 710 nm (Ferguson and Fielding 1971) and 900 nm (Smith and Strens 1976) have been assigned to Fe^{2+}-Ti^{4+} charge transfer. The assignment of these transitions is complicated by a large number of potential transitions due to the presence of Fe^{3+}, Ti^{3+}, Fe^{2+} and Ti^{4+}. The transition at 560-590 nm is at an energy close to the energies of Fe^{2+}-Ti^{4+} charge transfer as well as the broad range of energies of Fe^{2+}-Fe^{3+} charge transfer. The ~5200 cm^{-1} halfwidth (Smith and Strens 1976) is more similar to halfwidths observed for Fe^{2+}-Fe^{3+} charge transfer (Chapter 5). Of the transitions which have been assigned to Fe^{2+}-Ti^{4+} charge transfer, this transition is the only one which could be supported by my data. This comparison is

limited by the presence of face-sharing ion-pairs in corundum as opposed to edge-sharing ion-pairs above. Another limiting factor to the validity of previous assignments is the lack of consideration of intensified Fe^{2+} transitions (Chapter 3). Further work is required to assess the appropriate assignments in blue and green corundums.

Similar dilemmas are faced in the interpretation of the optical spectra of minerals such as kyanite (Smith and Strens 1976) and sillimanite (Rossman et al. 1982), polymorphs of Al_2SiO_5, and dumortierite, $Al_7BO_3(SiO_4)_3O_3$ (Rossman, unpublished data). Transition elements substitute for Al^{3+} in these minerals. Trivalent cations generally predominate, and divalent and tetravalent cations must occur together for charge compensation. Thus Fe^{2+}-Ti^{4+} pairs are generally accompanied by Fe^{2+}-Fe^{3+} pairs, and multiple charge transfer transitions as well as intensified Fe^{2+} transitions must be differentiated. Blue varieties of these minerals possess similar optical spectra with a band at ~600 nm (halfwidth ~5000 cm^{-1}) that has been assigned to Fe^{2+}-Ti^{4+} charge transfer. A comparison of these bands with the examples of Fe^{2+}-Ti^{4+} charge transfer presented in this paper would suggest that such assignments are unlikely. Further support for this contention is obtained from another polymorph of Al_2SiO_5. A band at 480 nm with a halfwidth of 6500 cm^{-1} (Smith and Strens 1976) has been assigned to Fe^{2+}-Ti^{4+} charge transfer in andalusite. These characteristics are similar to those outlined above and

should be directly comparable to these aluminum minerals.

REFERENCES

Alfors, JT and Pabst, A (1984) Titanian taramellites in western North America. Am Mineral 69:358-373

Alfors, JT and Putman, GW (1965) Revised chemical analyses of traskite, verplankite and muirite from Fresno County, California. Am Mineral 50:1500-1503

Allen, GC and Hush, NS (1967) Intervalence transfer absorption. Part 1. Qualitative evidence for intervalence-transfer absorption in inorganic systems in solution and in the solid state. Prog Inorg Chem 8:357-389

Bancroft, GM, Burns, RG, and Maddock, AG (1967) Oxidation state of iron in neptunite from Mössbauer spectroscopy. Acta Crystallogr 22:934-935

Bence, AE and Albee, AL (1968) Empirical correction factors for electron microanalysis of silicates and oxides. J Geol 76:382-403

Blasse, G (1981) Charge transfer in mixed metal oxides: their consequences and influence on physical properties. Comments Inorg Chem 1:245-256

Borisov, SV, Klevtsova, RF, Bakakin, VV and Belov, NV (1965) The crystal structure of neptunite. Kristallografiya 10:815-821 (transl. Sov Phys Crystallogr 10:684-689, 1966)

Brown, DB, ed. (1980) Mixed Valence Compounds. Theory and Applications in Chemistry, Physics, Geology, and Biology. Holland: Reidel, 519 pp.

Buerger, MJ, Burnham, CW and Peacor, DR (1962) Assessment of the several structures proposed for tourmaline. Acta Crystallogr 15:583-590

Burns, RG (1981) Intervalence transitions in mixed-valence minerals of iron and titanium. Ann Rev Earth Planet Sci 9:345-383

Burns, RG, Parkin, KM, Loeffler, BM, Abu-Eid, RM and Leung, IS (1976) Visible-region spectra of the moon: progress toward characterizing the cations in Fe-Ti bearing minerals. Proc 7th Lunar Sci Conf, Suppl 7, Geochim Cosmochim Acta 3:2561-2578

Canillo, E, Mazzi, F and Rossi, G (1966) The crystal structure of neptunite. Acta Crystallogr 21:200-208

Creutz, C (1983) Mixed valence complexes of d^5-d^6 metal centers. Prog Inorg Chem 30:1-73

Faye, GH, Manning, PG, Gosselin, JR and Tremblay, RJ (1974) The optical absorption spectra of tourmaline: importance of charge-transfer processes. Can Mineral 12: 370-380

Ferguson, J and Fielding, PE (1971) The origins of the colours of yellow, green and blue sapphires. Chem Phys Lett 10:262-265

Ford, WE (1909) Neptunite crystals from San Benito County, California. Am J Sci 27:235-240

Malinovskii, YuA, Pobedimskaya, EA and Belov, NV (1976) Crystal structure of traskite. Dokl Akad Nauk SSSR 229:1101-1104 (transl. Sov Phys Dokl 21:426-428, 1976)

Mao, HK, Bell, PM and Virgo D (1977) Crystal-field spectra of fassaite from the Angra dos Reis meteorite. Earth Planet Sci Lett 35:352-356

Mazzi, F and Rossi, G (1980) The crystal structure of taramellite. Am Mineral 65:123-128

Robin, MB and Day, P (1967) Mixed valence chemistry--a survey and classification. Adv Inorg Chem Radiochem 10:248-422

Robbins, DW and Strens, RGJ (1972) Charge-transfer in ferromagnesian silicates: the polarized electronic spectra of trioctahedral micas. Mineral Mag 38:551-563

Rossman, GR (1975) Spectroscopic and magnetic studies of ferric iron hydroxy sulfates: intensification of color in ferric iron clusters bridged by a single hydroxide ion. Am Mineral 60:698-704

Rossman, GR, Grew, ES and Dollase, WA (1982) The colors of sillimanite. Am Mineral 67:749-761

Smith, G (1977) Low-temperature optical studies of metal-metal charge-transfer transitions in various minerals. Can Mineral 15:500-507

Smith, G (1978) A reassessment of the role of iron in the 5,000-30,000 cm^{-1} region of the electronic absorption spectra of tourmaline. Phys Chem Minerals 3:343-373

Smith, G and Strens RGJ (1976) Intervalence transfer absorption in some silicate, oxide and phosphate minerals. In: The Physics and Chemistry of Minerals and Rocks, Strens, RGJ (ed.). New York: Wiley and Sons, pp. 583-612

Chapter 5

Characteristics of Intervalence Charge Transfer in Minerals

Introduction

The intense color of compounds which contain both Fe^{2+} and Fe^{3+} ions prompted the recognition of intervalence charge transfer (IVCT) transitions more than 30 years ago (Allen and Hush 1967). In the case of Fe^{2+}-Fe^{3+} compounds, these optical transitions correspond to the transfer of an electron from Fe^{2+} to Fe^{3+}. Studies of a large number of mixed-valence ion-pairs in chemical compounds (Robin and Day 1967; Allen and Hush 1967; Hush 1967) firmly established the experimental and theoretical basis of IVCT transitions. These studies provided a basis for the recognition of Fe^{2+}-Fe^{3+} charge transfer transitions in mineral spectra. Smith and Strens (1976) and Burns (1981) have reviewed IVCT assignments in minerals.

In spite of the predominance of Fe^{2+}-Fe^{3+} ion-pairs, the certain recognition of Fe^{2+}-Fe^{3+} charge transfer transitions in mineral spectra is often not possible. The characteristics of transitions which have been assigned to Fe^{2+}-Fe^{3+} charge transfer encompass wide variations. In addition, another effect of Fe^{2+}-Fe^{3+} interaction, intensified Fe^{2+} transitions, share many of the most frequently used characteristics of Fe^{2+}-Fe^{3+} charge transfer transitions (Chapter 3). The polarization of these transitions along the vector between the interacting cations is a well established characteristic which can be used, with a suitable structure, to differentiate ion-pair transitions from transitions within the d levels of a transition element

(crystal field transitions). The energy of Fe^{2+}-Fe^{3+} charge transfer transitions (Smith and Strens 1976) and temperature response (Smith 1977) have also been used as diagnostic criteria. These characteristics were established by empirical observations of limited examples of IVCT transitions in minerals. Most theoretical treatments of IVCT transitions which were developed for chemical systems do not support these characteristics (Creutz 1983; Day 1981). The width of Fe^{2+}-Fe^{3+} charge transfer transitions has also been proposed as a diagnostic characteristic (Smith and Strens 1976) but is often not considered.

Many of the uncertainties regarding the characteristics of IVCT transitions in minerals are due to an inadequate data base of unambiguous examples and the lack of a suitable theoretical framework. Amthauer and Rossman (1984) have examined stoichiometric Fe^{2+},Fe^{3+}-minerals which should provide definite examples of Fe^{2+}-Fe^{3+} charge transfer. The characteristics of these samples and previous, well-defined examples are examined in this paper to evaluate the reliability of diagnostic characteristics. The characteristics of these examples will be compared to theoretical predictions. Characteristics which could be used to differentiate Fe^{2+}-Fe^{3+} charge transfer from intensified Fe^{2+} transitions will also be discussed.

Experimental

The temperature dependence of Fe^{2+}-Fe^{3+} charge transfer was studied using samples previously examined by Amthauer and Rossman (1984) and euclase (GRR# 1/15/79) from Rhodesia (Miami area). The samples provided by Amthauer and Rossman include rockbridgeite (LA# 7603) from Hagendorf, Germany, babingtonite (CIT# 9883) from Bombay, India, and lazulite (LA# 4608) from Graves Mt., Georgia. The compositions of these samples are given in Table 2 of Amthauer and Rossman (1984). Chemical analysis of the euclase was obtained using a MAC5-SA5 electron microprobe. Blue zones contained 0.06% FeO, 35.1% Al_2O_3 and 42.1% SiO_2. BeO and H_2O could not be analyzed in this way. Data reduction was accomplished using the methods of Bence and Albee (1968).

Optical spectra were obtained in a manner similar to that described in Rossman (1975). Low temperature spectra were obtained by placing the sample on a coldfinger immersed in liquid nitrogen in a quartz dewar. Temperatures were monitored using a copper-constantan thermocouple placed sightly above the sample. Temperature variation during a spectrum was limited to 80 to 86 K. Room temperature spectra were measured in the same apparatus without moving the sample to insure quantitative comparisons.

Magnetic susceptibility measurements of powdered samples of rockbridgeite and babingtonite were taken on a S.H.E. model VTS magnetometer/susceptometer. Data for the empty Al sample container were used to correct the raw data.

Results and Discussion

Charge Transfer Energies

Fe^{2+}-Fe^{3+} charge transfer has been assigned to transitions which range in energy from 11500 cm^{-1} (Ferguson and Fielding 1971) to 17500 cm^{-1} (Rossman 1974). The energy of a charge transfer transition is related to the ionization potential of the donor cation (Fe^{2+} in this case) and the electron affinity of the acceptor cation. Although theoretical studies have made advances in the interpretation of the band area and the width of IVCT transitions, the energy has not proven amenable to quantitative interpretation nor a priori calculation (Day 1981; Creutz 1983). Smith and Strens (1976), however, found a linear correlation between Fe^{2+}-Fe^{3+} and Fe^{2+}-Ti^{4+} charge transfer energies and the separation of the interacting cations in silicate, oxide and phosphate minerals. These correlations have been used to assign transitions in minerals with known structures. Although the similarity of the nearest neighbor environment among these minerals may have left internuclear distance as the most important factor determining energy, the recent chemical studies referred to above would suggest that factors other than nearest neighbor anions and cation separation affect charge transfer energies. The correlation proposed by Smith and Strens can be reexamined in light of a large increase in the number of unambiguous examples of Fe^{2+}-Fe^{3+} charge transfer in minerals. Figure 1 shows the relationship between the energy of Fe^{2+}-Fe^{3+} charge transfer

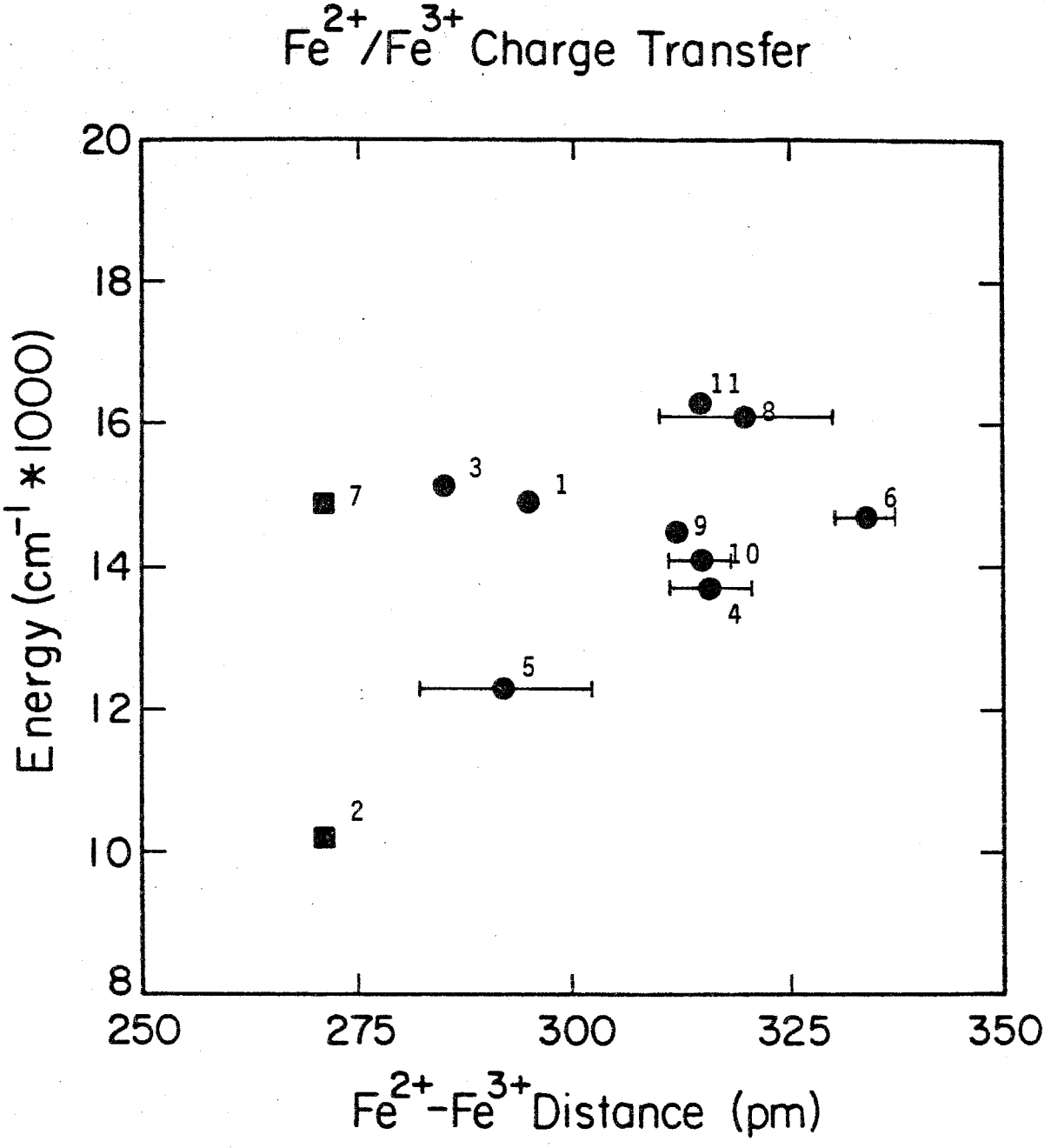

Fig. 1 Fe^{2+}-Fe^{3+} charge transfer transition energy vs internuclear distance. squares: face-shared octahedra circles: edge-shared octahedra Sample key: Table 1

and the distance between the cations for this expanded data set. The sources of the data included in this figure are presented in Table 1. No correlation between energy and distance is indicated. Although the specific energy of Fe^{2+}-Fe^{3+} charge transfer cannot be used diagnostically, Fe^{2+}-Fe^{3+} charge transfer transitions can be expected to fall between 10000 and 17000 cm^{-1}.

Effect of Temperature on Intensity

Many other transitions, particularly crystal field transitions, occur in the large energy range of Fe^{2+}-Fe^{3+} charge transfer transitions. The variation of intensity with temperature has been used extensively to differentiate charge transfer transitions in mineral spectra. An increase in intensity with decreasing temperature is taken to be characteristic of charge transfer transitions in general (Smith and Strens 1976; Smith 1977). This belief is based on empirical studies of Fe^{2+}-Fe^{3+} systems. Confidence in the reliability of this behavior is diminished by a previous lack of recognition of intensified Fe^{2+} transitions which appear to exhibit the same temperature response (Chapter 3). In addition, the general theoretical treatment of charge transfer transitions does not predict this behavior. The most familiar chemical example of Fe^{2+}-Fe^{3+} charge transfer in Prussian Blue exhibits very little change in intensity (Ludi 1980). In accord with the PKS theory (Wong and Schatz 1981), this transition shows no detectable increase in integrated intensity with decreasing temperature. However,

Table 1 Sample Key to Fig. 1

Mineral	Fig. 1 code	Source of Optical Data	Source of Structural Data
Euclase	1	this paper	Mrose & Appleman (1962)
Rockbridgeite	2	"	Moore (1970)
Vivianite	3	Amthauer & Rossman (1984)	Mori & Ito (1970)
Aegirine	4	"	Clark et al. (1969)
Ilvaite	5	"	Beran & Bittner (1974)
Babingtonite	6	"	Araki & Zoltai (1972)
Lazulite	7	"	Moore (1970)
Glaucophane	8	Burns (1970)	Papike & Clark (1968)
Orthopyroxenes	9	"	Burnham et al. (1971)
Biotite	10	Smith (1977)	Hazen & Burnham (1973)
Chloritoid	11	Hålenius et al. (1981)	Hanscom (1975)

the Fe^{2+} ions in Prussian Blue are distinctly different from those in most minerals in one important sense, they are diamagnetic ions which cannot interact magnetically with their Fe^{3+} neighbors. Cox (1980) and Girerd (1983) have suggested that magnetic exchange will alter the temperature response of charge transfer transitions. A larger data set of unambiguous examples of Fe^{2+}-Fe^{3+} charge transfer is required to evaluate the reliability of an inverse temperature response as a diagnostic characteristic.

Amthauer and Rossman (1984) have coupled Mössbauer and optical studies of Fe^{2+}-Fe^{3+} minerals to quantitatively characterize Fe^{2+}-Fe^{3+} charge transfer. The temperature response of Fe^{2+}-Fe^{3+} charge transfer in these samples is presented here. Lazulite, $MgAl_2(PO_4)_2(OH)_2$, contains Fe^{2+} and Fe^{3+} ions in face-sharing Mg and Al octahedra (Moore 1970). A transition at 668 nm has been assigned to Fe^{2+}-Fe^{3+} charge transfer. Figure 2 illustrates the gamma-polarized spectrum of lazulite at 296 K and 83 K. The area of the 668 nm band increases by 9% at 83 K. This behavior contrasts sharply with the temperature response of crystal field transitions. The area of a crystal field transition either decreases with decreasing temperature or remains constant.

Figure 3 illustrates the beta-polarized spectrum of euclase, $BeAlSiO_4OH$. Iron cations occur in edge-shared octahedral chains predominantly occupied by aluminum (Mrose and Appleman 1962). These spectra point out the difficulty

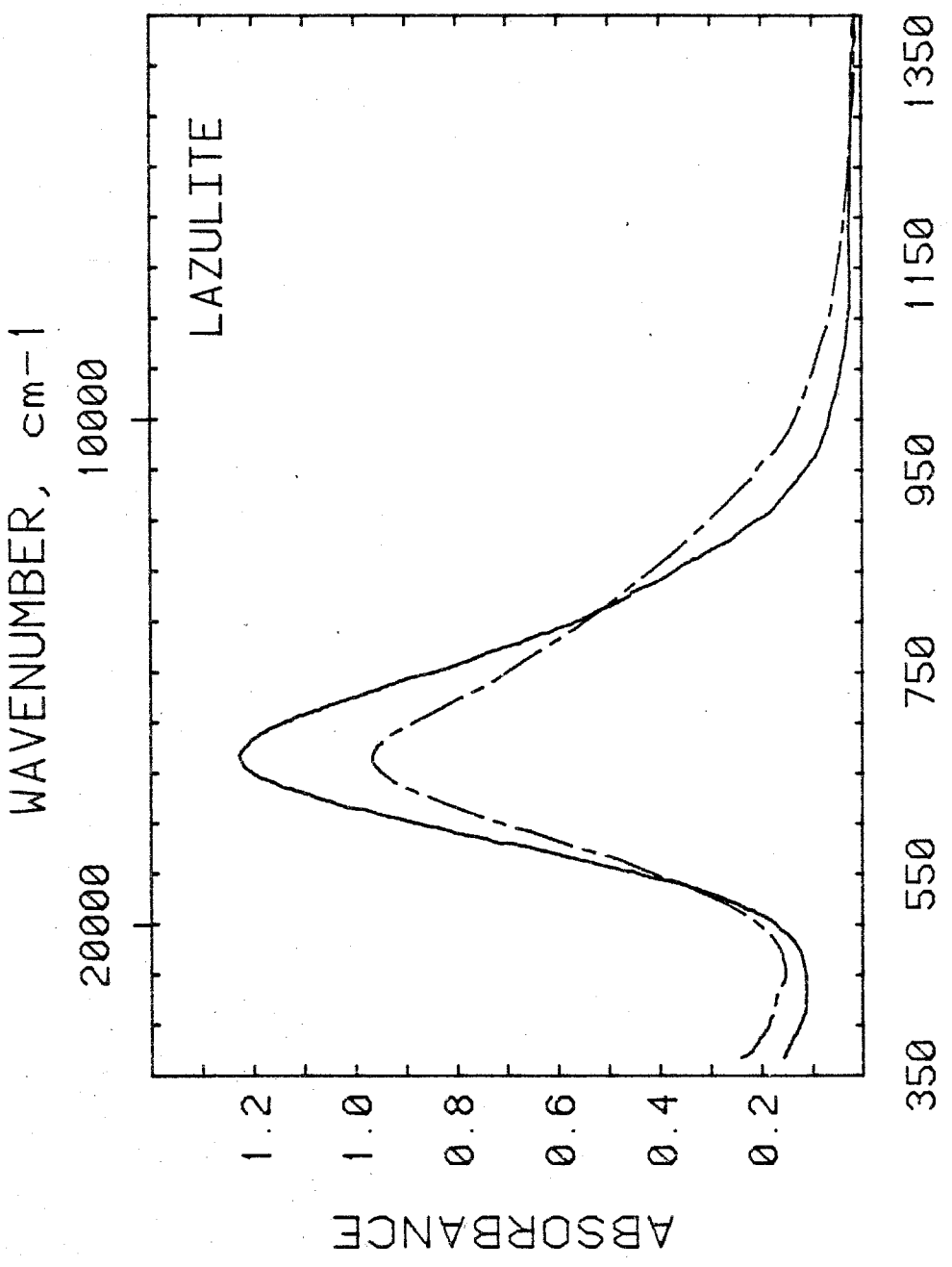

Fig. 2 E⊥Z polarized absorption spectra of lazulite. Sample thickness = 0.092 mm
Temperatures: 296 K -- broken line 83 K -- solid line

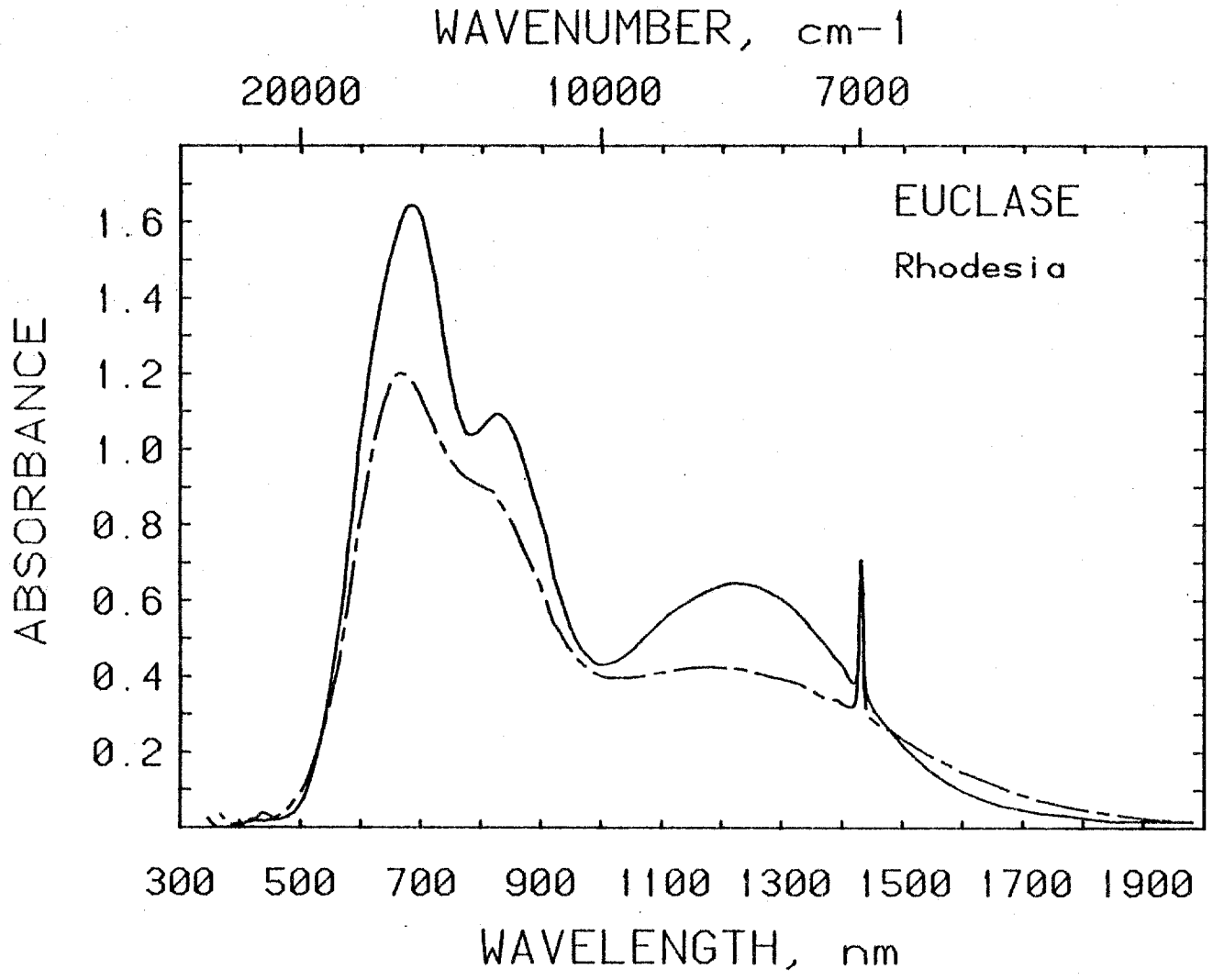

Fig. 3 E⊥Y polarized absorption spectra of euclase. Sample thickness = 0.300 mm
Temperatures: 296 K -- broken line 83 K -- solid line

of distinguishing Fe^{2+}–Fe^{3+} charge transfer from intensified Fe^{2+} transitions. At most Fe^{2+}–Fe^{3+} and Fe^{2+}–Ti^{4+} charge transfer transitions would be expected to contribute to this spectrum. However, three transitions exhibit intensity increases at low temperature. The two transitions at 860 and 1250 nm have wavelengths typical of Fe^{2+} transitions and have slightly different intensity ratios in different polarizations than does the 670 nm band. The restriction of Fe^{2+} ions to one site and the width of the 670 nm band (~4000 cm^{-1}) permits an assignment to Fe^{2+}–Fe^{3+} charge transfer. The area of the 670 nm transition increases by 20% at 83 K. Similar increases characterize the 860 and 1250 nm bands.

The inhomogeneity of the lazulite and euclase samples did not permit a comparison of their temperature responses with magnetic behavior as measured by magnetic susceptibility. However, the magnetic and optical properties of rockbridgeite, $(Fe^{2+},Mn)Fe^{3+}_4(PO_4)_3(OH)_5$, and babingtonite, $Ca_2(Fe^{2+},Mn)Fe^{3+}Si_5O_{14}OH$, can be correlated and provide a significant test of the theories of Cox (1980) and Girerd (1983). Figure 4 illustrates the variation of the intensity of Fe^{2+}–Fe^{3+} charge transfer (980 nm) in rockbridgeite with temeperature. A 10% increase in area is observed at 83 K. The temperature response of Fe^{2+}–Fe^{3+} charge transfer (680 nm) in babingtonite is shown in Fig. 5. This transition maintains an approximately constant area at 296 and 83 K. Cox and Girerd both agree that ferromagnetic exchange should

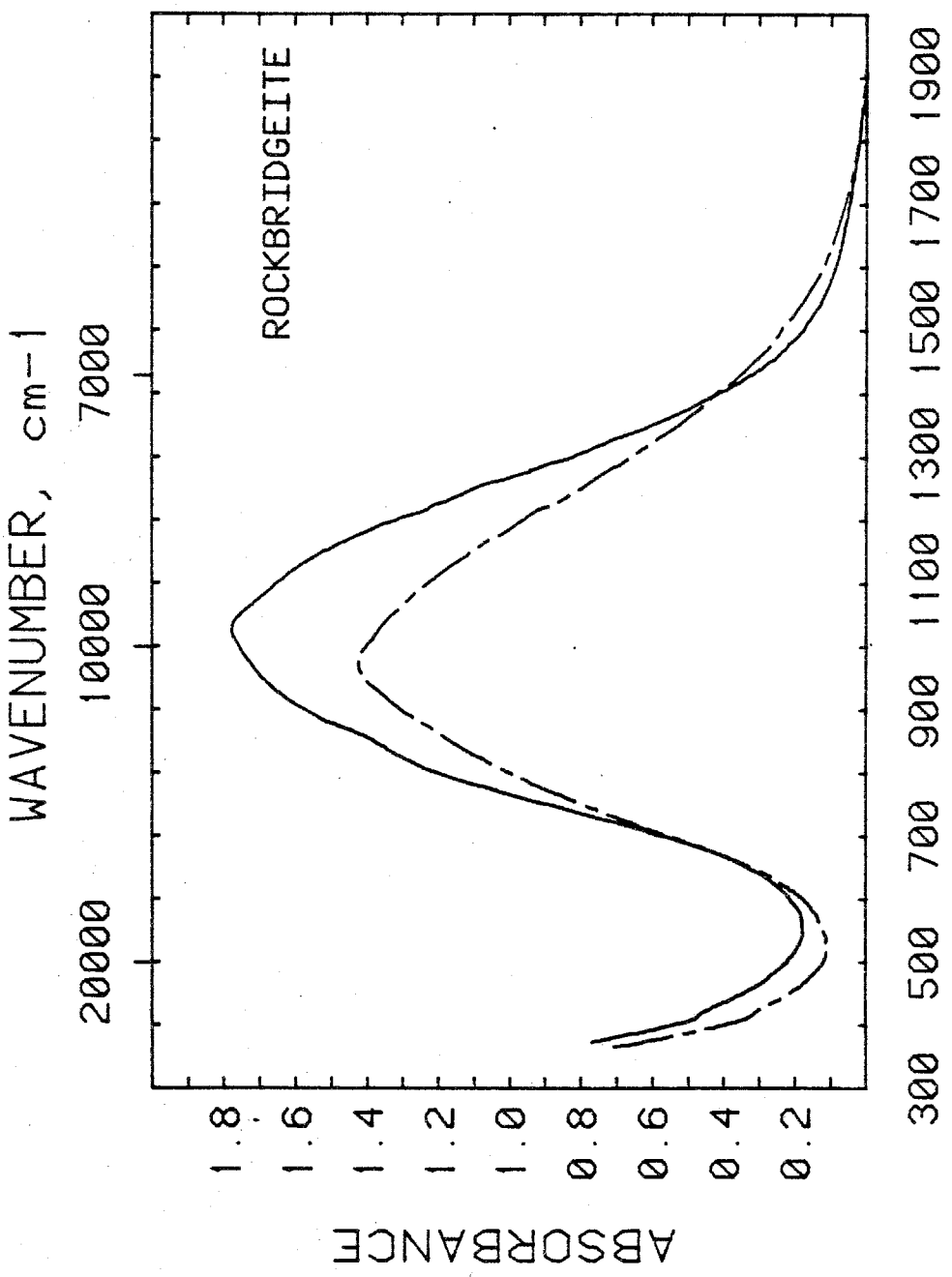

Fig. 4 E⊥Z polarized absorption spectra of rockbridgeite. Sample thickness = 0.060 mm
Temperatures: 296 K -- broken line 83 K -- solid line

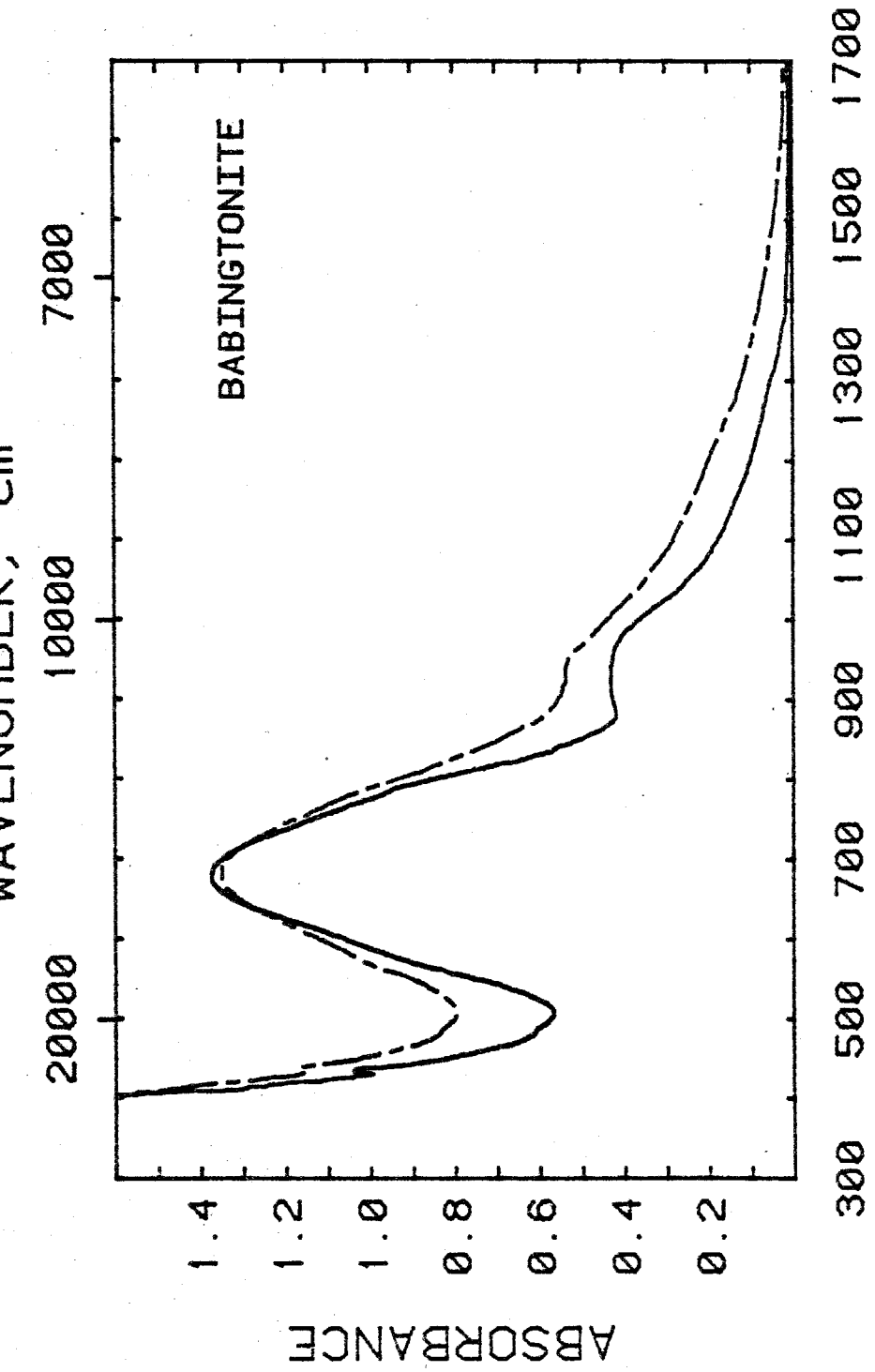

Fig. 5 E⊥c polarized absorption spectra of babingtonite. Sample thickness = 0.077 mm
Temperatures: 296 K -- broken line 83 K -- solid line

produce an intensity increase at low temperature and that antiferromagnetic exchange produces an intensity decrease at low temperature. Figures 6 and 7 illustrate the effective magnetic moment per iron atom at various temperatures for rockbridgeite and babingtonite, respectively. The nature of the magnetic interaction can be determined through a qualitative examination of these data. An antiferromagnetic interaction below 30 K is indicated in babingtonite. Between 296 and 83 K, however, no magnetic interaction is evident. The lack of an intensity increase at low temperature is consistent with the theoretical expectation. Rockbridgeite exhibits multiple magnetic interactions which may be related to interactions within and among different clusters. A transition to a ferromagnetic region occurs at ~100 K. The proposed effect of this behavior is confirmed by the observed increase in charge transfer intensity at low temperature.

Although these results confirm the theories of Cox and Girerd, a consideration of Fe^{2+}-Ti^{4+} charge transfer indicates that other factors may also produce a temperature variation. Fe^{2+}-Ti^{4+} charge transfer generally exhibits smaller changes in intensity with temperature than Fe^{2+}-Fe^{3+} charge transfer (Smith 1977), but these theories would not predict any change because Ti^{4+} cannot interact magnetically. A 15% increase in the integrated intensity of Fe^{2+}-Ti^{4+} charge transfer in tourmaline occurs for a temperature change of 296 to 83 K (Chapter 4). The failure

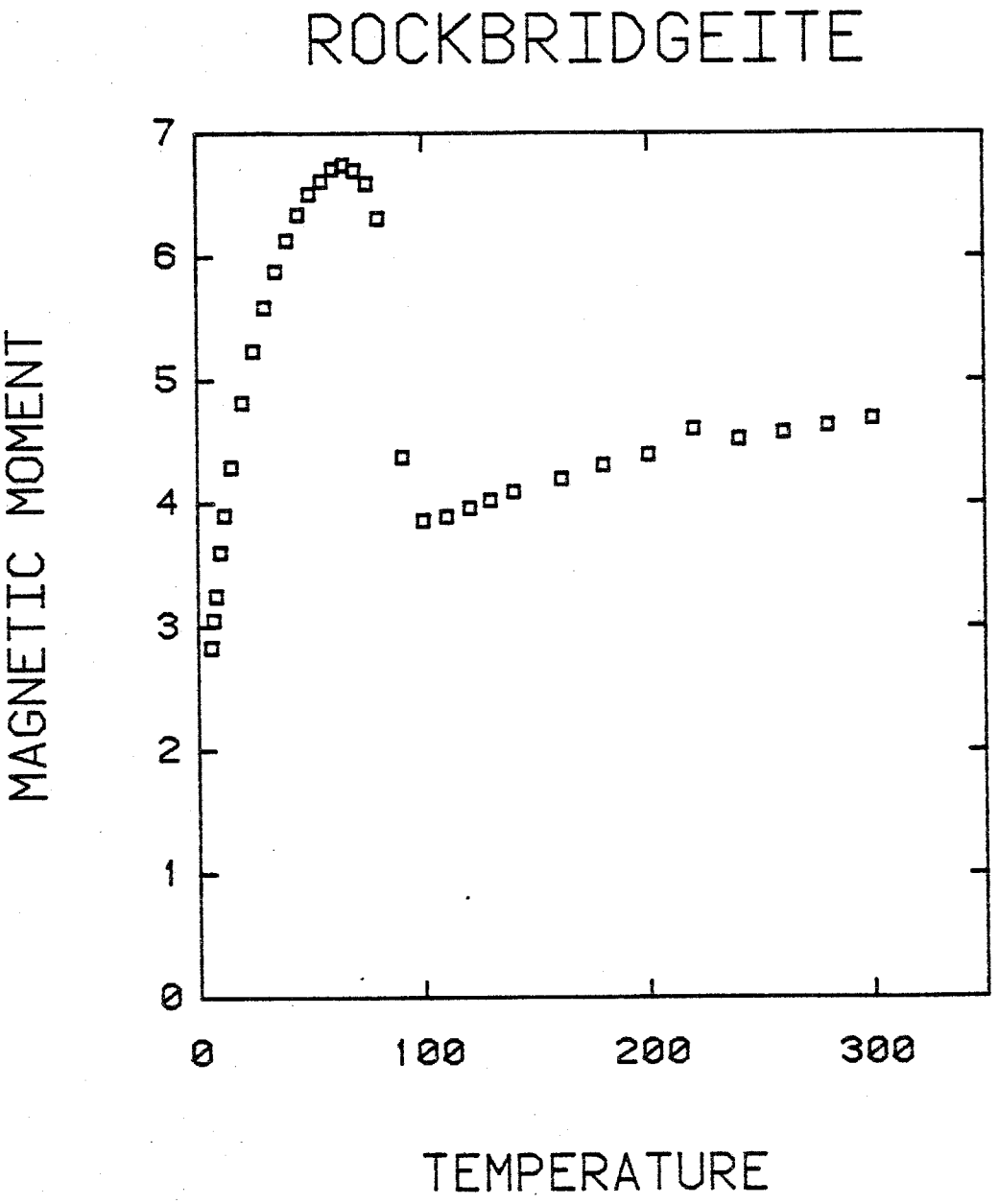

Fig. 6 Temperature (K) dependence of the effective magnetic moment (B.M.) of rockbridgeite

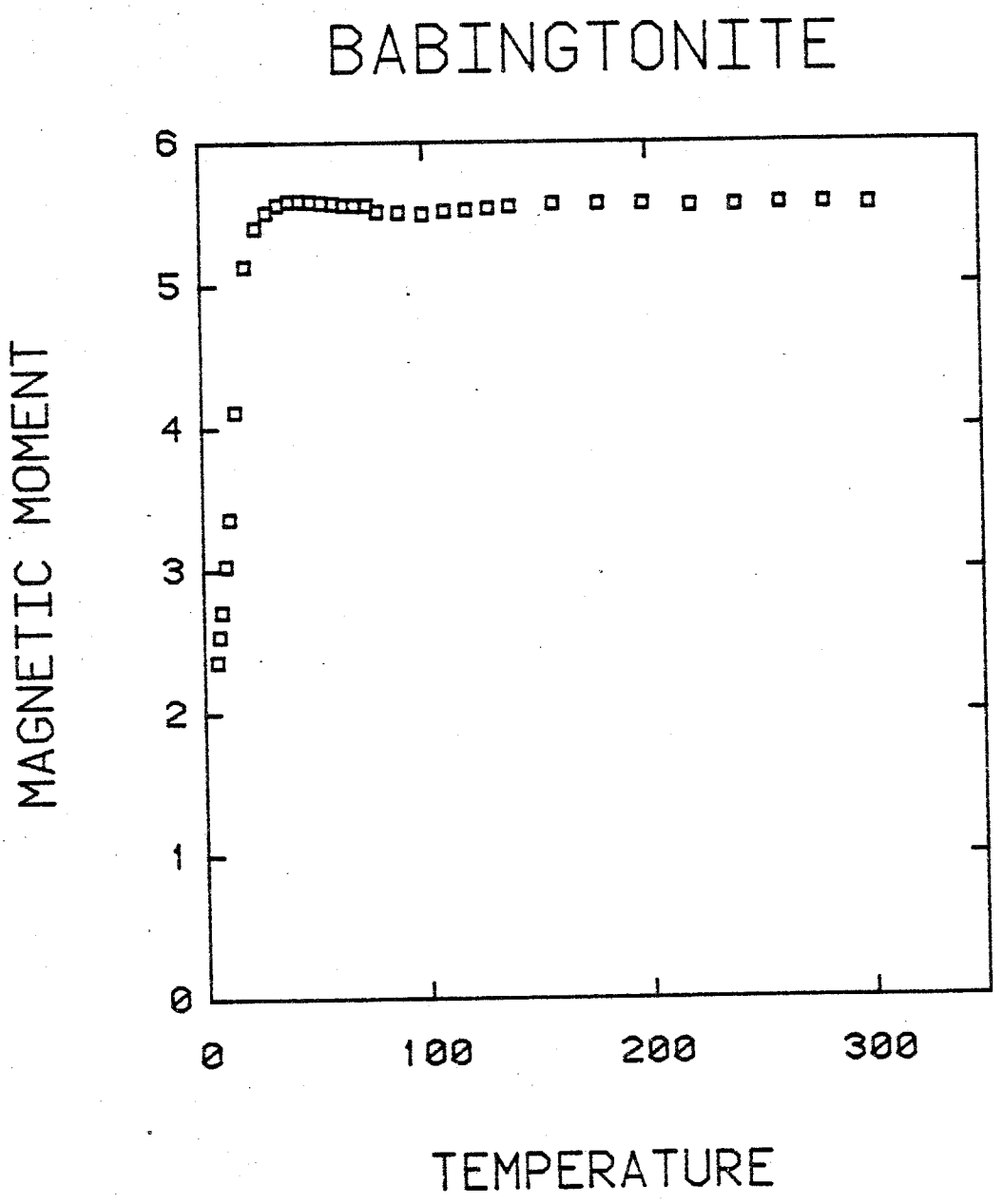

Fig. 7 Temperature (K) dependence of the effective magnetic moment (B.M.) of babingtonite

to account for intensity increase of Fe^{2+}-Ti^{4+} charge transfer transitions may be related to a possible limitation of the general theories for intervalence charge transfer which are focused upon symmetric, homonuclear systems.

Both experimental and theoretical studies indicate that IVCT transitions may not increase in intensity with decreasing temperature. Thus a decrease or lack of change in intensity does not eliminate a charge transfer assignment. In addition, an increase in intensity does not necessarily indicate a charge transfer assignment because intensified crystal field transitions exhibit the same behavior.

Widths of Charge Transfer Transitions

In a popular theoretical formulation by Hush (1967) the 300 K bandwidth at half intensity (Γ -- in cm^{-1}) of an IVCT transition is related to its energy (E) by the following formula:

$$\Gamma^2 = 2310 * (E - E_o)$$

where E_o is the difference in zero point energy between the two cations. IVCT transitions between cations in identical sites ($E_o = 0$) which have energies between 10000 and 17000 cm^{-1} would thus be expected to have halfwidths of 4800-6300 cm^{-1}. Theories which incorporate vibronic effects (Wong and Schatz 1981) suggest that these values are applicable to strongly localized systems. IVCT transitions of systems in which discrete valences are not distinguishable have much smaller halfwidths (Creutz 1983). The halfwidths of some

well established mineralogical examples of Fe^{2+}–Fe^{3+} charge transfer are shown in Table 2. The halfwidths of crystal field transitions may be as low as 100 cm^{-1} and generally do not exceed 3500 cm^{-1}. Intensified Fe^{2+} transitions maintain the energy and width of the related transitions of non-interacting Fe^{2+}. Thus the evaluation of transition widths should permit the differentiation of IVCT transitions from crystal field transitions and intensified Fe^{2+} transitions. As can be seen in Table 2, the majority of Fe^{2+}–Fe^{3+} charge transfer transitions have widths which agree with that predicted by Hush. However, a few of the transitions assigned to Fe^{2+}–Fe^{3+} charge transfer have widths which are low enough to overlap with the widths of crystal field transitions. Delocalized valences could produce a lower width as indicated above, but Mössbauer spectra of biotite (Annersten 1974) indicate very little delocalization. Very different local environments of Fe^{2+} and Fe^{3+} could also produce a small decrease in width but would not be expected to be more significant in biotite than the other minerals presented in Table 2. It is possible that a better assignment of the transitions in biotite and chlorite would be intensified Fe^{2+} transitions, but such an assignment eliminates Fe^{2+}–Fe^{3+} charge transfer from the spectrum. The relative influence of these two different effects of Fe^{2+}–Fe^{3+} interaction is not known. Thus, while a large halfwidth undoubtedly indicates a charge transfer transition, further studies are required to differentiate

Table 2 Widths of Fe^{2+}-Fe^{3+} Charge Transfer Transitions

Mineral	Energy (cm^{-1})	Halfwidth (cm^{-1})	Reference
Lazulite	14900	5250	Amthauer & Rossman (1984)
Euclase	14900	~4000	this paper
Rockbridgeite	10200	~5200	"
Babingtonite	14700	~6000	"
Voltaite	16500	~5000	Beveridge & Day (1979)
Glaucophane	16130	6600	Smith & Strens (1976)
Biotite	14300	3150	"
Chlorite	14100	3575	"

broad crystal field transitions from IVCT transitions.

As was indicated in Chapter 4, Fe^{2+}-Ti^{4+} charge transfer transitions have halfwidths which range between 6500 and 9000 cm^{-1}. Halfwidth is definitely the most reliable criterion to identify these transitions.

Summary

Charge transfer transitions occur in mineral spectra together with crystal field transitions and intensified crystal field transitions. Many of the characteristics ascribed to charge transfer transitions have not proven accurate or unique. Transition energies can rarely be used to differentiate crystal field and charge transfer transitions. An inverse temperature response of intensity is shared by intensified Fe^{2+} transitions and is not necessarily expected of charge transfer transitions. Polarization along the vector between the interacting cations is also characteristic of intensified Fe^{2+} transitions. Large halfwidths are generally the most reliable characteristic of charge transfer transitions. However, some overlap with crystal field transitions cannot be dismissed. The response of crystal field and charge transfer transitions to pressure variations (Abu-Eid 1976; Mao 1976) have been examined and may prove to be a useful diagnostic tool. As yet, however, intensified Fe^{2+} transitions have not been studied at variable pressures. A combination of width, temperature response and polarization behavior should permit the differentiation of single ion

transitions and ion-pair transitions. The differentiation of intensified Fe^{2+} transitions and Fe^{2+}-Fe^{3+} charge transfer transitions is limited primarily by the uncertainty regarding widths of charge transfer transitions.

REFERENCES

Abu-Eid, RM (1976) Absorption spectra of transitions metal bearing minerals at high pressures. In: The Physics and Chemistry of Minerals and Rocks, Strens RGJ (ed.). London: Wiley and Sons, pp. 641-675

Allen, GC and Hush, NS (1967) Intervalence transfer absorption. Part 1. Qualitative evidence for intervalence-transfer absorption in inorganic systems in solution and in the solid state. Prog Inorg Chem 8:357-389

Amthauer, G and Rossman, GR (1984) Mixed valence of iron in minerals with cation clusters. Phys Chem Minerals 11:37-51

Annersten, H (1974) Mössbauer studies of natural biotites. Am Mineral 59:143-151

Araki, T and Zoltai, T (1972) Crystal structure of babingtonite. Z Kristallogr 135:355-373

Bence, AE and Albee, AL (1968) Empirical correction factors for electron microanalysis of silicates and oxides. J Geol 76:382-403

Beran, A and Bittner, H (1974) Untersuchungen zur Kristallchemie des Ilvaits. Tschermaks Mineral Petrogr Mitt 21:11-29

Beveridge, D and Day, P (1979) Charge transfer in mixed-valence solids. Part 9. Preparation, characterization, and optical spectroscopy of the mixed-valence mineral voltaite [aluminum pentairon(II) tri-iron(III)

dipotassium dodecasulphate 18-hydrate] and its solid solutions with cadmium(II). J Chem Soc, Dalton Trans 1979:648-653

Burnham, CW, Ohashi, Y, Hafner, SS and Virgo, D (1971) Cation distribution and atomic thermal vibrations in an iron-rich orthopyroxene. Am Mineral 56:850-876

Burns, RG (1970) Mineralogical Applications of Crystal Field Theory. Cambridge: Cambridge Univ. Press. 224 pp.

Burns, RG (1981) Intervalence transitions in mixed-valence minerals of iron and titanium. Ann Rev Earth Planet Sci 9:345-383

Clark, JR, Appleman, DE and Papike, JJ (1969) Crystal-chemical characterization of clinopyroxenes based on eight new structure refinements. Mineral Soc Am Special Paper 2:31-50

Cox, PA (1980) Electron transfer between exchange-coupled ions in a mixed-valency compound. Chem Phys Lett 69:340-343

Creutz, C (1983) Mixed valence complexes of d^5-d^6 metal centers. Prog Inorg Chem 30:1-73

Day, P (1981) Theory and experiments on valence delocalization in mixed-valence compounds. Comments Inorg Chem 1:155-167

Ferguson, J and Fielding, PE (1971) The origins of the colours of yellow, green and blue sapphires. Chem Phys Lett 10:262-265

Girerd, J-J (1983) Electron transfer between magnetic ions in mixed valence binuclear systems. J Chem Phys 79:1766-1775

Hålenius, U, Annersten, H and Langer, K (1981) Spectroscopic studies on natural chloritoids. Phys Chem Minerals 7:117-123

Hanscom, RH (1975) Refinement of the crystal structure of monoclinic chloritoid. Acta Crystallogr B31:780-784

Hazen, RM and Burnham, CW (1973) The crystal structures of one-layer phlogopite and annite. Am Mineral 58:889-900

Hush, NS (1967) Intervalence-transfer absorption. Part 2. Theoretical considerations and spectroscopic data. Prog Inorg Chem 8:391-444

Ludi, A (1980) Descriptive chemistry of mixed-valence compounds. In: Mixed-Valence Compounds. Theory and Applications in Chemistry, Physics, Geology and Biology, Brown DB (ed.). Holland: Reidel, pp. 25-47

Mao, HK (1976) Charge transfer processes at high pressure. In: The Physics and Chemistry of Minerals and Rocks, Strens RGJ (ed.). London: Wiley and Sons, pp. 573-581

Moore, PB (1970) Crystal chemistry of the basic iron phosphates. Am Mineral 55:135-169

Mori, H and Ito, T (1970) The structure of vivianite and symplesite. Acta Crystallogr 3:1-6

Mrose, ME and Appleman, DE (1962) The crystal structures and the crystal chemistries of väyrynenite, (Mn,Fe)$BePO_4OH$, and euclase, $BeAlSiO_4OH$. Z Kristallogr 117:16-36

Papike, JJ and Clark,J (1968) The crystal structure and cation distribution of glaucophane. Am Mineral 53:1156-1173

Robin, MB and Day, P (1967) Mixed valence chemistry--a survey and classification. Adv Inorg Chem Radiochem 10:248-422

Rossman, GR (1974) Lavender jade. The optical spectrum of Fe^{3+} and $Fe^{2+} - Fe^{3+}$ intervalence charge transfer in jadeite from Burma. Am Mineral 59:868-870

Rossman, GR (1975) Spectroscopic and magnetic studies of ferric iron hydroxy sulfates: intensification of color in ferric iron clusters bridged by a single hydroxide ion. Am Mineral 60:698-704

Smith, G (1977) Low-temperature optical studies of metal-metal charge-transfer transitions in various minerals. Can Mineral 15:500-507

Smith, G and Strens RGJ (1976) Intervalence transfer absorption in some silicate, oxide and phosphate minerals. In: The Physics and Chemistry of Minerals and Rocks, Strens, RGJ (ed.). New York: Wiley and Sons, pp. 583-612

Wong, KY and Schatz, PN (1981) A dynamic model for mixed-valence compounds. Prog Inorg Chem 28:369-449

Chapter 6

Summary

The prevalence of ion-pair interactions in minerals which contain edge- or face-sharing octahedra is indicated by the number of distinct ion-pair transitions which were recognized in tourmalines. These assignments were made possible by the great compositional diversity of the tourmaline group. In general, however, the qualitative interpretation of mineral spectra relies upon the characteristics of specific transitions which are relatively invariant. Minerals with stoichiometric concentrations of the desired cations can be used to obtain quantitative absorption intensities as well as reliable qualitative characteristics. These minerals were generally emphasized in this study.

The pleochroism of tourmalines, particularly macroscopically black samples, is frequently related to what appear to be extremely anisotropic Fe^{2+} transitions to the casual observer. An indication that they are not ordinary Fe^{2+} transitions is evident in intensity increases of these transitions in the most intense polarization upon partial oxidation of Fe^{2+} in the sample. The quantitative relationship of intensity to Fe^{2+}-Fe^{3+} pairs was determined through combined optical and Mössbauer studies. The intensity of Fe^{2+} absorption in Fe^{2+}-Fe^{3+} pairs is ~1200 $M^{-1}cm^{-1}$. This is much larger than the molar absorptivities associated with the most distorted sites and compares to a value of ~5 $M^{-1}cm^{-1}$ for non-interacting Fe^{2+} in tourmaline. This large change in intensity should provide a sensitive

probe of Fe^{3+} ions. Such considerations have been employed to monitor the effects of gamma irradiation. The most useful characteristics which can be used to differentiate these transitions from unintensified bands are the polarization characteristics and the general increase in intensity with decreasing temperature. These distinctions are essential if crystal field transitions are to be used quantitatively. The differentiation of Fe^{2+}-Fe^{3+} charge transfer transitions from intensified Fe^{2+} transitions is somewhat more difficult. In principle, the characteristic width of Fe^{2+} crystal field transitions which is maintained by the intensified transitions should be distinctly lower than Fe^{2+}-Fe^{3+} charge transfer transitions. However, a few transitions which have been assigned to Fe^{2+}-Fe^{3+} charge transfer have unusually low widths.

The concentrated Fe,Ti-minerals which have been examined have been characterized by consistent features which should be easily differentiated from both crystal field and Fe^{2+}-Fe^{3+} charge transfer transitions. The wavelengths of Fe^{2+}-Ti^{4+} charge transfer in the samples examined in this study and those that have been previously assigned with certainty lie between 400 and 500 nm. They are also characterized by extremely large halfwidths which range between 6500 and 9000 cm^{-1}. Some uncertainty regarding the assignment of transitions between 500 and 600 nm is produced when sapphire is considered. The difference in face-sharing and edge-sharing systems cannot be evaluated

presently. In contrast to the consistency of the width and energy, absorptivities vary between 200 and 4000 $M^{-1}cm^{-1}$. Thus although Fe^{2+}-Ti^{4+} charge transfer should be recognizable in mineral spectra, quantitative interpretations will have to be based on calibrations of specific systems.

It is somewhat ironic that these transitions appear to have consistent features and that the characteristics of well established transitions were brought into question by this study. Intensified Fe^{3+} transitions have been studied extensively in chemical systems and the characteristics of these transitions compare well with most mineralogical examples. The transitions of Fe^{3+} in tourmaline, however, bear little resemblance to them. The transition energy of one Fe^{3+} ion-pair is much lower than that of both unintensified and intensified examples of Fe^{3+} transitions and has a much larger width. The second possesses very unusual intensity ratios of components of the three Fe^{3+} transitions. Other characteristics such as polarization and magnitude of the intensity increase are consistent among all groups. These assignments were based upon optical studies of samples which were partially reduced and oxidized and comparisons within a group of Fe^{3+}-rich samples. In addition, a very similar spectrum is exhibited by coalingite.

An empirical correlation between cation separation and charge transfer energy has been used diagnostically as well

as an expected increase in intensity with decreasing temperature. A review of the characteristics of Fe^{2+}-Fe^{3+} charge transfer transitions with emphasis on the relationship of intensity to temperature did not permit these characteristics and left halfwidth as the only generally reliable characteristic. The correlation of temperature response to magnetic exchange in 2 Fe^{2+}-Fe^{3+} minerals was found to support recent theoretical proposals by Cox and Girerd. The temperature response of Fe^{2+}-Ti^{4+} charge transfer, however, could not be accommodated by theory.

Appendix

OH Vibrations as a Chemical Probe in Tourmaline

Investigations of the infrared spectra of micas and other sheet silicates (Farmer 1974) and amphiboles (Strens 1974) have demonstrated the variation of OH vibration frequency with the cations which are bonded to the OH group. Frequency shifts can be correlated to changes in the electronegativity and the charge of the cations. Increases in electronegativity and charge shift the OH stretching vibration to lower energy. These variations can be used to differentiate among the various tourmaline end members and the two basic tourmaline compositional series.

Hydroxyl groups in tourmaline occur in two different crystallographic environments which are illustrated in Fig. 1. The labels in this figure are related to the formula $XY_3Z_6Si_6O_{18}(BO_3)_3(OH)_4$. One (O(1)H) out of four OH ions per formula unit is coordinated to three Y-site cations. The remaining three (O(3)H) are bonded to one Y-site cation and two Z-site cations. Because the Y-site cations are generally divalent or have an average charge of +2 and the Z-site cations are generally trivalent, these two OH groups are separated in frequency. In addition, the O(1)H vibration is shifted to higher energy because the OH group points toward the X-site cation, further increasing this separation. Variations in the X-, Y-, and Z-site cations as well as hydrogen and X-site vacancies give rise to 4-7 distinct bands.

Polarized spectra of polished ac sections were obtained using a Cary 17I spectrophotometer and Glan-Thomson calcite

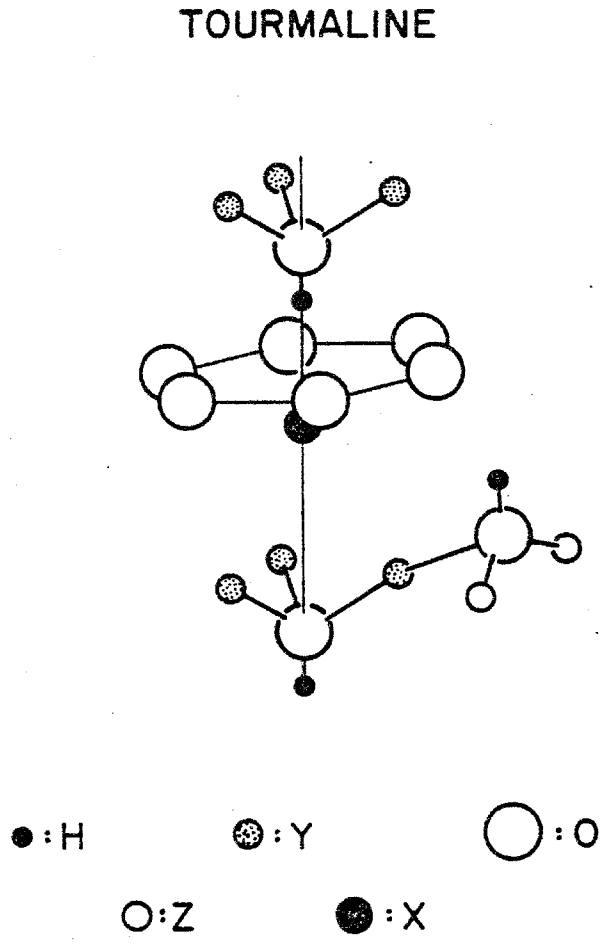

Fig. 1 A portion of the tourmaline structure selected to show the environment of the OH groups. The thin vertical line is the c-axis. (Taken from Gebert and Zemann (1965))

Table 1 Sample Descriptions

Sample	Color	Locality	Archival Code
D1	brown	Yinnietharra, Australia	CIT# 12683
D2	brown	Bryant Lake, NY	CIT# 12684
T16	colorless	Madagascar	CIT# 13657
EC	colorless	Afghanistan	GRR# 1/27/80
EB4	blue	Afghanistan	GRR# 1/27/80
T22	black	Blue Lady Mine, San Diego Co., CA	GRR# 8/10/83

Table 2 Electron Microprobe Analyses of Tourmalines

Sample	Na_2O	CaO	MgO	FeO	MnO	TiO_2	Al_2O_3	ZnO	SiO_2	F
EC	1.89	0.28	BDL	0.08	1.90	BDL	41.8	NA	37.5	0.9
EB4	2.75	0.30	BDL	3.67	2.17	0.02	37.6	0.22	37.1	1.8
T22	2.01	0.06	BDL	12.2	0.89	0.04	35.0	0.59	35.2	1.4
T16	0.75	3.92	BDL	0.18	0.21	0.02	39.1	NA	37.4	1.5
D1	2.93	0.37	11.6	0.46	BDL	1.09	32.0	NA	37.2	0.1
D2	0.77	4.25	14.3	0.38	BDL	0.58	28.7	NA	36.5	0.3

BDL -- below detection limits NA -- not analyzed

polarizers. Descriptions and compositions of the tourmalines discussed here are presented in Tables 1 and 2. Samples which were used for optical studies were too thick for examination of the fundamental vibrations between 3800 and 3450 cm^{-1}. The first overtone vibrations between 7400 and 6800 cm^{-1} (1350-1500 nm) which are much less intense were utilized. The E"$\subseteq$ polarization of these transitions indicates an orientation of the OH vector along the c-axis (Gebert and Zemann 1965).

Variations in the charge of the X-, Y- and Z-site cations produce the major OH bands in Fe,Mg-tourmalines. Figure 2 illustrates the spectrum of a dravite and Figure 3 the spectrum of a uvite. Both samples deviate from the end member compositions by containing ~1% TiO_2. The largest band (1430 nm) can be assigned to the most abundant group in both samples -- Mg(Y)Al(Z)$_2$O(3)H. The O(1)H bands are the lowest wavelength bands (excluding the non OH band at 1310 nm) and can be assigned by comparison of these two spectra. Dravites and uvites differ in the X-site cation toward which this hydroxyl group is directed. Dravites contain predominantly Na^+ in this site and uvites contain Ca^{2+}. Their comparison indicates the assignment of Ca(X)Mg(Y)$_3$O(1)H to the 1350 nm band and Na(X)Mg(Y)$_3$O(1)H to the 1370 nm band. Uvites also differ from dravites in the Z site. Excess Mg which enters the Z-site (normally occupied by Al) and H-defects charge compensate for the Ca^{2+} ion (Dunn et al. 1977a). Mg(Y)Mg(Z)Al(Z)O(3)H groups are

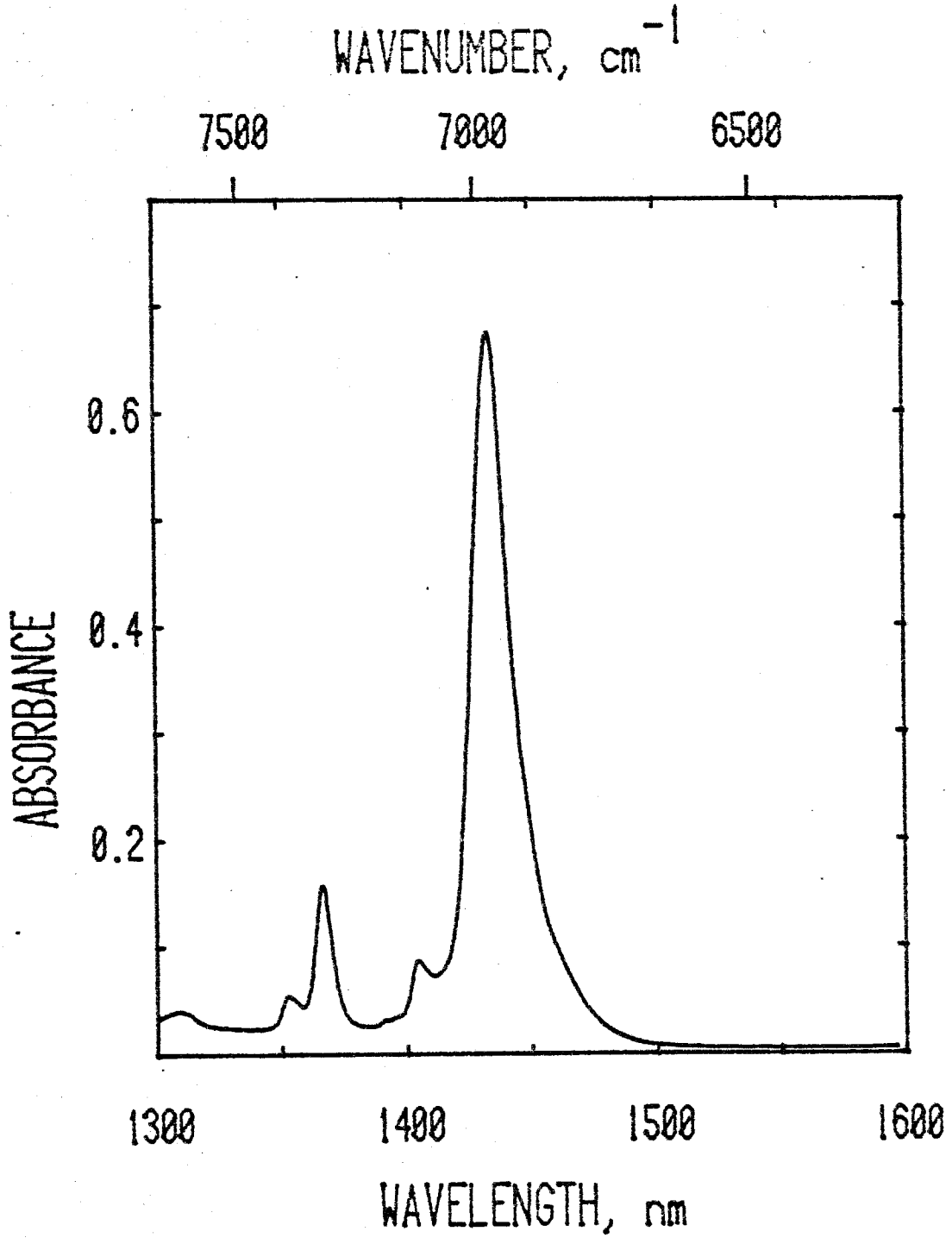

Fig. 2 E⊥c polarized absorption spectrum of tourmaline D1.

Sample thickness = 0.680 mm

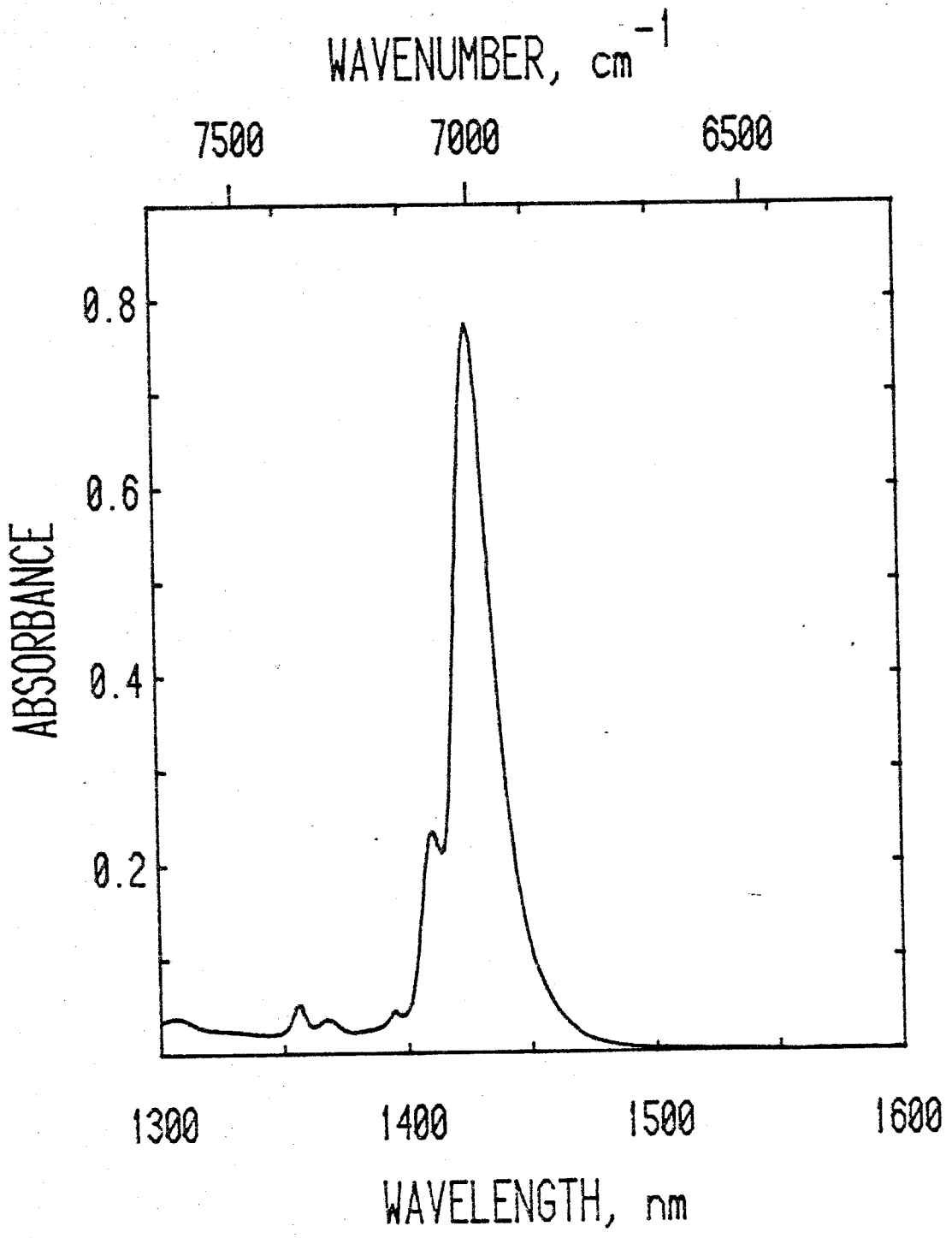

Fig. 3 E⊥c polarized absorption spectrum of tourmaline D2

Sample thickness = 0.738 mm

expected to absorb at a lower wavelength than the 1430 nm band. The band at 1410 nm in Fig. 3 can be assigned to this group. Na vs Ca is also indicated by a slight shift of the 1430 nm band to lower wavelength in uvites. OH bands which absorb in the region 1370-1410 nm are related to charge differences in the Y site and cannot be assigned by simple comparison.

These spectra are distinctly different from those of the elbaite-schorl compositional series. Figure 4 illustrates the spectrum of a sample which is representative of the elbaite end member (X=Na Y=Li,Al Z=Al). The most common groups in this composition are $Li(Y)Al(Z)_2O(3)H$ and $Al(Y)Al(Z)_2O(3)H$. The two largest bands can be assigned to these groups. The charge difference between these groups would indicate the assignment of the 1470 nm band to $Al(Y)Al(Z)_2O(3)H$ and the 1425 nm band to $Li(Y)Al(Z)_2O(3)H$. This can be confirmed by comparison to liddicoatite (X=Ca Y=Li,Al Z=Al). Charge compensation for Ca is attained by excess Li and H-defects (Dunn et al. 1977b). Excess Li is evident by the increase in the intensity ratio of the 1420 nm band and the 1465 nm band (Fig. 5). In addition to this difference, the effect of Ca can also be seen as shifts of the two major bands to lower wavelength. The higher wavelength shoulders can be related to a small amount of Na. The influence of Ca is much more difficult to see in the O(1)H bands. Large amounts of Mn and Fe can substitute into both elbaite-liddicoatites and dravite-uvites but do not

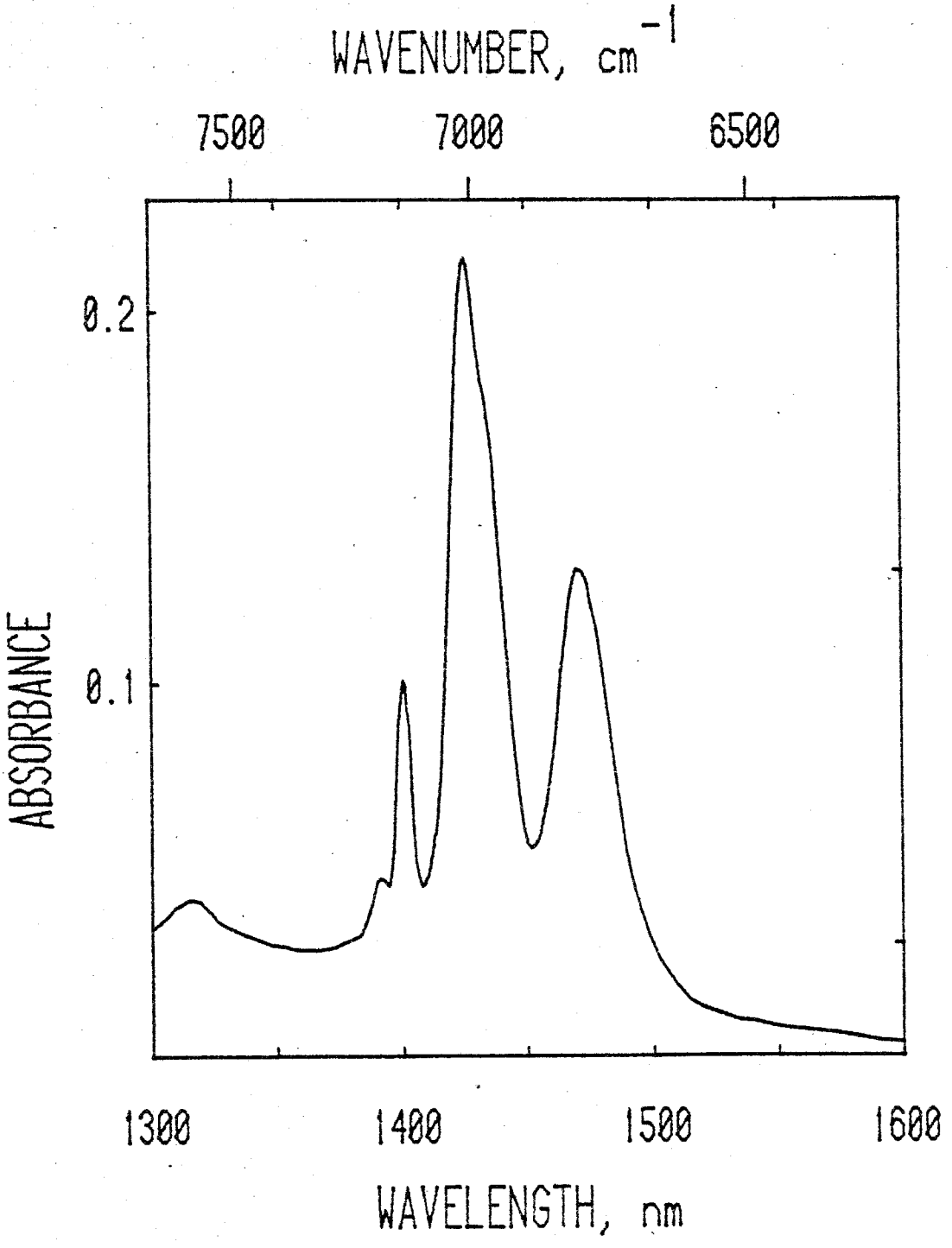

Fig. 4 E⊥c polarized absorption spectrum of tourmaline EC.

Sample thickness = 0.384 mm

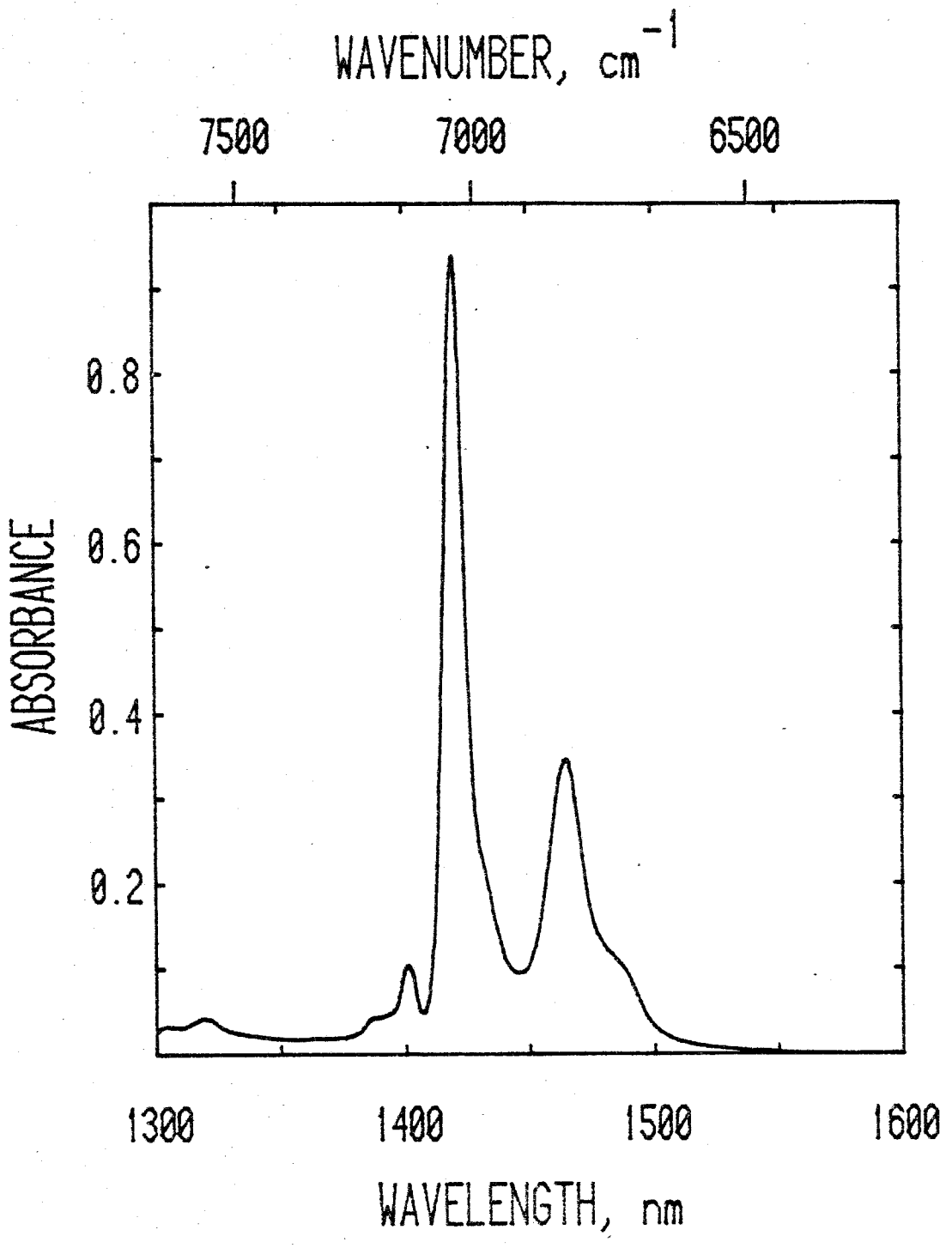

Fig. 5 E⊥c polarized absorption spectrum of tourmaline T16

Sample thickness = 1.005 mm

produce large changes in the OH spectra of the latter because they are generally divalent and substitute into the Y-site. A new transition develops in elbaites, however, at approximately the same position as the Mg(Y)Al(Z)$_2$O(3)H band in dravites and uvites. Figure 6 illustrates the spectrum of an elbaite with intermediate Fe, Mn contents. The 1437 nm band can be assigned to (Fe,Mn)(Y)Al(Z)$_2$O(3)H groups. Figure 7 illustrates the spectrum of a schorl in the elbaite-schorl series. Although the Fe(Y)Al(Z)$_2$O(3)H band is the most intense feature, the 1425 and 1470 nm bands indicate the correct compositional group. The use of OH vibrations to differentiate Fe,Mg-tourmalines from elbaite-schorl tourmalines depends upon the 1425 nm band specifically and will not be possible at compositions closer to the schorl end member. A hydroxyl band at 1470 nm can also be found in Fe,Mg-tourmalines if Fe^{3+} is present or there is excess Al.

The O(1)H groups in elbaites can be assigned to the remaining OH transitions between 1350 and 1410 nm. The complexity of this region indicates a potential for more detailed chemical analysis. However, the large number of possible groups is too large for simple interpretations. More complete analyses including Li and H would also be essential to interpretation.

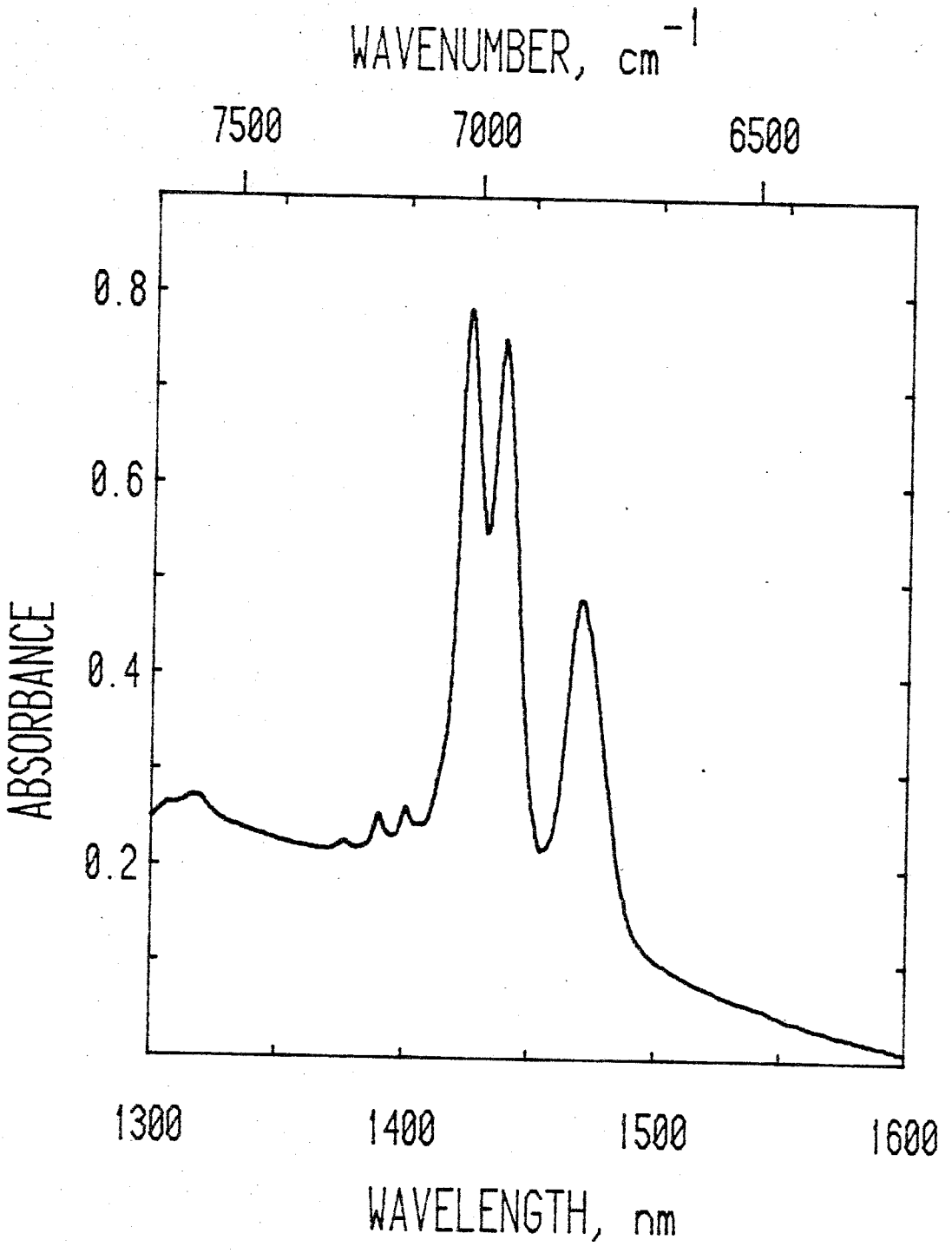

Fig. 6 E$\perp$c polarized absorption spectrum of tourmaline EB4. Sample thickness = 1.032 mm

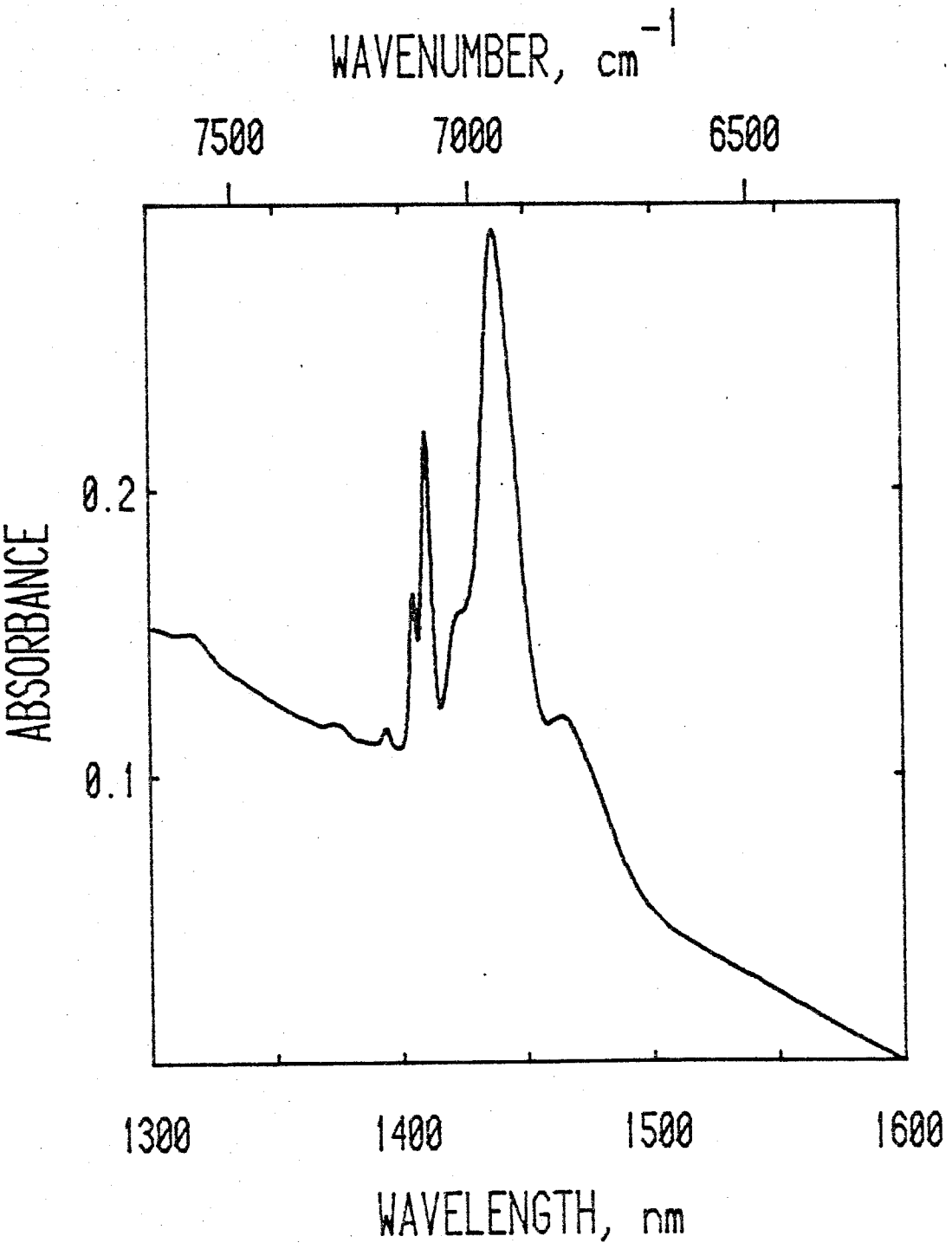

Fig. 7 E$\perp$c polarized absorption spectrum of tourmaline T22. Sample thickness = 0.253 mm

REFERENCES

Dunn, PJ, Appleman, D, Nelen, J and Norberg, J (1977a) Uvite, a new(old) member of the tourmaline group and its implications for collectors. Mineral Record 8:100-108

Dunn, PJ, Appleman, D and Nelen, JA (1977b) Liddicoatite, a new calcium end-member of the tourmaline group. Am Mineral 62:1121-1124

Farmer, VC (1974) The layer silicates. In: The Infrared Spectra of Minerals, Farmer, VC (ed.). London: The Mineralogical Society, pp. 331-363

Gebert, W and Zemann, J (1965) Messung des Ultrarot-pleochroismus von Mineralen II. Der Pleochroismus der OH-Streckfrequenz in Turmalin. Neues Jb Mineral Mh 1965:232-235

Strens, RGJ (1974) The common chain, ribbon, and ring silicates. In: The Infrared Spectra of Minerals, Farmer, VC (ed.). London: The Mineralogical Society, pp. 305-330